nagra.

Arbeitsbericht NAB 22-02

TBO Stadel-2-1: Data Report

Dossier IX Rock-mechanical and Geomechanical Laboratory Testing

September 2022

E. Crisci, L. Laloui & S. Giger

National Cooperative
for the Disposal of
Radioactive Waste

Hardstrasse 73
P.O. Box
5430 Wettingen
Switzerland
Tel. +41 56 437 11 11

nagra.ch

nagra.

Arbeitsbericht NAB 22-02

TBO Stadel-2-1: Data Report

Dossier IX Rock-mechanical and Geomechanical Laboratory Testing

September 2022

E. Crisci[1], L. Laloui[2] & S. Giger[3]

[1] Nesol - Numerical Engineering Solutions
EPFL Innovation Park Building D
[2] Laloui Consulting, Vevey
[3] Nagra

Keywords:
STA2-1, Nördlich Lägern, TBO, deep drilling campaign, geomechanics, geomechanical laboratory testing, triaxial tests, oedometric tests

National Cooperative for the Disposal of Radioactive Waste

Hardstrasse 73
P.O. Box
5430 Wettingen
Switzerland
Tel. +41 56 437 11 11

nagra.ch

Nagra Arbeitsberichte ("Working Reports") present the results of work in progress that have not necessarily been subject to a comprehensive review. They are intended to provide rapid dissemination of current information.

This NAB aims at reporting drilling results at an early stage. Additional borehole-specific data will be published elsewhere.

In the event of inconsistencies between dossiers of this NAB, the dossier addressing the specific topic takes priority. In the event of discrepancies between Nagra reports, the chronologically later report is generally considered to be correct. Data sets and interpretations laid out in this NAB may be revised in subsequent reports. The reasoning leading to these revisions will be detailed there.

This report was finalised in June 2023.

This Dossier was prepared by a project team consisting of:
E. Crisci (test coordination, formal analysis, QC and writing)
S. Giger (project administration, conceptualisation and writing)
L. Laloui (review and supervision)

The present report was prepared based on numerous contractor reports, to which many people from different laboratories contributed, namely B. Bohloli, T.S. Faleide, H. Smith, J. Stenebråten, R. Stankovic, V. Vajdova, R. Ewy, A. Ferrari, M. Rosone, F. Sandrone, M. Violay, H. Baumgartner, S. Louis, and J. Menningen.

Editorial work: P. Blaser and M. Unger

The Dossier has greatly benefitted from technical discussions with external and internal experts. Their input and work are very much appreciated.

Table of Contents

List of Tables

List of Figures

1 Introduction

1.1 Context

To provide input for site selection and the safety case for deep geological repositories for radioactive waste, Nagra has drilled a series of deep boreholes ("Tiefbohrungen", TBO) in Northern Switzerland. The aim of the drilling campaign is to characterise the deep underground of the three remaining siting regions located at the edge of the Northern Alpine Molasse Basin (Fig. 1-1).

In this report, we present the results from the Stadel-2-1 borehole.

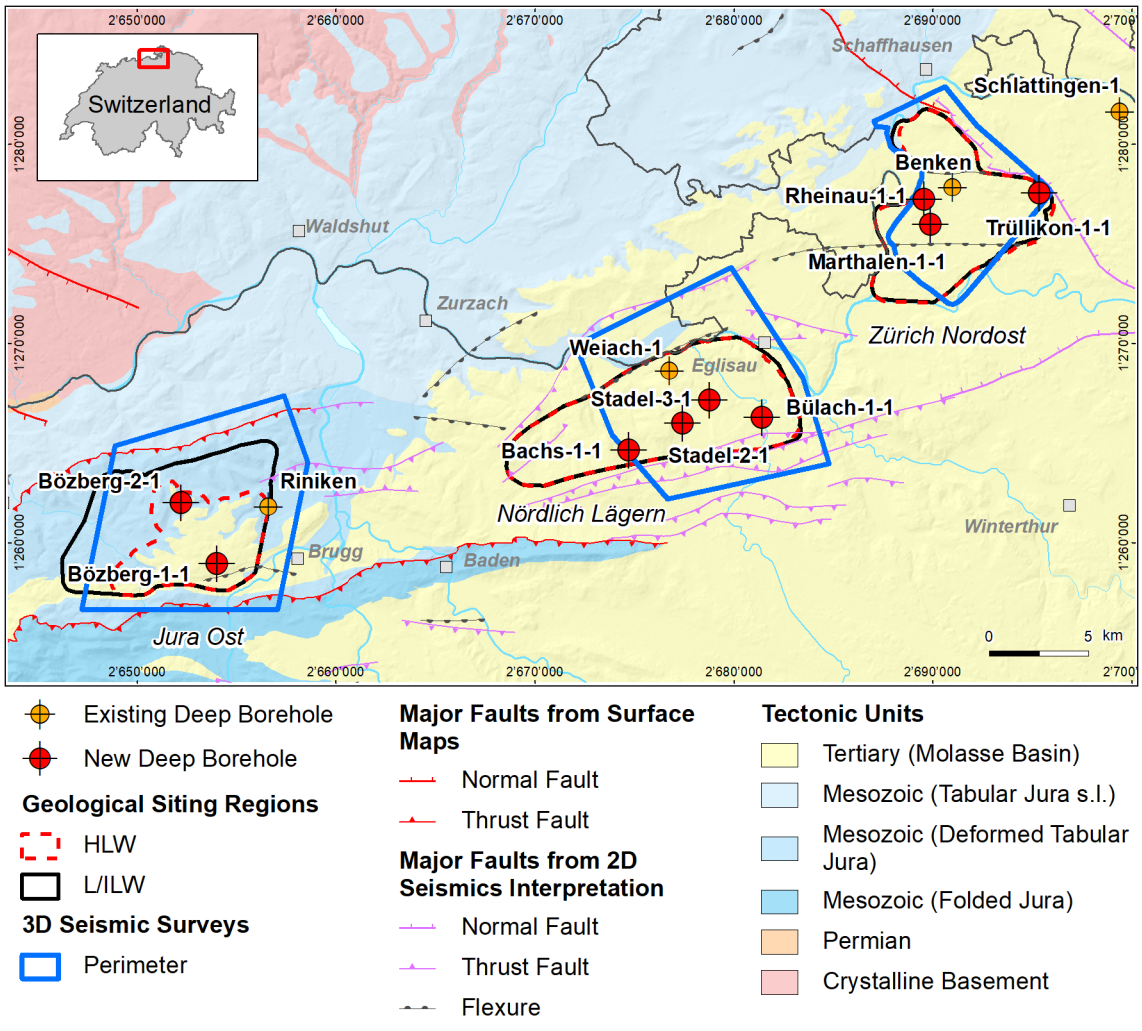

Fig. 1-1: Tectonic overview map with the three siting regions under investigation

1.2 Location and specifications of the borehole

The Stadel-2-1 (STA2-1) exploratory borehole is the seventh borehole drilled within the framework of the TBO project. The drill site is located in the central part of the Nördlich Lägern siting region (Fig. 1-2). The vertical borehole reached a final depth of 1'288.12 m (MD)[1]. The borehole specifications are provided in Tab. 1-1.

Tab. 1-1: General information about the STA2-1 borehole

Siting region	Nördlich Lägern
Municipality	Stadel (Canton Zürich / ZH), Switzerland
Drill site	Stadel-2 (STA2)
Borehole	Stadel-2-1 (STA2-1)
Coordinates	LV95: 2'677'447.617 / 1'265'987.019
Elevation	Ground level = top of rig cellar: 417.977 m above sea level (asl)
Borehole depth	1'288.12 m measured depth (MD) below ground level (bgl)
Drilling period	25th January – 8th July 2021 (spud date to end of rig release)
Drilling company	Daldrup & Söhne AG
Drilling rig	Wirth B 152t
Drilling fluid	Water-based mud with various amounts of different components such as[2]: 0 – 670 m: Bentonite & polymers 670 – 1'051 m: Potassium silicate & polymers 1'051 – 1'117 m: Water & polymers 1'117 – 1'288.12 m: Sodium chloride brine & polymers

The lithostratigraphic profile and the casing scheme are shown in Fig. 1-3. The comparison of the core versus log depth[3] of the main lithostratigraphic boundaries in the STA2-1 borehole is shown in Tab. 1-2.

[1] Measured depth (MD) refers to the position along the borehole trajectory, starting at ground level, which for this borehole is the top of the rig cellar. For a perfectly vertical borehole, MD below ground level (bgl) and true vertical depth (TVD) are the same. In all Dossiers depth refers to MD unless stated otherwise.

[2] For detailed information see Dossier I.

[3] Core depth refers to the depth marked on the drill cores. Log depth results from the depth observed during geophysical wireline logging. Note that the petrophysical logs have not been shifted to core depth, hence log depth differs from core depth.

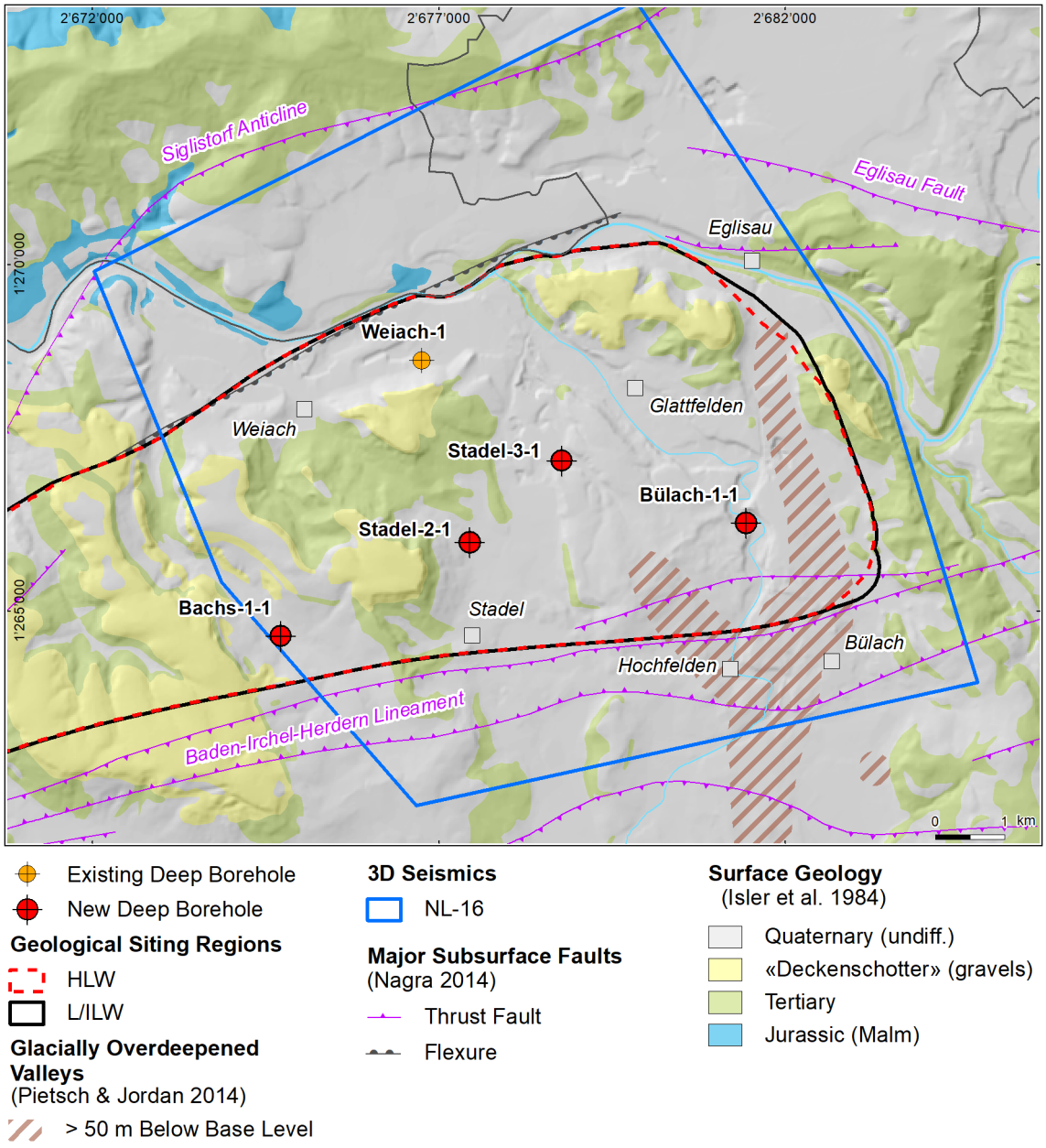

Fig. 1-2: Overview map of the investigation area in the Nördlich Lägern siting region with the location of the STA2-1 borehole in relation to the boreholes Weiach-1, BUL1-1, STA3-1 and BAC1-1

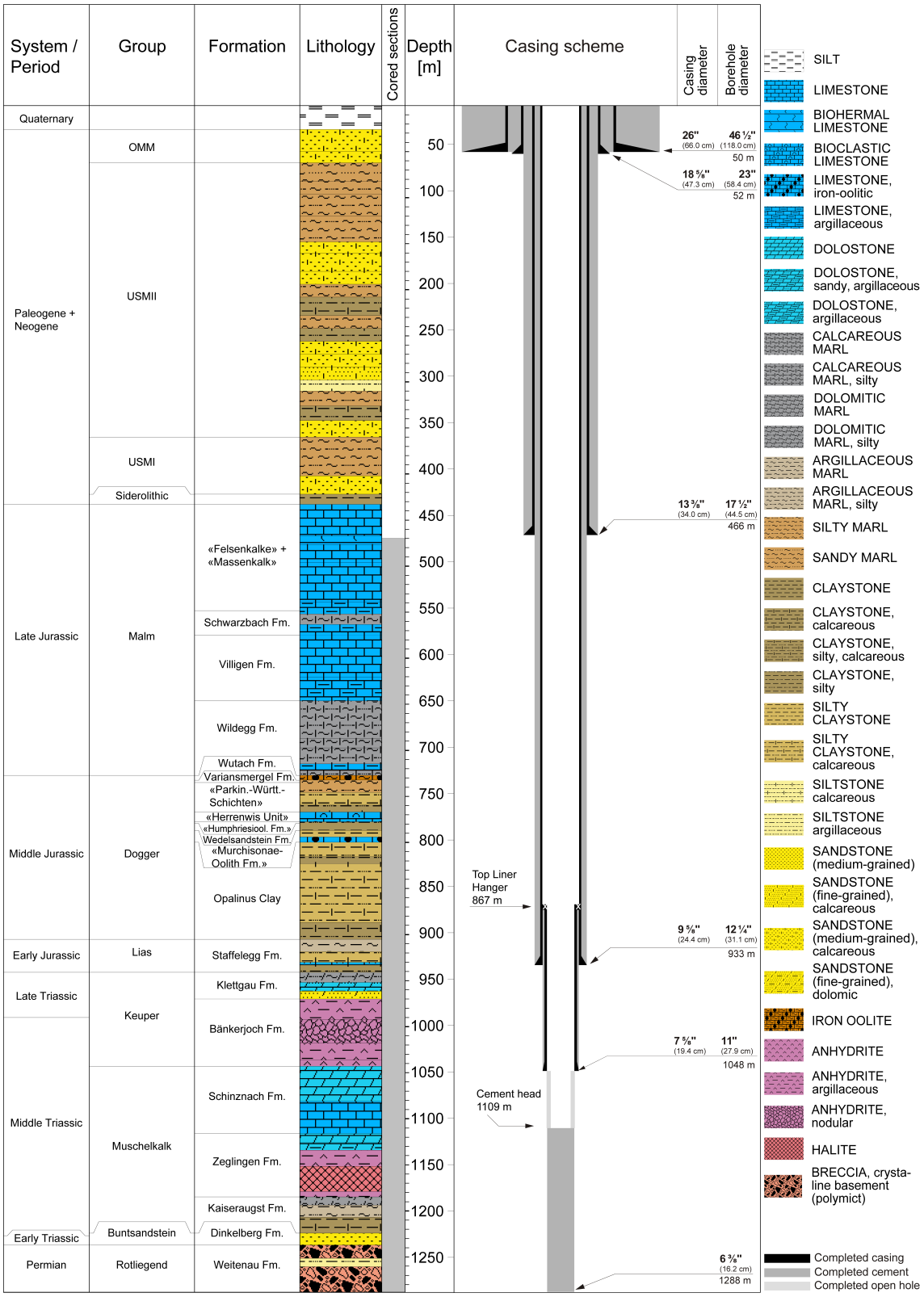

Fig. 1-3: Lithostratigraphic profile and casing scheme for the STA2-1 borehole[4]

[4] For detailed information see Dossier I and III.

Tab. 1-2: Core and log depth for the main lithostratigraphic boundaries in the STA2-1 borehole[5]

System / Period	Group	Formation		Core depth in m (MD)	Log depth in m (MD)	
Quaternary				**26.0**		—
Paleogene + Neogene	OMM			62.0		—
	USM			422.0		—
	Siderolithic			**433.0**		—
Jurassic	Malm	«Felsenkalke» + «Massenkalk»		548.35	548.62	—
		Schwarzbach Formation		575.08	575.45	—
		Villigen Formation		646.23	646.63	—
		Wildegg Formation		727.18	728.20	—
	Dogger	Wutach Formation		732.16	733.25	—
		Variansmergel Formation		734.92	735.95	—
		«Parkinsoni-Württembergica-Schichten»		767.02	768.05	—
		«Herrenwis Unit»		777.54	778.47	—
		«Humphriesioolith Formation»		779.34	780.27	—
		Wedelsandstein Formation		786.85	787.79	—
		«Murchisonae-Oolith Formation»		799.67	800.67	—
		Opalinus Clay		905.20	906.87	—
	Lias	Staffelegg Formation		**940.89**	**941.42**	—
Triassic	Keuper	Klettgau Formation		969.87	970.52	—
		Bänkerjoch Formation		1043.07	1043.62	—
	Muschelkalk	Schinznach Formation		1116.01	1116.69	—
		Zeglingen Formation		1184.72	1185.42	—
		Kaiseraugst Formation		1224.20	1225.07	—
	Buntsandstein	Dinkelberg Formation		**1237.01**	**1237.94**	—
Permian	Rotliegend	Weitenau Formation	final depth	1288.12	1288.87	

[5] For details regarding lithostratigraphic boundaries see Dossier III and IV; for details about depth shifts (core goniometry) see Dossier V.

1.3 Documentation structure for the STA2-1 borehole

NAB 22-02 documents the majority of the investigations carried out in the STA2-1 borehole, including laboratory investigations on core material. The NAB comprises a series of stand-alone dossiers addressing individual topics and a final dossier with a summary composite plot (Tab. 1-3).

This documentation aims at early publication of the data collected in the STA2-1 borehole. It includes most of the data available approximately one year after completion of the borehole. Some analyses are still ongoing (e.g. diffusion experiments, analysis of veins, hydrochemical interpretation of water samples) and results will be published in separate reports.

The current borehole report will provide an important basis for the integration of datasets from different boreholes. The integration and interpretation of the results in the wider geological context will be documented later in separate geoscientific reports.

Tab. 1-3: List of dossiers included in NAB 22-02

Black indicates the dossier at hand.

Dossier	Title	Authors
I	TBO Stadel-2-1: Drilling	P. Hinterholzer-Reisegger
II	TBO Stadel-2-1: Core Photography	D. Kaehr & M. Gysi
III	TBO Stadel-2-1: Lithostratigraphy	P. Jordan, P. Schürch, H. Naef, M. Schwarz, R. Felber, T. Ibele & H.P. Weber
IV	TBO Stadel-2-1: Microfacies, Bio- and Chemostratigraphic Analysis	S. Wohlwend, H.R. Bläsi, S. Feist-Burkhardt, B. Hostettler, U. Menkveld-Gfeller, V. Dietze & G. Deplazes
V	TBO Stadel-2-1: Structural Geology	A. Ebert, S. Cioldi, E. Hägerstedt & H.P. Weber
VI	TBO Stadel-2-1: Wireline Logging, Pressure-meter Testing and Micro-hydraulic Fracturing	J. Gonus, E. Bailey, J. Desroches & R. Garrard
VII	TBO Stadel-2-1: Hydraulic Packer Testing	R. Schwarz, R. Beauheim, S.M.L. Hardie & A. Pechstein
VIII	TBO Stadel-2-1: Rock Properties, Porewater Characterisation and Natural Tracer Profiles	C. Zwahlen, L. Aschwanden, E. Gaucher, T. Gimmi, A. Jenni, M. Kiczka, U. Mäder, M. Mazurek, D. Roos, D. Rufer, H.N. Waber, P. Wersin & D. Traber
IX	TBO Stadel-2-1: Rock-mechanical and Geomechanical Laboratory Testing	E. Crisci, L. Laloui & S. Giger
X	TBO Stadel-2-1: Petrophysical Log Analysis	S. Marnat & J.K. Becker
	TBO Stadel-2-1: Summary Plot	Nagra

1.4 Scope and objectives of this dossier

The dossier at hand is organised as follows:

- Chapter 2 presents the aims of the laboratory testing programmes and introduces the laboratories involved.
- Chapter 3 provides an overview of core sampling, conditioning and storage methods, and also explains the non-destructive method used to evaluate core integrity prior to shipping to the laboratories.
- Chapter 4 introduces the testing methods used in the testing programmes and provides an overview of the executed tests per formation.
- Chapter 5 documents the results of the rock-mechanical testing programme.
- Chapter 6 documents the triaxial and the oedometric test results of the geomechanical testing programme. Given the greater complexity of the testing procedure and the relevance of the test results for site evaluation, these test results are more rigorously documented than the rock-mechanical test results.
- A short discussion on the representativeness of the results is provided in Chapter 7.

Furthermore, large documentation of the performed tests is reported in the appendix, and includes:

A – Photo documentation of the rock-mechanical testing programme

B – XCT (medical X-ray tomography) cross-sections, with indication of the section used for geomechanical testing

C – Diagnostic plots of the triaxial tests (geomechanical testing programme)

D – Mineralogical analysis (geomechanical testing programme)

E – Triaxial test results (geomechanical testing programme)

F – Test results in oedometric conditions (geomechanical testing programme)

2 Aims of the study and overview of the testing programme

2.1 Aims of the study and distinction of rock-mechanical and geomechanical testing programmes

For site characterisation, rock-mechanical and geomechanical properties are used for the following applications:

1. Supporting data for the detailed analysis and interpretation of in situ micro-hydraulic fracturing tests
2. Parametrise 3D geomechanical numerical models with (sub-)formation properties to assess the spatial variability of the stress tensor
3. Design of underground repository access structures
4. Hydro-mechanical properties of the host rock Opalinus Clay and its confining units
5. Volumetric behaviour (consolidation and swelling) and hydraulic properties of the host rock Opalinus Clay and its confining units

To address points 1. to 3. «standard» rock-mechanical tests were performed on core material in the stratigraphic interval Malm to Rotliegend, except for Opalinus Clay. «Standard» here means that the tests were performed according to national and international standards, notably the suggested methods of the International Society of Rock Mechanics (*cf.* Section 4.2). Standard tests were performed within the **"rock-mechanical testing programme"**.

In contrast, laboratory testing under points 4. and 5. were conducted using specialised protocols (*cf.* Section 4.3) combining rock-mechanical and soil mechanical aspects. Specifically, these protocols account for 1) the higher requirements of the low-permeability and fluid-sensitive Opalinus Clay and its argillaceous confining units to obtain robust test results, and 2) for the greater relevance of these units to evaluate the safety of a future repository. Tests performed using the specialised protocols are hereafter assigned to the **"geomechanical testing programme"**.

2.2 Overview of testing programme and contractors

2.2.1 Rock-mechanical testing programme

The rock-mechanical testing programme with core material of the STA2-1 borehole comprised the following testing methods:

- Fracture toughness using semi-circular bend specimen (FT)
- Uniaxial compressive strength (UCS)
- Triaxial compressive strength (TRX)

The following laboratories were contracted:

- Experimental Rock Mechanics Laboratory at EPFL (Switzerland). Main contacts were Federica Sandrone and Marie Violay.
- Gesteinslabor Dr. Eberhard Jahns (Germany). Main contacts were Hansjörg Baumgartner, Sarah Louis and Johanna Menningen.
- NGI (Norway). Main contact was Bahman Bohloli.

2.2.2 Geomechanical testing programme

The geomechanical testing programme was specifically designed for Opalinus Clay and its confining units and comprised of the following testing methods with cores from the STA2-1 borehole:

- Triaxial deformation tests with various stress paths (TRX)
- Constant-head permeability phases (PERM) performed in oedometric apparati
- Triaxial compression tests perfomed in laterally constrained conditions (K0), including for some tests constant-head permeability phases

Three laboratories were contracted for the geomechanical testing campaign:

- NGI (Norway), main contact was Bahman Bohloli
- Sintef (Norway), main contact was Jørn Stenebråten
- RSTD (USA), main contact was Russel Ewy
- DI (Italy), main contact was Alessio Ferrari

Each laboratory is identified with a letter, used in the test results labelling (A = NGI, B = Sintef, C = RSTD, D = DI).

Specialised protocols were developed in recent years to evaluate hydro-mechanical properties of Opalinus Clay in both high-pressure oedometric tests (Favero 2017, Ferrari et al. 2016, Crisci et al. 2019) and triaxial deformation tests (Favero et al. 2018, Giger et al. 2018). In the case of triaxial testing, the testing procedures were further validated in a benchmarking study (Minardi et al. 2019, Minardi et al. 2020).

3 Core sampling, storage and XCT scanning

3.1 Core sampling and conditioning

Cores used for geomechanical or rock-mechanical analyses (hereafter referred to as GM cores) represent one of nine major categories sampled at the borehole. Each of these categories has special requirements to minimise potential effects on laboratory analyses, and hence special conditioning methods. Target exposure time to atmosphere was set to 20 minutes for all GM cores to allow geological description and documentation (incl. core scanner for photographic description). A complete archive of core photographs, and exposure time to atmosphere prior to embedding the cores in resin is made in Nagra's internal QA/QC documentation.

Fig. 3-1: Sampling and storage workflow of GM cores

(a) Inserting core directly into PVC tube (no plastic film). (b) Rack of PVC tubes during curing with clamp bar in core at the front row (left side). (c) Labelled PVC tubes with core and top spacer (used for clamping) embedded in epoxy resin. (d) Custom made core box used for transporting and archiving. Example pictures are from borehole Bülach-1-1 (Crisci et al. 2021a).

The cores were then immediately inserted in PVC tubes, and axially constrained with bar clamps (Fig. 3-1). The annulus was then filled with epoxy (Sikadur-52). The annulus between the core and the PVC tube was chosen to be very small (nominal 3.2 mm) to ensure that no excessive temperature from curing of the epoxy develops[6]. Further details of the conditioning procedure are provided in the field manual (Rufer 2019).

A total of 78 GM cores with a cumulative length of 35 metres were conditioned in this way. Additional 3 cores were sampled later at the core storage facility. This was done to enable permeability testing to complement the in situ testing programme (hydraulic packer tests in the «Humphriesioolith Formation» and the Klettgau Formation, respectively) where no conditioned core was secured, and only for hard rocks not sensitive to water exchange (drying).

3.2 Evaluation of core quality using XCT Scanning

To evaluate core integrity prior to shipping to the testing laboratories, all GM cores from Opalinus Clay and its confining units in the Upper Dogger and Lias (Staffelegg Formation) were analysed using medical X-ray computer tomography (XCT). Details of the applied XCT method can be found in Keller & Giger (2019). The obtained image data had a voxel size of 0.25 × 0.25 × 0.4 mm. By stacking individual scans, a virtual cross-section could be obtained for each core (Fig. 3-2). It is noted that the CT-number is a proxy for material density. This enabled the detection of small cracks and a physical representation of the variability of material properties. These cross-sections were the basis for the selection of sub-coring for the geomechanical testing programme (Chapter 6 and Appendix B).

[6] Maximum measured temperature in the laboratory was < 27 °C.

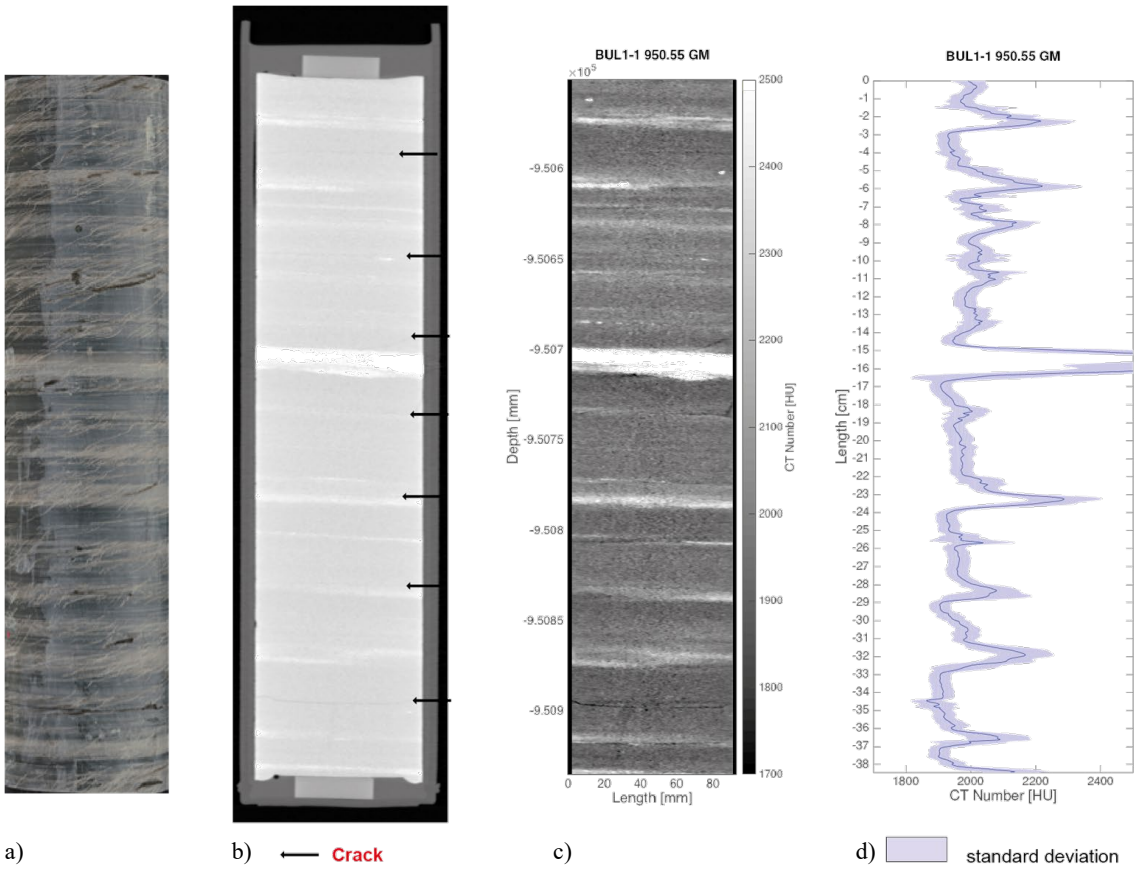

Fig. 3-2: Cross-section of XCT stack

(a) core picture; (b) entire core in PVC tube and resin (both dark grey) and embedded spacers (light grey – subhorizontal cracks are indicated by arrows); (c) optimised image for the core only; (d) vertical profile with CT number (Hounsfield Units). Example pictures are from borehole Bülach-1-1 (Crisci et al. 2021a).

4 Testing methods and overview of executed tests

4.1 Convention of sample geometry

Sedimentary geomaterials typically display transversely isotropic mechanical properties which are related to the orientation of the bedding. To study this anisotropic response, cylindrical specimens were tested in three orientations with respect to bedding (Fig. 4-1).

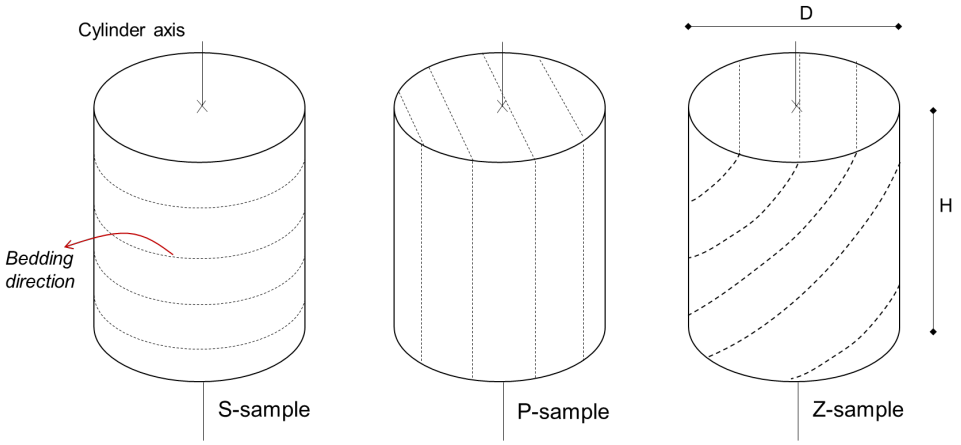

Fig. 4-1: Terminology of specimens in relation to bedding orientation

In this report, the following convention applies:

- S-samples: the cylinder axis is perpendicular to bedding direction
- P-samples: the cylinder axis is parallel to bedding direction
- Z-samples: the cylinder axis is at an angle with respect to bedding.

The convention applies to all kind of tests, however the ratio of diameter (D) to height (H) of the specimen is different. The ratio ranges from $D:H \approx 1/2$ for triaxial and uniaxial tests, to $D:H \approx 1.4$ in Brazilian tests and $D:H \approx 2.5$ for oedometric tests.

4.2 Rock-mechanical testing programme – testing methods

4.2.1 Fracture toughness

Two methods were used to constrain fracture toughness: (i) the semi-circular bending method, and (ii) the modified ring method. For the semi-circular bending (SCB) test, specimens were prepared according to the ISRM recommended specifications (Kuruppu et al. 2014). Specimens were cut with a blade and water at room temperature as a cutting fluid, and in each specimen, a 23 mm long notch was cut. In the semi-circular notched specimen sketched in Fig. 4-2, a is the length of the notch, R is the core radius, B is the specimen thickness, and s is the distance between the base supports for the test. P denotes the applied load. The specimen is submitted to a monotonically increasing compressive load applied at the central loading roller of the three-point bend loading at a constant displacement rate of about 0.2 mm/min until it reaches failure.

The second method used was the modified ring (MR) test (Thiercelin 1988), which is considered to yield a more stable fracture growth. In MR tests, the specimen is a hollow cylinder with two diametrically opposed flat-loading surfaces, in order to reduce crushing damages nearby the load application point (Fig. 4-2b). The internal hole is notched with two diametrically opposed notches about 5 mm long (indicated by *c* in Fig. 4-2b) and 1 mm wide each. The notch direction is either aligned or perpendicular to the bedding planes.

During the test, the specimen is submitted to a monotonically increasing compressive load (F) applied on the flat-loading surface at a constant displacement rate of about 0.02 mm/s until the cracks show stable propagation. The test is stopped before the cracks reach the loading surfaces, thus avoiding the influence of the compressive state of stress induced in these portions of the sample and reducing the boundary conditions effects related to the sample geometry. The vertical displacement is measured with a digital transducer while the crack mouth opening is measured with an extensometer measuring horizontal displacement of the internal hole walls. The sample is also equipped with two strain gauges.

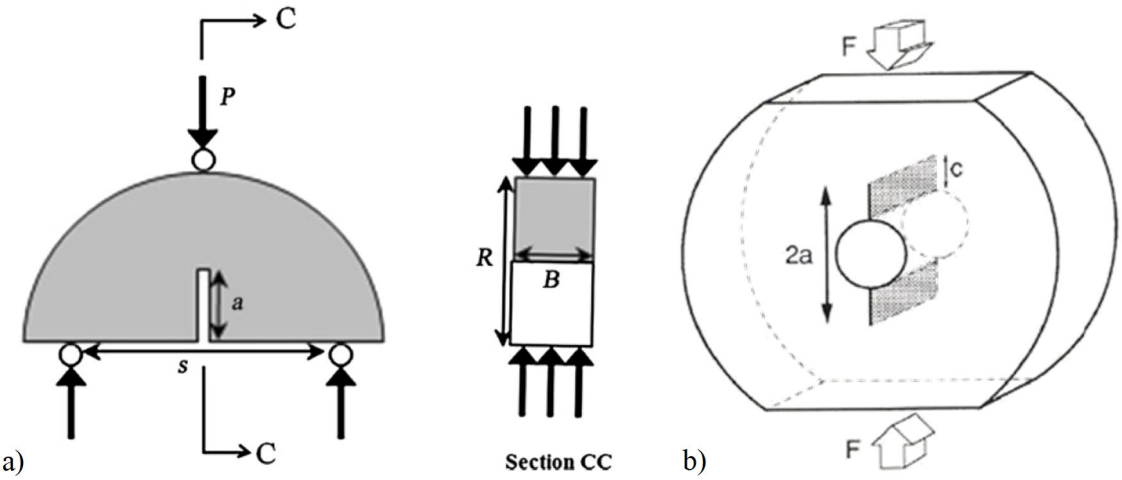

Fig. 4-2: Testing geometries used to constrain fracture toughness

(a) Semi-circular bending (SCB) test geometry after Kuruppu et al. (2014). (b) Modified ring (MR) test geometry after Fischer et al. (1996).

4.2.2 Unconfined compressive strength test

Unconfined compressive strength (UCS) tests were done according to ASTM standard D7012-14e1 (ASTM 2014).

Test specimens have a diameter of 25.4 mm and a length of at least 50.8 mm (length:diameter ratio of 2:1). Testing plugs were drilled either perpendicular to bedding (so-called "S" direction) or parallel to bedding (so-called "P" direction). The plugs were drilled with a diamond tipped hollow bit. Cooling during drilling and trimming was performed with the low viscous volatile mineral oil Ilocut EDM 180 (Castrol). Plug trimming to the required length was carried out with a diamond chop saw with slow constant velocity feeding. The accuracy in plane parallelism is in accordance with ASTM D4543-19 (ASTM 2019).

The UCS tests were performed on a digitally controlled, servo-hydraulic testing machine with a maximum load range of 600 kN (accuracy class 1) and at a constant strain rate of approximately 10^{-5} s^{-1}.

Axial deformation of the specimen was measured with either one or two LVDT displacement transducers. Measurements were either done directly at the specimen or corrected for load frame deformation. Radial deformation of the specimen is measured diametric with a transverse extensometer (Fig. 4-3).

Throughout this report, the strains are calculated as the ratio of the variation in height (or diameter) to the initial height (or diameter).

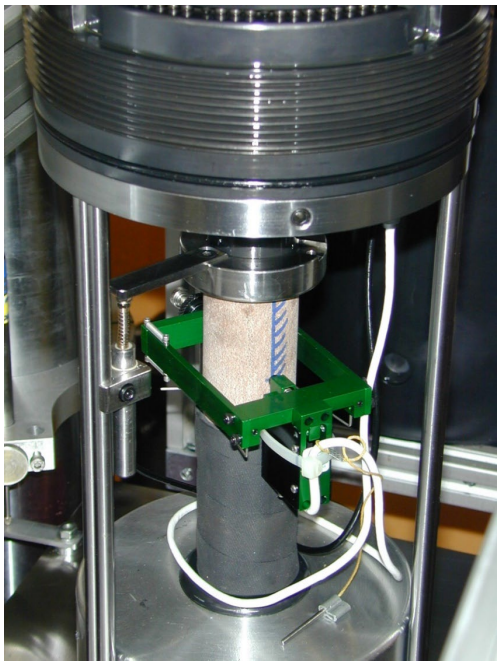

Fig. 4-3: UCS testing configuration

Note axial LVDT and transverse extensometer. Specimen diameter is 25.4 mm.

4.2.3 Triaxial deformation test

Triaxial deformation tests (TRX) were done according to ASTM standard D7012-14e1 (ASTM 2014) for single-stage procedure, but also included an unloading/reloading cycle before peak strength (below).

Test specimens have the same dimensions as for the UCS tests (diameter 25.4 mm, length 50.8 mm) and were prepared in the same manner (*cf.* Section 4.2.2). The accuracy in plane parallelism is also in accordance with ASTM D4543-19 (ASTM 2019).

Axial (average of three LVDTs) and radial deformation of the specimen (diametric with one single strain gauge) were measured 'in-vessel' to avoid the load frame deformation being included in the results of the deformation of the individual specimen (Fig. 4-4). The measurement range of the LVDTs is ±5 mm; their sensitivity in the range between 9 and 60 mV; non-linearity is 0.15% full scale. Three LVDTs were used to observe specimen distortions that may influence the strength measurements in a non-acceptable manner. The differential axial load (strain gauge) also was measured 'in vessel' with a load cell mounted directly below the specimen to eliminate the influence of piston friction effects to the stress measurement. A 600 kN load cell of accuracy class 0.5 was used for the tests.

The artificial brine was composed of demineralised water and 5 g/l NaCl. The pistons are perforated to enable drained conditions. One of the two labs involved used side drains, the other did not. No spherical seats were used. All the important parameters were recorded automatically with different intervals, adjusted to expected speed of changes. No smoothing or filtering algorithms were applied.

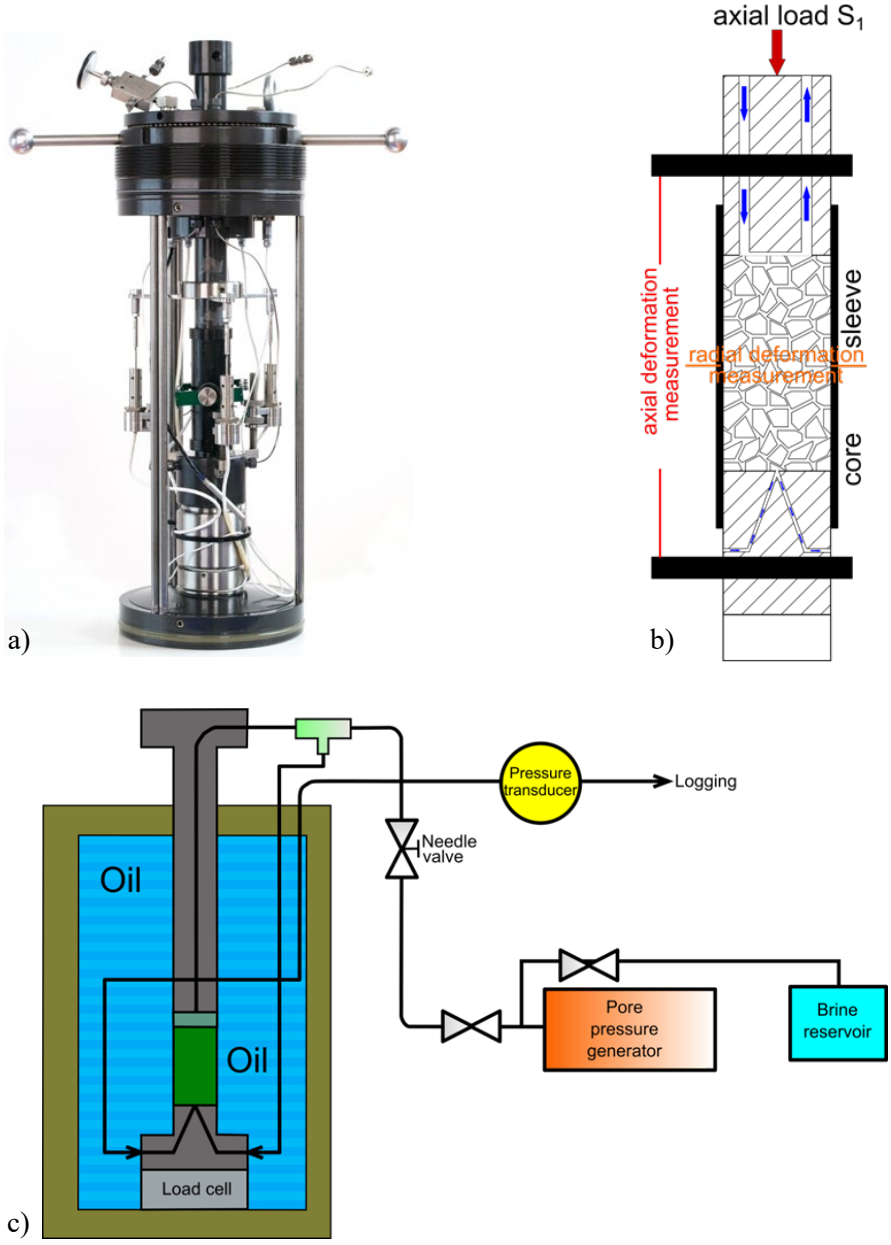

Fig. 4-4: Triaxial testing configuration used for rock-mechanical testing

Specimen in membrane with axial and radial strain sensors, pore fluid line and ultrasonics (a), schematic of the specimen (b) and the pressure cell with pore fluid system (c).

During all phases of the tests, ultrasonic velocities, both P- and S-waves, were logged and monitored according to ISRM standards (Aydin 2014). The piezometer resonance frequency was 1 MHz.

The theoretically possible stress paths in a triaxial testing configuration with two independent controls (axial and radial stress) are illustrated in Fig. 4-5 in mean total stress (p) versus deviatoric stress (q) space, where:

$$p = \frac{\sigma_a + 2\sigma_r}{3} \tag{4-1}$$

$$q = \sigma_a - \sigma_r \tag{4-2}$$

Where σ_a and σ_r are the total axial (direction of the cylinder axis) and radial (direction perpendicular to the cylinder axis) stress, respectively.

The upper part of the plane (compression part) summarises the stress paths that induce axial compression of the tested specimen. The shear path can be induced by either increasing the axial stress σ_a (CTC path), reducing the radial stress σ_r (RTC path) or increasing σ_a and reducing σ_r at the same time (TC path) keeping the mean total stress constant. The stress paths that induce an axial extension of the specimen are illustrated below the p-axis in Fig. 4-5. The axial extension can be induced by either decreasing the axial stress (RTE path), increasing the radial stress (CTE), or decreasing σ_a and increasing σ_r at the same time (TE path) keeping the mean total stress constant. Therefore, when the term 'reduce' is used to define the stress path, it means that one of the two stresses is decreased while the other is kept constant. On the other hand, when the term 'conventional' is used to define the stress path, it means that one of the two stresses is increased and the other is kept constant. It is noted that the illustrations in Fig. 4-5 are the stress paths for total stress only, so the tests can be conducted in either drained or undrained conditions. This means that the submitted loading conditions may differ based on the porewater pressure generation during undrained testing. For the triaxial tests of the rock-mechanical testing programme, only CTC stress paths were executed.

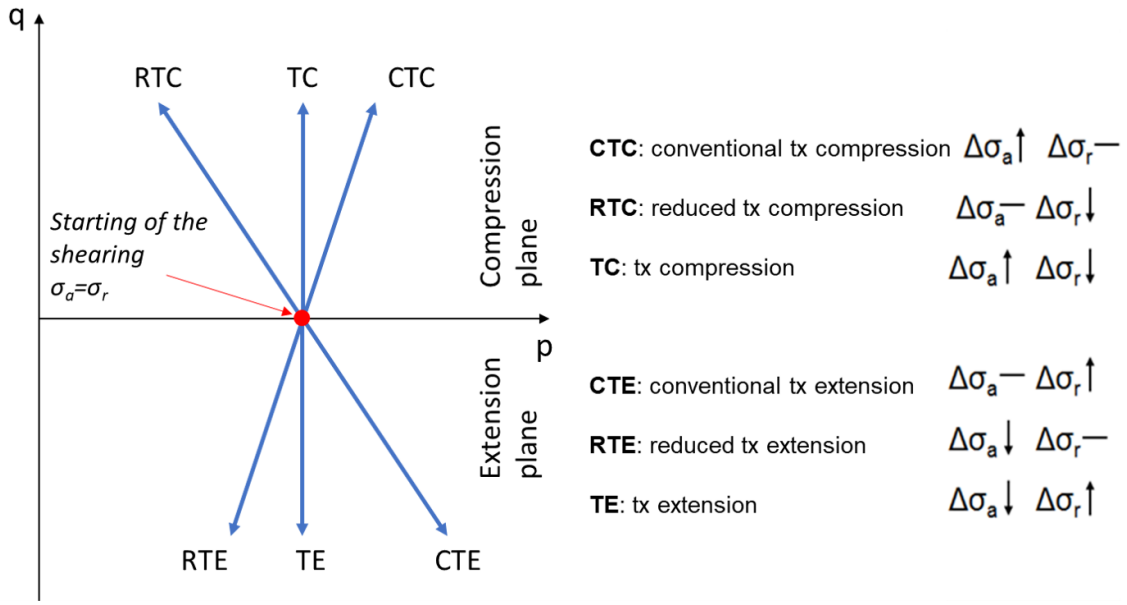

Fig. 4-5: Summary of possible stress paths that can be used to perform triaxial tests

On the right side, it is indicated which of the two stresses (axial σ_a and radial σ_r) is increased or decreased.

Test procedure

The testing procedure consisted of a maximum of four main phases:

1. Isotropic loading phase, during which the radial confining pressure and the axial load are increased simultaneously. The needle valve to the pore pressure generator is opened after the total stress has reached an equivalent value of 2 MPa. Both total mean stress (p) and fluid pressure (u_w) are then increased in concert to their respective target values: 10 to 15 MPa for p and 5 MPa for u_w.

2. *Selected tests only:* the pore-fluid-coupling parameter during isotropic loading (Skempton's B value) is evaluated in undrained conditions. During the Skempton's B test, the change in pore pressure over time (Δu_w) is determined as a function of the change in isotropic pressure increase over time (Δp) (u_w is allowed to equilibrate at least for 20 minutes up to 8 – 24 hours):

$$B = \frac{\Delta u_w}{\Delta p} \tag{4-3}$$

   In the present case two to three Skempton's B tests were carried out per specimen with confining pressure increase Δp of 1 or 2 MPa.

3. *Selected tests only:* a consolidation phase is performed to determine the consolidation coefficient c_{vi}. An isotropic total stress increase (or decrease) is applied to the specimen and the deformations in time are recorded and analysed. The deformation evolves according to the dissipation of the porewater over- (or under-) pressure induced by the load variation. Calculation of the consolidation coefficient c_{vi} (in mm^2/h) is done according to the following equation (Head 1998):

$$c_{vi} = \frac{\pi D^2}{\lambda t_{100}} \tag{4-4}$$

   with D as the plug diameter and t_{100} as the theoretical time to 100% consolidation. The theoretical time t_{100} is found by extrapolating the linear portion of the volumetric strain versus square root of the experimental time curve (with time in h) to the final strain value. Lastly, λ is a constant depending on drainage boundary conditions.

4. The fourth testing phase is the shearing phase or triaxial test, applying a constant deviatoric stress or strain rate. The standard strain rate was 10^{-6} s^{-1} but was adjusted based on theoretical calculations (Head 1998) using the consolidation coefficient determined in phase 3 or considering lithology and water content.

The shearing phase of the triaxial tests was preceded in selected cases by a Skempton's B test for verification of specimen saturation and, subsequently, by a determination of the consolidation coefficient c_v as base for strain rate calculation. However, in the rock mechanics programme of STA2-1 cores, consolidation coefficients were not determined. Instead, strain rates were chosen based on lithological criteria (rock type, water content and mechanical properties based on UCS test results) and previous experiences (*cf.* Crisci et al. 2021a and 2021b).

Generally, clay-rich rocks, such as clay- and siltstones or marls were tested at lower strain rates than limestones, sandstones and anhydrites. The strain rate of the single-stage triaxial tests ranged between 10^{-6} s^{-1} and 2×10^{-7} s^{-1}.

4.3 Geomechanical testing programme – testing methods

4.3.1 Synthetic pore fluid

The artificial porewater (APW) used in the geomechanical tests is based on the recipe derived from the investigations in the Schlattingen borehole (Mäder in Wersin et al. 2013), and the composition is reported in Tab. 4-1. This recipe defines a porewater saturated with respect to calcite and dolomite under atmospheric CO_2 partial pressure (lab conditions).

Towards the end of the geomechanical testing programme, the porewater chemistry was also constrained for the STA2-1 core material (*cf.* Dossier VIII). These investigations confirm the general Na-Cl water type. The salinities in the Dogger section are somewhat higher than in the APW; e.g. chloride concentrations in Opalinus Clay and in the Dogger above the OPA are in the range of 7 – 8 g g/L (APW: 6.7 g/L)). From the base of OPA, the values decrease to the Keuper aquifer to c. 4 g/L. In addition to saturation with carbonate minerals, the investigations suggest that the porewaters are at or close to saturation with respect to the sulphate mineral celestite. But the APW was not changed for the final geomechanical tests, to be consistent with earlier tests. Finally, the slightly higher ionic strength in the porewater found in the STA2-1 core is not anticipated to have a significant effect on hydromechanical properties (Witteveen et al. 2013, Ewy 2014, Tuttolomondo 2021).

Tab. 4-1: Recipe used for the preparation of the APW

Compound	mmol/kg_{H2O}	g/kg_{H2O}
NaCl	115.26	6.7356
$NaHCO_3$	0.54	0.0456
$CaCl_2$ $2H_2O$	11.91	1.7510
KCl	2.55	0.1902
$MgCl_2$ $6H_2O$	9.17	1.8635
Na_2SO_4	24.00	3.4089

4.3.2 Triaxial deformation test (specialised protocol)

To assess the mechanical properties of the Opalinus Clay and confining units, dedicated testing protocols were established (Minardi et al. 2019).

The extraction of the specimens was carefully performed in order to minimise water content loss during the operation. All involved laboratories used a drilling machine. All labs used hydrocarbons as cooling fluids during the drilling of the specimens.

Computed tomography of the cores after drilling was used to identify the most suitable sections for extracting test specimens *(cf.* Appendix A). The target zones were selected upon Nesol's and Nagra's guidance.

The conventional testing procedure indicated by Nagra to carry out triaxial tests foresaw the following steps (Fig. 4-6):

1. An initial isotropic total stress (0.5 – 1 MPa) is applied to the specimen to ensure contact with the axial piston. The saturation of the specimen is then performed at constant volume to minimise specimen disturbance (i.e. fissure opening during resaturation); axial and radial stresses are progressively increased to keep the specimen's volume constant while it is put in contact with fluid at low back pressure. Next, the fluid back-pressure is increased to at least 2 MPa (the total stresses are also increased to keep the effective stress constant) (*ss1*), to dissolve possible air remaining in the tubing or the material. This procedure allows the determination of the axial and radial swelling pressures. The confining stress is then set equal to the axial stress (*ss2*). A pore pressure increment step is performed either at this stage (*ss3*) or before the shearing phase in order to reach the target confinment.
2. The assessment of the specimens' saturation is carried out by measuring the Skempton's B coefficient (B check test). Two to three isotropic undrained loadings are performed. More steps are applied when unsatisfactory values are obtained.
3. Drained consolidation or swelling of the specimen is performed to reach the target consolidation stress; consolidation effective stresses range between 7 and 20 MPa. The pore fluid pressure is kept constant to 8 – 10 MPa during consolidation.
4. The final stage is the shearing of the specimens at constant axial strain rate. An unloading/ reloading loop is performed, then the specimen is sheared until the specimen's failure and achievement of the post-peak constant deviatoric stress, in undrained or drained conditions.

The laboratories involved in the triaxial testing programme with specialised protocols, prepared cylindrical specimens respecting the diameter (D) to height (H) ratio $D:H \approx 0.5$. In particular, the specimen nominal diameters are:

- Lab A: $D = 25.0$ mm
- Lab B: $D = 25.0$ mm
- Lab C: $D = 19.1$ mm

The labs used two drainage systems: Lab A and B used both radial drainage and drainage at the two edges, while Lab C used radial drainage and drainage at one edge of the cylinder. The strain rates to apply during shearing were defined according to the drainage conditions and the specimen dimensions (i.e., drainage length). Water content after testing was determined by oven-drying at 105 °C for several days until constant weight.

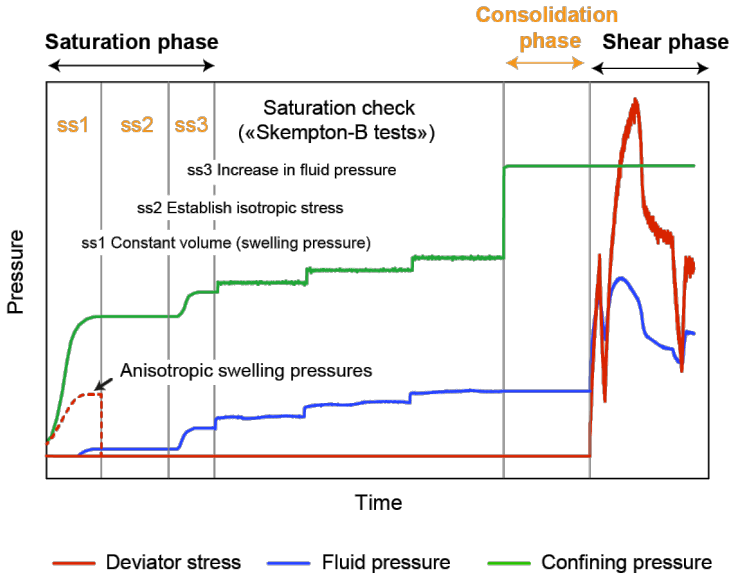

a) **Orange: (sub)phases wtih drained boundary conditions**

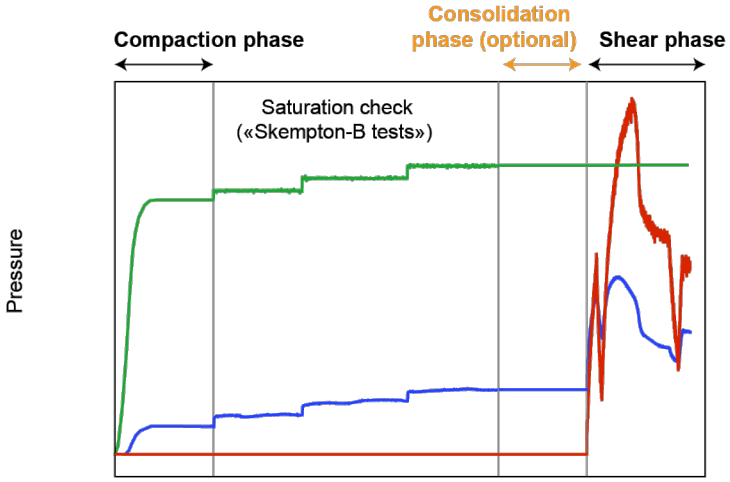

b)

Fig. 4-6: Pressure – time sequence of triaxial deformation tests (specialised protocol)

(a) conventional and (b) alternative testing procedures for undrained boundary conditions during the shear phase.

4.3.3 Triaxial tests in lateral strain-prevented conditions

Specimens for triaxial tests in zero lateral strain conditions are cylindrical, with a diameter (D) to height (H) ratio $D:H = 1$. The nominal dimensions of the specimens are:

- Lab A: $D = 25.0$ mm
- Lab B: $D = 37.0$ mm

The extraction of the specimens was carefully performed in order to minimise water-content loss during the operation. The laboratories used a drilling machine, and hydrocarbons as cooling fluids during the drilling of the specimens, as for the other triaxial samples (Section 4.3.2).

Four tests were conducted in triaxial test apparati, reproducing the zero lateral strain conditions typical of oedometric conditions. 2 tests were conducted by Lab B on Opalinus Clay samples, and 2 tests were conducted by Lab A with core samples from the Villigen Formation and the «Murchisonae-Oolith Formation».

The test consisted of an isochoric saturation phase, followed by 2 load – unload cycles of different amplitudes, performed in zero lateral strain conditions.

The loading was conducted in drained conditions, in axial strain rate control. The radial stress was adjusted continuously by a feedback loop to impose the zero radial strain condition.

During the tests from Lab A, permeability tests were also conducted at a pre-defined stage during the compression. A pressure gradient of 1 to 2 MPa was applied, and the water flow was measured. The stresses and pressure gradient were kept constant during the permeability test until steady-state conditions were achieved. Then, the same pore pressure was applied at the two ends of the specimen, and the load and unload phases were continued in zero lateral strain conditions.

The results allow evaluating the coefficient of earth pressure at rest, K0, defined as the ratio of the minor and the major principal effective stresses under conditions of complete confinement (zero strain) in the direction of the minor principal stress. With reference to the field stress conditions, K0 is the ratio between the horizontal (parallel to the bedding planes) and the vertical (perpendicular to the bedding planes) effective stress.

4.3.4 Permeability tests in oedometric conditioms

Specimens for oedometric testing are of cylindrical shape, with a diameter (D) to height (H) ratio $D:H \geq 2.5$. The nominal dimensions of the specimens are:

- Lab D: $D = 35.0$ mm; $H = 12.5$ mm

The operators cut a pre-defined section of the core with a saw, through the PVC tube to minimise exposure of the geomaterial to the atmosphere. Then, the obtained slice is cut into a smaller piece to be handled within a lathe machine. No air nor water is used during the sawing process. Planarity and parallelism of the bases are verified, and the dimensions of sawn specimens are measured.

The specimen is then put into the oedometric ring, a rigid metallic ring to constrain the radial strains; silicon grease was placed on the internal surface of the ring to reduce the friction between the specimen and the metallic ring.

For 3 tests, Lab D filled the gap between the sample and the ring with bentonite. Bentonite filler was used to avoid water shortcut between the sample and the ring, and it was considered to have a significantly lower permeability then the rock under investigation..

The specimen disks are loaded axially, and deformation is recorded with time.

Specimens are resaturated within the apparatus in isochoric conditions. The axial deformations are kept constant by increasing the axial stress. Pore pressure is applied from the bottom side of the specimen at 50 kPa. When the swelling pressure generated by saturation at isochoric conditions stabilises, pore pressure equal to 50 kPa is applied at the top side of the specimen. Displacements are monitored throughout this stage of the test. Once the axial stress has stabilised, the mechanical loading phase of the test can start. Load to the target stress level is applied.

A constant-head permeability test (PERM) is performed at this stage, increasing the pore pressure at the bottom side and measuring the fluid flow through the specimen. The axial stress and pressure gradient are kept constant during the permeability test until steady-state conditions are achieved.

After completion of the test, the oedometer cell is dismantled, and the specimen is dried in the oven to measure the water content (oven-drying at 105 °C for several days until constant weight).

4.4 Lithostratigraphy and test overview

4.4.1 Lithostratigraphy of tested core material

A brief summary is provided here on lithological characteristics of the formations of which cores were used in geomechanical testing. Further details on lithology can be found in Dossier III ('TBO Stadel-2-1: Lithostratigraphy').

- **«Felsenkalke» + «Massenkalk»**: Bedded (Felsenkalke) to poorly or non-bedded limestones (Massenkalk).
- **Schwarzbach Formation**: Calcareous to argillaceous marls.
- **Villigen Formation**: Thick-bedded limestone.
- **Wildegg Formation**: Calcareous marl with interlayers of limestone.
- **«Murchisonae-Oolith Formation»**: A very heterogeneous succession of siltstone, argillaceous marl to claystone and limestone beds. The tested interval (796 m) is an iron-oolitic, reddish-brown, cross-bedded bioclastic limestone.
- **Opalinus Clay**: Silty claystone with silty to sandy lenses. The following subdivision was specified:
  - **799.67 – 823.50 m** **Subunit 1**: **«Sub-unit with silty calcareous beds» (23.83 m)**: Claystone to silty claystone with discrete heterogeneities, in particular silty calcareous beds and nodules.
  - **823.50 – 839.72 m** **Subunit 2**: **«Upper silty sub-unit» (16.22 m)**: Claystone to silty claystone with frequent lenses, typically centimetres wide and several millimetres thick (flaser structure).
  - **839.72 – 886.97 m** **Subunit 3**: **«Mixed clay-silt-carbonate sub-unit» (47.25 m)**: Silty claystone, devoid of marked characteristics typical for the other subunits.
  - **886.97 – 905.20 m** **Subunit 4**: **«Clay-rich sub-unit» (18.23 m)**: Homogeneous claystone with high clay-mineral content (mostly > 60 wt.-%).
- **Klettgau Formation**: Heterogeneous succession dominated by playa sediments with mostly silty claystone and dolocretes. The tested interval for PERM tests (965 m) is from the Ergolz Member.
- **Bänkerjoch Formation**: Succession of anhydrite, dolomitic marl, dolostone and sandstone. Both tested samples are anhydrites, with the one from 986 m characterised as chicken wire texture (anhydrite as nodules in argillaceous matrix).
- **Schinznach Formation**: Succession of dolomites and dolostones, partly dolomitised limestones and micritic limestones, and bituminous claystones.
- **Kaiseraugst Formation**: Succession of claystone to marly, partly bituminous and dolomitic marl, with interbeds of limestone, dolostone and sandstone.

- **Weitenau Formation**: Siliciclastic pre-Mesozoic sediments. Mostly matrix-supported breccia, with matrix of siltstone and claystone and larger sub-rounded components of granite and gneiss. Fanglomerates consisting of crystalline basement components.

4.4.2 Test overview

A total of 69 rock-mechanical and geomechanical tests were conducted on a total of 20 cores from borehole STA2-1 (Tab. 4-2). The number of tests in the geomechanical testing programme is smaller than in the rock-mechanical testing programme. However, typical testing times in the geomechanical programme were 12 to 30 days for TRX+ tests. This is one order of magnitude longer than the typical TRX test in the rock-mechanical testing programme.

Cores without proper initial conditioning (PVC = 0 in Tab. 4-2) were generally only used for lithologies not sensitive to water exchange, i.e. without any macroscopic indication of damage at the time of sampling in the storage facility.

Tab. 4-2: Overview of performed tests

The red border illustrates the clay-mineral rich interval of Opalinus Clay (focus of geo-mechanical testing programme). PVC indicates whether cores were conditioned in resin and core barrel on site (1) or later wrapped in aluminium foil off-site (0). TRX = triaxial test, UCS = unconfined compressive strength test, FT= fracture toughness, TRX+ = TRX with specialised protocols, PERM = constant-head permeability tests, K0 = zero leteral strain conditions.

Core-ID	**Formation**	**Top**	**Length**	**Bottom**		**Rock-mechanical testing programme**			**Geomechanical testing programme**		
						Standard rock-mechanical tests			**Special protocols**		**Other**
STA2-1		[m]	[cm]	[m]	**PVC**	**TRX**	**UCS**	**FT**	**TRX+**	**PERM**	**K0**
484.16/40-GM	«Felsenkalke» + «Massenkalk»	484.16	40	484.56	1		3				
561.28/40-GM	Schwarzbach	561.28	40	561.68	1	1	2				
596.14/50-GM	Villigen	596.14	50	596.64	1	2	2				
626.41/35-GM		626.41	35	626.76	1	1				1	1
679.25/50-GM	Wildegg	679.25	50	679.75	1			11			
701.18/50-GM		701.18	50	701.68	1		2				
795.80/40-GM	«Murchisonae-Oolith»	795.80	40	796.20	1	3				1	1
814.52/40-GM	Opalinus Clay	814.52	40	814.92	1						1
842.52/40-GM		842.52	40	842.92	1				8		
845.28/45-GM		845.28	45	845.73	1						1
861.81/44-GM		861.81	44	862.25	1			6			
896.99/50-GM		896.99	50	897.49	1				1		
903.62/49-GM		903.62	49	904.11	1				1		
960.94/34-GM	Klettgau	960.94	34	961.28	1		2				
965.15/50-GM		965.15	50	965.65	0					5	
985.98/45-GM	Bänkerjoch	985.98	45	986.43	1	2	2				
1073.70/36-GM	Schinznach	1'073.70	36	1'074.06	1		2				
1108.70/40-GM		1'108.70	40	1'109.10	1	1	2				
1220.14/37-GM	Kaiseraugst	1'220.14	37	1'220.51	1		2				
1273.20/50-GM	Weitenau	1'273.20	50	1'273.70	1		2				
Total					**19**	**10**	**21**	**17**	**10**	**7**	**4**

5 Rock-mechanical testing

5.1 Fracture toughness

With the SCB method, the fracture toughness is obtained from the peak load P_{max} recorded during the test:

$$K_{Ic} = P_{max} \frac{\sqrt{\pi a}}{2\,R\,B} Y' \tag{5-1}$$

Y' is a dimensionless factor which depends on the distance between the two supports (s). It is defined as:

$$Y' = -1.297 + 9.516\left(\frac{s}{2R}\right) - \left(0.47 + 16.457\,\frac{s}{2R}\right)\beta + \left(1.071 + 34.401\frac{s}{2R}\right)\beta^2 \tag{5-2}$$

with $\beta = a/R$.

With the MR method, crack length was inverted from a theoretical compliance curve (Saxena & Hudak 1978) obtained in finite element simulations. If the crack length is accurate, K_{Ic} is computed from those simulations where crack propagation is stable.

Typical test results for both methods are illustrated in Fig. 5-1.

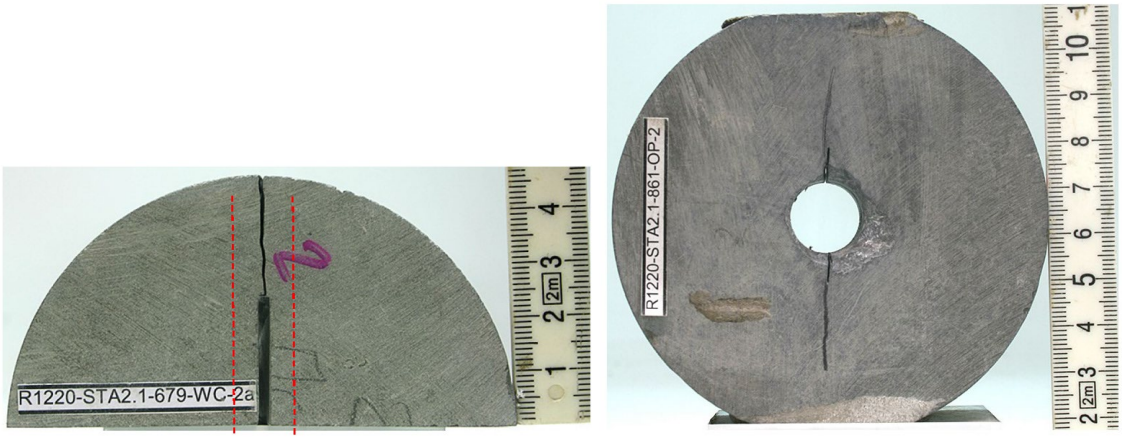

Fig. 5-1: Example of test specimens after testing

Left: SCB test method, with red line showing the field of valid fracture propagation. Right: MR test method (cracks highlighted with a pencil line).

To compare the results of different methods, both SCB and MR testing methods were applied to a core interval in the Wildegg Formation. For Opalinus Clay, only the MR method was applied, as it is considered to yield a more stable crack growth (Tab. 5-1).

Tab. 5-1: Test results of conducted fracture tougness tests

Last column depicts standard deviation.

Testing method	**Formation**	**Number of tests**	**Depth range** [m]	**K_{Ic}** [MPa.m$^{1/2}$]	**σ** [MPa.m$^{1/2}$]
SCB	Wildegg	6	679 – 680	0.51	0.13
MR	Wildegg	5	679 – 680	0.33	0.04
MR	Opalinus Clay	3	861 – 862	0.24	0.05

5.2 Unconfined compressive strength tests (UCS)

A total of 21 UCS tests were performed by two laboratories (Tab. 5-2). Photographs of the specimens before and after testing can be found in Appendix A.

At the linear portion of the axial load cycle, an unloading/reloading cycle was performed by reducing the axial stress to 1/3 of the actual load, and hysteresis was observed. The cycle was performed for determining the elastic properties of the rock. The Young's modulus E (in GPa) was determined as an average reload modulus using the slope of the rising portion of the hysteresis as the ratio between the axial load change $\Delta\sigma_a$ (in MPa) and the induced axial strain $\Delta\varepsilon_a$ (dimensionless) according to the equation:

$$E = \frac{\Delta\sigma_a}{\Delta\varepsilon_a} \tag{5-3}$$

The Poisson's ratio (ν) is calculated as the negative ratio between the delta in radial $\Delta\varepsilon_r$ and axial strain $\Delta\varepsilon_a$:

$$\nu = -\frac{\Delta\varepsilon_r}{\Delta\varepsilon_a} \tag{5-4}$$

An example of calculation of tangent E modulus is reported in Fig. 5-2.

Following the hysteresis, the axial load was again increased until peak strength was reached, and the specimen was allowed to fail. The compressive peak strength was derived from the peak value of the axial load.

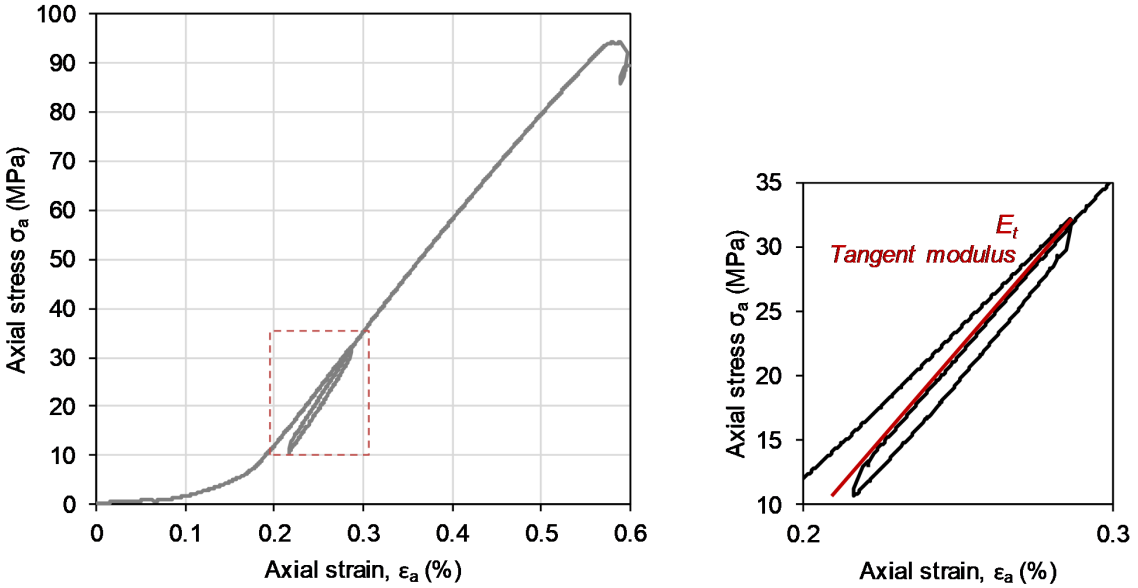

Fig. 5-2: Stress – strain diagram for UCS test

On the right zoom into the unloading/reloading loop, and the definition of tangent and secant Young's moduli. Example from test BUL1-1_661UCS_S1 (Crisci et al. 2021a).

Tab. 5-2: Test results from UCS tests

Young's modulus refers to E_{50}. For specimen geometry see Fig. 4-1.

Test-ID STA2-1	**Specimen geometry**	**Average depth**	**Bulk density**	**Water content**	**Young's modulus**	**Poisson's ratio**	**Peak strength**	**Strain at peak strength**
		[m]	[g/cm^3]	[wt.-%]	[GPa]	[-]	[MPa]	[%]
484UCS_S2	S	484.34	2.689	0.14	12.64	0.06	107.20	0.58
484UCS_S3	S	484.52	2.701	0.20	24.58	0.08	122.05	0.67
484UCS_S4	S	484.21	2.704	0.20	35.78	0.18	98.50	0.39
561UCS_S1	S	561.32	2.591	2.65	14.75	0.22	62.30	0.78
561UCS_S2	S	561.55	2.628	1.86	20.29	0.19	83.35	0.66
596UCS_S2	S	596.58	2.671	0.47	30.77	0.15	146.58	0.53
596UCS_S1	S	596.18	2.678	0.51	33.92	0.18	117.39	0.49
701UCS_S1	S	701.22	2.596	2.89	13.57	0.22	67.88	0.91
701UCS_S2	S	701.56	2.570	3.34	8.97	0.18	37.93	0.95
961UCS_S1	S	961.04	2.559	4.43	23.20	0.09	58.75	0.50
961UCS_S2	S	961.25	2.749	2.65	25.12	0.13	118.46	0.58
986UCS_S1	S	986.07	2.806	1.23	27.41	0.10	72.50	0.43
986UCS_S2	S	986.34	2.753	1.46	31.98	0.19	178.22	0.68
1073UCS_S1	S	1'073.73	2.571	4.85	21.09	0.16	99.08	0.71
1074UCS_S2	S	1'074.03	2.473	6.39	15.98	0.15	63.67	0.63
1108UCS_S1	S	1'108.75	2.685	1.06	31.17	0.15	151.37	0.51
1109UCS_S2	S	1'109.06	2.719	0.75	27.39	0.15	197.84	0.73
1220UCS_S1	S	1'220.18	2.597	3.60	7.33	0.15	26.57	0.73
1220UCS_S2	S	1'220.45	2.630	2.89	9.61	0.16	33.68	0.59
1273UCS_S1	S	1'273.24	2.538	2.31	13.49	0.16	35.29	0.55
1273UCS_S2	S	1'273.60	2.558	2.03	14.51	0.12	45.31	0.58

The relatively large lithologic variability of tested specimens is reflected by the test results, ranging just over one order of magnitude both for Young's moduli and strength.

5.3 Triaxial deformation tests

A total of 10 triaxial tests were performed. Photographs of the specimens before and after testing can be found in Appendix A.

Basic properties and test conditions are provided in Tab. 5-3. The water content reported refers to the final, post-test measurement.

Skempton's B values were constrained in 3 tests[7].

Ultrasonic velocities were recorded throughout the tests, and the tabulated values in Tab. 5-3 were constrained at the start of the shear phase.

Triaxial test results from the shear phase are provided in Tab. 5-4.

[7] The tabulated values in Tab. 5-3 are not corrected for potential equipment compliance.

Tab. 5-3: Basic properties and triaxial test results from consolidation and saturation stage
For specimen geometry see Fig. 4-1.

Test-ID	**Specimen geometry**	**Average depth**	**Bulk density**	**Water content**	**Pore pressure**	**Confining pressure**	**Consolidation coefficient**	**Skempton's B**	**P-wave velocity**	**S-wave velocity**
		[m]	[g/cm^3]	[wt.-%]	[MPa]	[MPa]	[mm^2/s]	[-]	[m/s]	[m/s]
561TRX_S1	S	561.32	2.59	8.34	7.2	22	-	-	4'076	2'142
596TRX_S1	S	596.18	2.68	1.37	5.0	15.0	-	-	5'982	3'151
596TRX_S3	S	596.58	2.67	1.22	5.0	15.0	-	-	5'917	3'084
TRX8_626_56	S	626.56	2.66	1.12	8.0	15.0	0.002	-	6'246	2'306
TRX9_796_13	S	796.13	2.67	7.08	5.0	10.0	-	0.85	4'047	2'021
TRX10_796_13	S	796.13	2.68	7.30	5.0	15.0	0.03	0.77	4'132	2'159
TRX11_796_13	S	796.13	2.67	7.05	5.0	20.0	-	0.80	4'190	2'086
986TRX_S1	S	986.07	2.80	2.14	5.0	15.0	-	-	5'240	2'818
986TRX_S2	S	986.34	2.74	2.65	5.0	15	-	-	5'294	2'891
1108TRX_S1	S	1'108.75	2.66	2.41	5.0	15	-	-	5'819	3'073

Tab. 5-4: Triaxial test results from the shear phase

Test-ID	**Stress path**	**Strain Rate**	**Young's modulus**	**Poisson's ratio**	**Deviatoric stress at peak ($q = \sigma 1 - \sigma 3$)**	**Radial total stress at peak ($\sigma 3$)**	**Pore pressure at peak**	**Axial strain at peak**	**Post-peak q**	**Pore pressure at post-peak**
		[1/s]	[GPa]	[-]	[MPa]	[MPa]	MPa]	[%]	[MPa]	[MPa]
561TRX_S1	CTCU	1E-06	14.6	0.33	56.7	22	10.8	0.9	54.5	10.7
596TRX_S1	CTCU	1E-06	37.0	0.26	282.4	15	8.0	1.0	92.3	0.5
596TRX_S3	CTCU	1E-06	33.8	0.25	202.0	15	9.6	0.8	66.9	0.5
TRX8_626_56	CTCU	5E-07	48.4	0.30	228.3	15	0.7	0.9	102.0	0.0
TRX9_796_13	CTCU	2E-07	10.8	0.39	40.0	10	5.4	0.4	26.0	1.2
TRX10_796_13	CTCU	2E-07	20.6	0.28	47.1	15	7.4	0.6	35.7	2.9
TRX11_796_13	CTCU	2E-07	10.1	0.22	50.6	20	8.7	0.8	40.9	4.2
986TRX_S1	CTCU	1E-06	23.3	0.15	75.5	15	9.2	0.8	47.7	2.8
986TRX_S2	CTCU	1E-06	27.3	0.32	180.9	15	7.4	1.1	88.7	0.5
1108TRX_S1	CTCU	1E-06	34.3	0.24	219.4	15	0.6	0.9	76.7	0.5

6 Geomechanical testing programme

In the STA2-1 geomechanical testing campaign, 10 triaxial tests were performed with specialised protocols. Two geometries (Section 5.1) were selected: S- and P-samples.

Four lateral strain prevented tests (K0) were conducted in triaxial apparati (including 2 constant-head permeability tests).

Five constant head permeability tests were conducted in one-dimensional conditions.

In the following sections, the test results of the experimental campaign are presented. First, the main geotechnical and intrinsic properties are reported (Section 6.1). Then, in Sections 6.2 and 6.3, the results of triaxial tests and lateral strain prevented tests in triaxial conditions are reported. Section 6.4 reports the results of the constant-head permeabilty tests.

6.1 Geotechnical and intrinsic properties of tested cores

6.1.1 Water content and Native activity

The laboratories involved in the testing campaign also determined basic properties of the tested specimens. The water content of the specimens before and after testing was determined, and the results are reported in Fig. 6-1.

For the triaxial tests, the first phase of each test consisted in imposing saturated conditions on the specimen by injecting water in isochoric conditions and measuring the generated swelling pressure (conventional testing procedure).

The water content before and after the tests generally differs, and in the case of undrained boundary conditions, the difference may primarily be attributed to resaturation in the rig. Additional sources of discrepancy between the water content before and after the tests can be attributed to the handling of the specimen when dismantling the tests (e.g. loss of solid mass while removing the specimen from the sleeve, drained unloading phases which allow further swelling and water content increase).

The water content and the Native activity of the material were also measured on trimming pieces from a part of the section from which testing specimens were extracted. The Native activity of a specimen corresponds to the value of relative humidity in equilibrium with the specimen's native state, with no variation of the initial water content[8].

The measurements were done by placing a piece of freshly cut material within a closed container and measuring the resulting (relative) humidity generated within the container (Ewy 2015) by the use of a psychrometer.

Resutls are reported in Fig. 6-2. All cores exhibit high Native activity, above 70%, indicating excellent preservation conditions.

[8] In a specimen in contact with controlled relative humidity, if water content increases, then that relative humidity value is greater than the Native activity value of the shale. Conversely, if there is a water content decrease, then that relative humidity value is less than the Native activity.

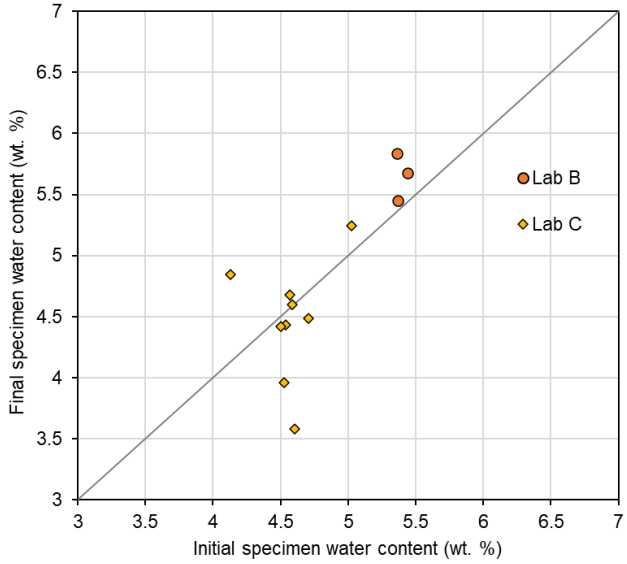

Fig. 6-1: Initial (at test) versus final water content of specimens in triaxial tests (Opalinus Clay)

Results grouped by laboratory.

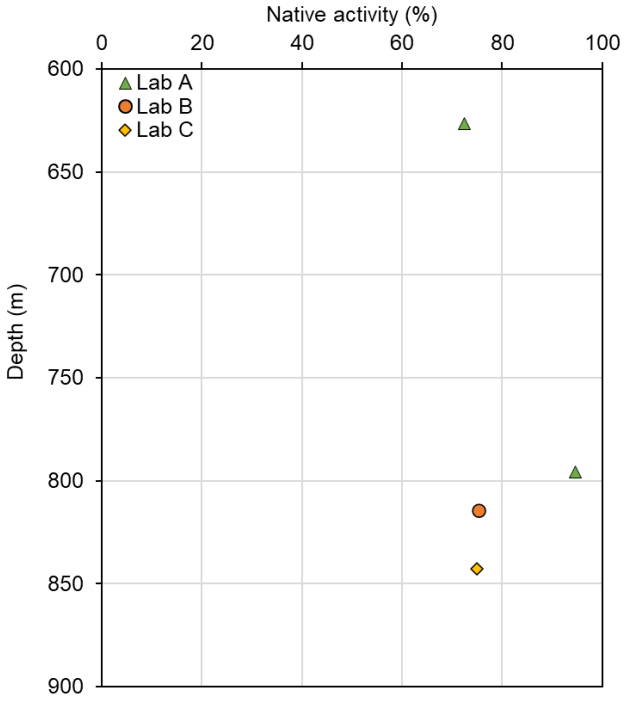

Fig. 6-2: Native activity of trimming material versus depth of collection

Results grouped by laboratory.

6.2 Triaxial deformation tests with specialised protocols

An overview of the performed tests is presented in Tab. 6-1. Each test is labelled with an ID indicating the main features of the test.

For example, the triaxial test ID B1_STA2_1_897_04P7CTCU indicates the laboratory that performed the test (B), a testing sequential number (1), the borehole name (STA2-1), the specimen depth (897.04 m), the specimen geometry (P), effective confinement before shearing (7 MPa), the stress path (CTCU).

It is reported in Tab. 6-1 for each tested specimen:

- Specimen ID, as described above
- Core depth [m]
- Geological formation, as presented in Section 4.4.1
- Specimen geometry
- Total confining stress, p_0 [MPa] at the beginning of the shearing phase
- Pore pressure [MPa] at the beginning of the shearing phase
- Effective confining stress p'_0 [MPa] at the beginning of the shearing phase
- Stress path, as presented in Fig. 4-5
- Indication of shearing in drained conditions (*d*)
- Initial void ratio, computed using a reference solid density[9] of 2.70 g/cm^3
- Initial porosity, computed using a reference solid density of 2.70 g/cm^3
- Initial and final water content.

The initial part of the ID (hereafter Specimen ID), including the laboratory and the sequential number is afterwards used as short code to quickly identify a specific test point in the entire set of results.

[9] Solid density measurements were conducted on specimens used for mineralogical analysis and are available in Appendix D.

Tab. 6-1: Conducted triaxial tests

Specimen ID, shearing phase characteristics, specimen initial (and final) conditions.

Specimen ID	**Specimen location and geometry**			**Shearing phase characteristics**				**Specimen initial conditions**			**Final water content, wf [%]**
	Core depth [m]	**Formation**	**Specimen geometry**	**Total confining stress, p_0** [Mpa]	**Pore pressure, u_{w0}** [MPa]	**Effective confining stress p'_0** [MPa]	**Stress path**	**Initial void ratio, e_0** [-]	**Initial porosity, n_0** [-]	**Initial water content, w_0** [%]	
C6_STA2_1_842_62P13CTCU	842.625	Opalinus Clay	P	22	9	13	CTCU	0.121	0.108	4.71	4.48
C7_STA2_1_842_62P8CTCU	842.625		P	17	9	8	CTCU	0.112	0.101	4.54	4.44
C8_STA2_1_842_63P11TC	842.625		P	20	9	11	TC	0.120	0.107	4.61	3.58
C9_STA2_1_842_63P8TC	842.625		P	17	9	8	TC	0.111	0.100	4.13	4.85
C2_STA2_1_842_63S7CTCU	842.625		S	16	9	7	CTCU	0.120	0.107	4.57	4.68
C3_STA2_1_842_62S13CTCU	842.625		S	22	9	13	CTCU	0.127	0.113	4.53	3.96
C4_STA2_1_842_63S20CTCU	842.625		S	29	9	20	CTCU	0.121	0.108	4.50	4.42
C5_STA2_1_842_63S18CTCU	842.625		S	29	11	18	CTCU	0.120	0.107	4.59	4.60
B1_STA2_1_897_04P7CTCU	897.035		P	16	9	7	CTCU	0.119	0.107	5.36	5.45
C1_STA2_1_903_67P7CTCU	903.665		P	16	9	7	CTCU	0.137	0.120	5.03	5.24

6.2.1 Saturation and consolidation phase

6.2.1.1 Swelling pressure

In the conventional triaxial procedure and in the K0 tests, the specimen saturation was conducted imposing isochoric conditions and monitoring the evolution of the axial and radial stress. The effective stress reached at the end of the saturation phase is called swelling pressure, and the results (grouped by S- and P-geometries, respectively) are reported in Fig. 6-3 versus the specimen initial water content (before saturation).

For specimens with S-geometry, the radial direction corresponds to the one of the bedding, while the axial direction is perpendicular to it. Swelling pressure was found to be higher in the axial direction.

On the other hand, in P-samples, the axial direction corresponds to the bedding direction, while the radial stress is obtained by maintaining close to zero the average of the deformation in the two radial directions, perpendicular and parallel to bedding.

It has to be noted that the experimental configuration adopted by Lab B, does not allow to sustain a confining pressure higher than the axial pressure. In STA2-1 saturation tests, P-samples showed a tendency of the confining pressure to rise above the axial pressure. Hence, the axial pressure was adjusted to the confining value, and the two values coincide in Fig. 6-3.

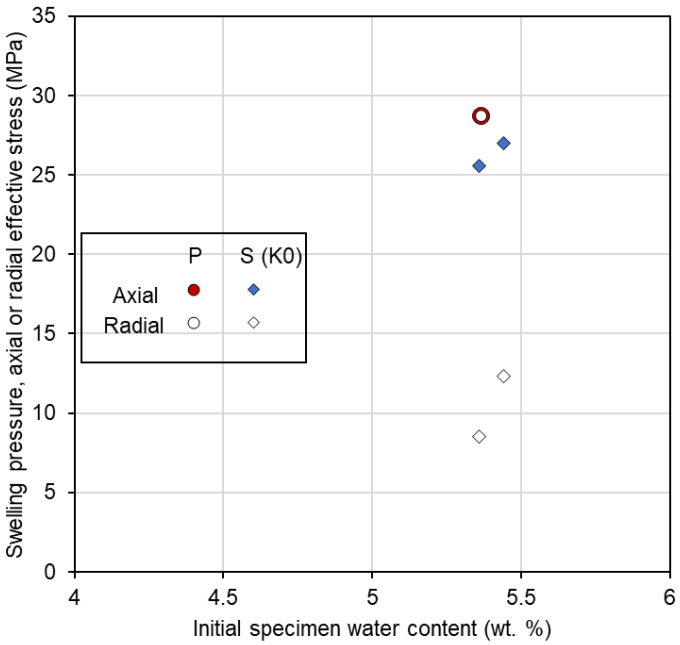

Fig. 6-3: Radial and axial swelling pressure versus initial specimen water content

S-samples (from K0 tests) and P-samples (triaxial tests).

6.2.1.2 B check tests

In each test, the specimen saturation was verified by performing Skempton's B checks. B values were computed over multiple steps. If the difference in B values among the steps was less than 10%, the average of the measurements was considered as the B coefficient and associated with the average effective confinement level at which B segments were performed. The values are reported in Fig. 6-4 for all results.

The compressibility of the apparatus can affect the accuracy of the measured B values. Wissa (1969) proposed a correction to the B value to consider the compressibility of the dead volume of water (i.e., the water in the drainage system) and the compressibility of the system (tubes and transducers). However, several researchers (e.g. Ghabezloo & Sulem 2010) show that the compressibility of modern types of steel tubes and transducers has a negligible impact on the B measurements compared to the dead water volume impact. Therefore, the results of the testing campaign have been analysed considering the dead water volume in each apparatus, and B values results ($B_{correct}$) were computed as (Wissa 1969, Favero et al. 2018):

$$B_{correct} = \frac{1}{\frac{1}{B_{obs}} - \frac{V_L}{V}\frac{K}{K_f\left(1-\frac{K}{K_s}\right)}} \tag{6-1}$$

where B_{obs} is the measured B value, V_L is the volume of fluid in the porewater lines, V is the volume of the specimen, K is the bulk modulus of the specimen, K_f the bulk modulus of the pore fluid and K_s the bulk modulus of the solid phase. Bulk and solid moduli K = 6 MPa and Ks = 50 MPa were considered for the corrections. The correction was applied for results of Lab B. It has to be noted that the dead volume in the apparatus from Lab B is ~ 700 mm^3. The results for the measured and corrected B values are reported in Fig. 6-4. An average value of 0.77 was calculated and marked as a dotted line in the graph.

During tests C4, C7 and C8 temperature fluctuation caused oscillation in the pore water pressure. B values for those tests are not reported.

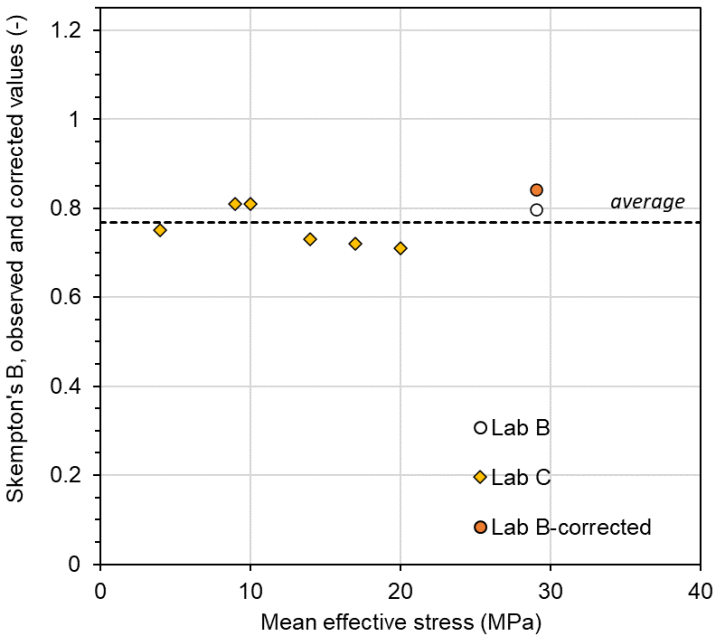

Fig. 6-4: Average Skempton's B values

B values versus the corresponding effective mean stress; data from STA2-1 (Opalinus Clay): Observed and corrected values accounting for dead water volume.

6.2.1.3 Consolidation phase

Drained consolidation phases were performed to achieve the target effective confining stress for shearing, and allow for determining the consolidation coefficient, according to Head (1998). The time to consolidate was obtained applying the square root of time method in the evaluation of the evolution of the volumetric strain. It is noted that the method refers to an instantaneous loading of the sample. In tests adopting the conventional method, the stress level at the end of saturation is higher than the target value for shearing, hence an unloading (with consequent swelling of the sample) was performed. Performing quasi-instantaneous loading or unloading is challenging, given the stress levels involved, and often a ramp of several hours needs to be used. Therefore, the consolidation coefficient obtained from these results may be underestimated. It is further noted that the values were obtained by considering the time to consolidate excluding the time required to load.

The obtained values for specimens of Opalinus Clay are reported in Fig. 6-5 versus the mean effective stress at the end of the consolidation phase.

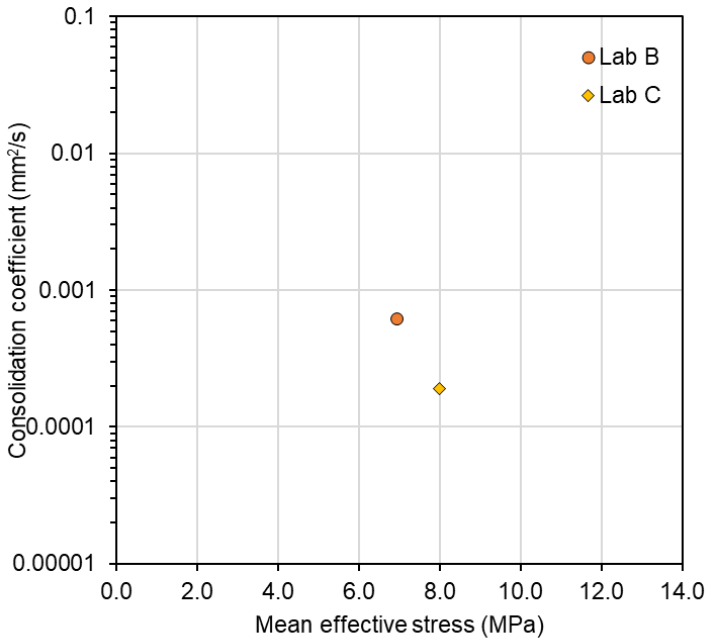

Fig. 6-5: Consolidation coefficient for Opalinus Clay specimens (all geometries)

6.2.2 Shearing phase

This section provides the results of the shearing phase of tests. The stress paths are reported in the $q - p'$ plane, where q is the deviatoric stress (Eq. 4-2) and p' is the mean effective stress, obtained by subtracting the porewater pressure u_w from the total stress (Eq. 4-1).

6.2.2.1 Stress paths of Opalinus Clay subunits

This section focuses on the stress paths obtained on Opalinus Clay specimens during the shearing phase of the tests. The behaviour of the tested specimens is characterised by a pronounced non-linearity before the peak stress and softening response after the peak. A similar evolution of the deviatoric stress (q) and porewater pressure (u_w) with the axial effective strain is observed among the tests (see Appendix B). The effective stress paths obtained on Opalinus Clay specimens are here grouped by the lithological sub-units (Fig. 6-6), as presented in Section 4.4.1.

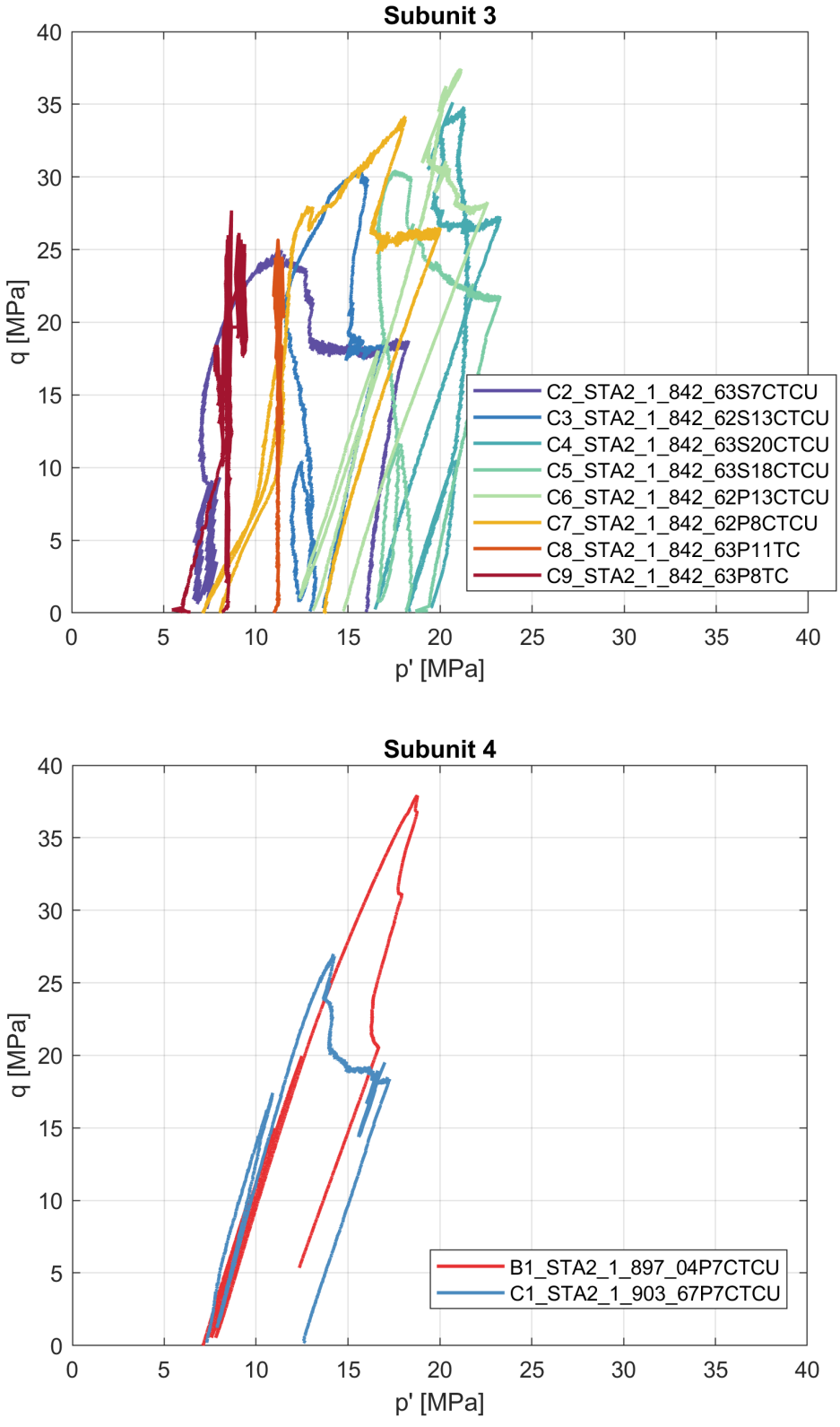

Fig. 6-6: Effective stress paths of tested specimens grouped by the lithological (sub-)unit

6.2.2.2 Elastic phase

The analysis of the elastic parameters for Opalinus Clay samples is presented in this section. Unloading/reloading cycles were performed to estimate the elastic response of the material during an unloading phase. As requested in the testing procedure, the cycles were carried out during the shearing of the specimens before the achievement of the peak stress.

During unloading and reloading, shales present a hysteretic and non-linear behaviour. Depending on the strain amplitude of the unloading/reloading loop, the secant moduli may vary considerably. The strains are calculated as the ratio of the variation in height (or diameter) to the initial height (or diameter). To eliminate the dependency of the moduli on the amplitude of the unloading loop, the elastic modulus for all analysed tests was computed as the secant modulus during unloading for a pre-fixed strain range, 0.02 – 0.04% from the beginning of the unloading phase (Fig. 6-7). The strain calculation refers to the initial specimen height. The strain amplitude was selected as common to all the analysed test results.

Small-strain moduli were also evaluated from the stress cycles (Fig. 6-7) according to the procedure presented in Giger et al. (2018). An example of elastic moduli evaluation is reported in Fig. 6-7, with reference to test BUL1_1_950_62S9CTCU_B (BUL1-1 testing campaign; Crisci et al. 2021a). The top graph in Fig. 6-7 shows the evolution of the secant moduli with the axial strain range used for their computation, for the unloading phase. A clear non-linear decrease of the modulus is observed with the axial strain, which reflects the non-linearity of the material's response. This feature highlights the importance of the axial strain range adopted to perform unloading/reloading cycles. Different ranges lead to different moduli, making a comparison among the tests difficult and misleading. Generally, larger strain ranges lead to lower moduli (Minardi et al. 2019).

A summary plot comparing small strain moduli and secant moduli is provided in Fig. 6-8. It is highlighted that small strain moduli are always higher than the secant moduli computed over the common strain range. Secant moduli from P- and S-samples are provided in Fig. 6-9, sorted by specimen final water content. In the case of P-tests, generally higher values of the undrained elastic moduli with respect to S-tests are observed.

In terms of radial response, the relationship between axial and radial deformations during the unloading phase of the cycles performed before the achievement of the peak stress was used $(-\Delta\varepsilon_r/\Delta\varepsilon_a)$ for the assessment of the undrained equivalent of the drained Poisson's ratio (ν). In the undrained conditions, deviations from the theoretical value of 0.5, typically obtained from the linear isotropic elasticity, are due to the anisotropic features of the material and possible poro-elastic effects. The computed parameters for the drained and undrained unloading loops are reported in Fig. 6-10 (also, Appendix E), divided by specimen geometry (S and P) and along with the corresponding elastic moduli.

For P-samples, usually the radial sensors detect the anisotropic response, with higher deformation in the direction perpendicular, compared to the direction parallel to the bedding plane. As a consequence, the Poisson's ratios computed using the strain perpendicular to bedding are higher than those parallel to bedding.

Ultrasonic velocities of P (Vp) and S (Vs) waves were also measured by Lab B and Lab C. Both laboratories measured the velocity of P and S waves in the axial direction (Vp and Vs).

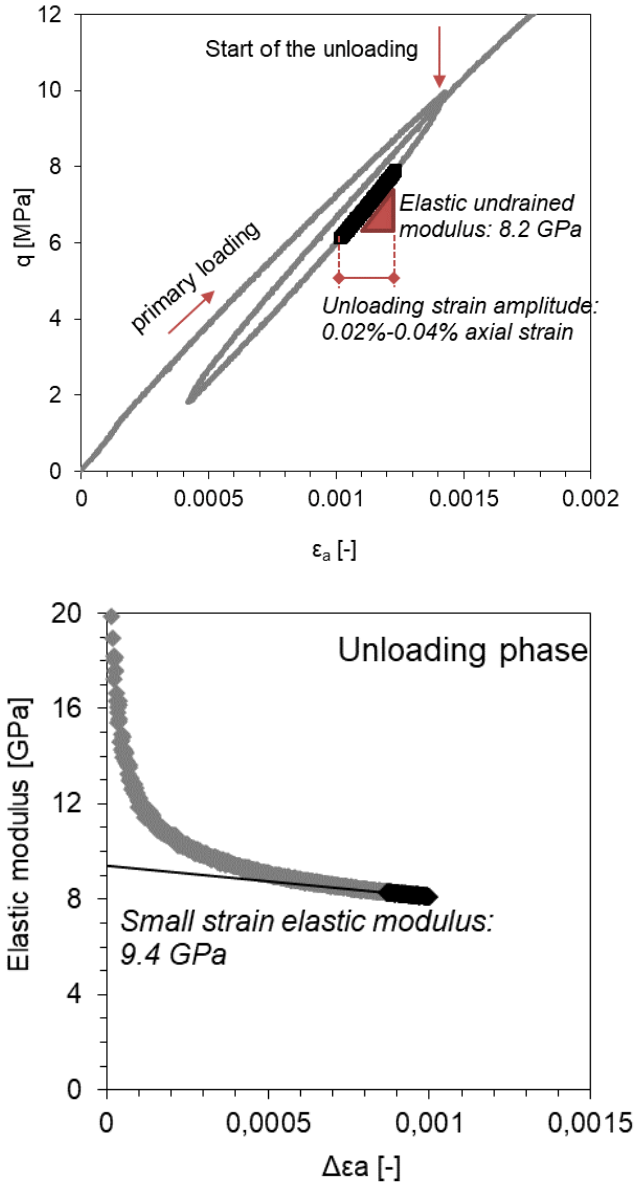

Fig. 6-7: Unloading/reloading cycle and small strain elastic modulus in triaxial tests

Determination of the elastic undrained moduli (E_u) during the unloading phase, for a pre-determined strain amplitude (top); small strain elastic modulus obtained on the unloading phase (bottom) (test BUL1_1_950_62S9CTCU_B; Crisci et al. 2021a).

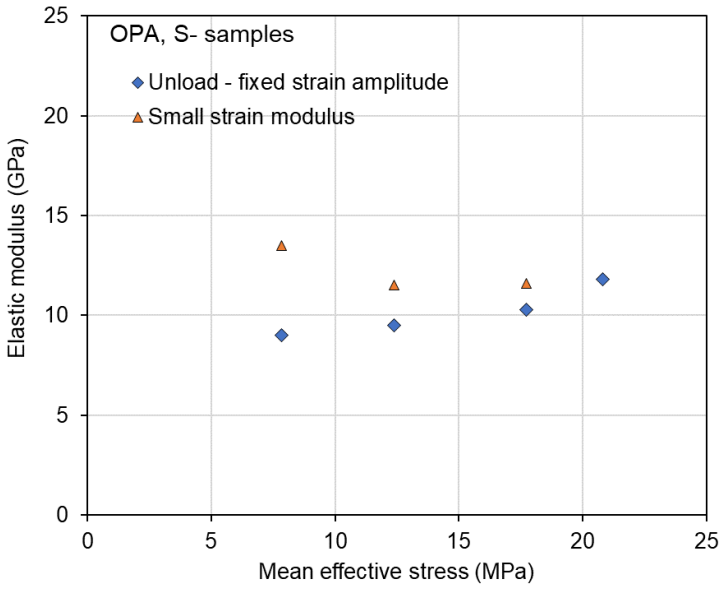

Fig. 6-8: Elastic undrained moduli calculated over an unloading (UL) path: modulus of a fixed strain interval and small strain extrapolation (S-samples)

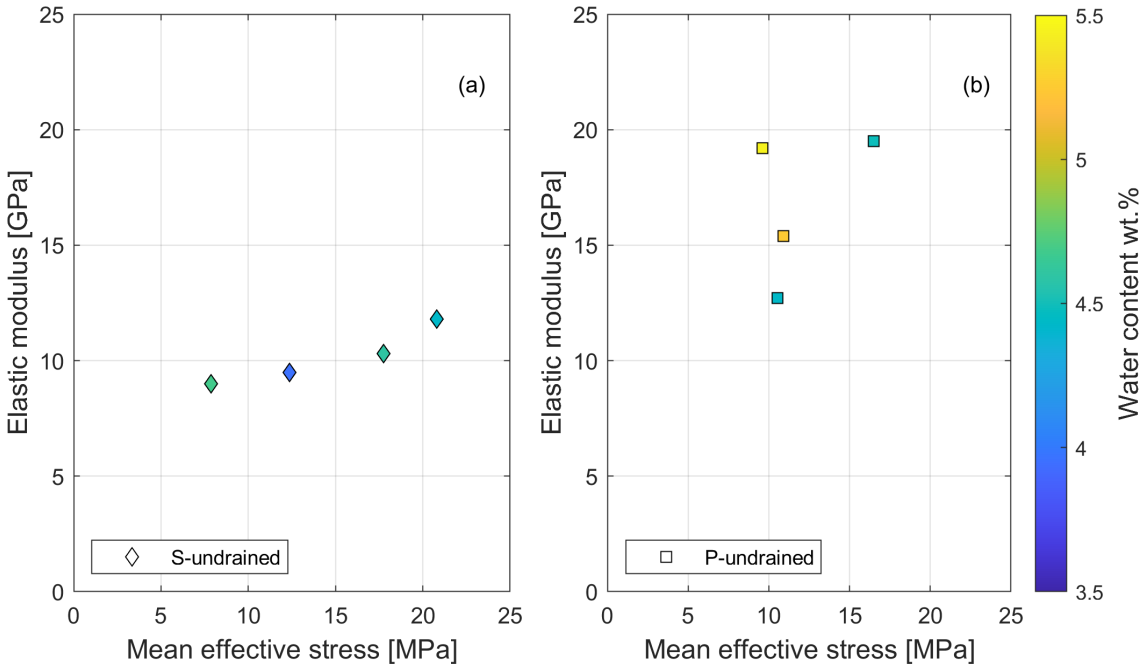

Fig. 6-9: Elastic undrained moduli, sorted by specimen final water content

Moduli are calculated over a fixed strain interval during an unloading (UL) path: P- and S-geometries, sorted by water content at the end of the test (final).

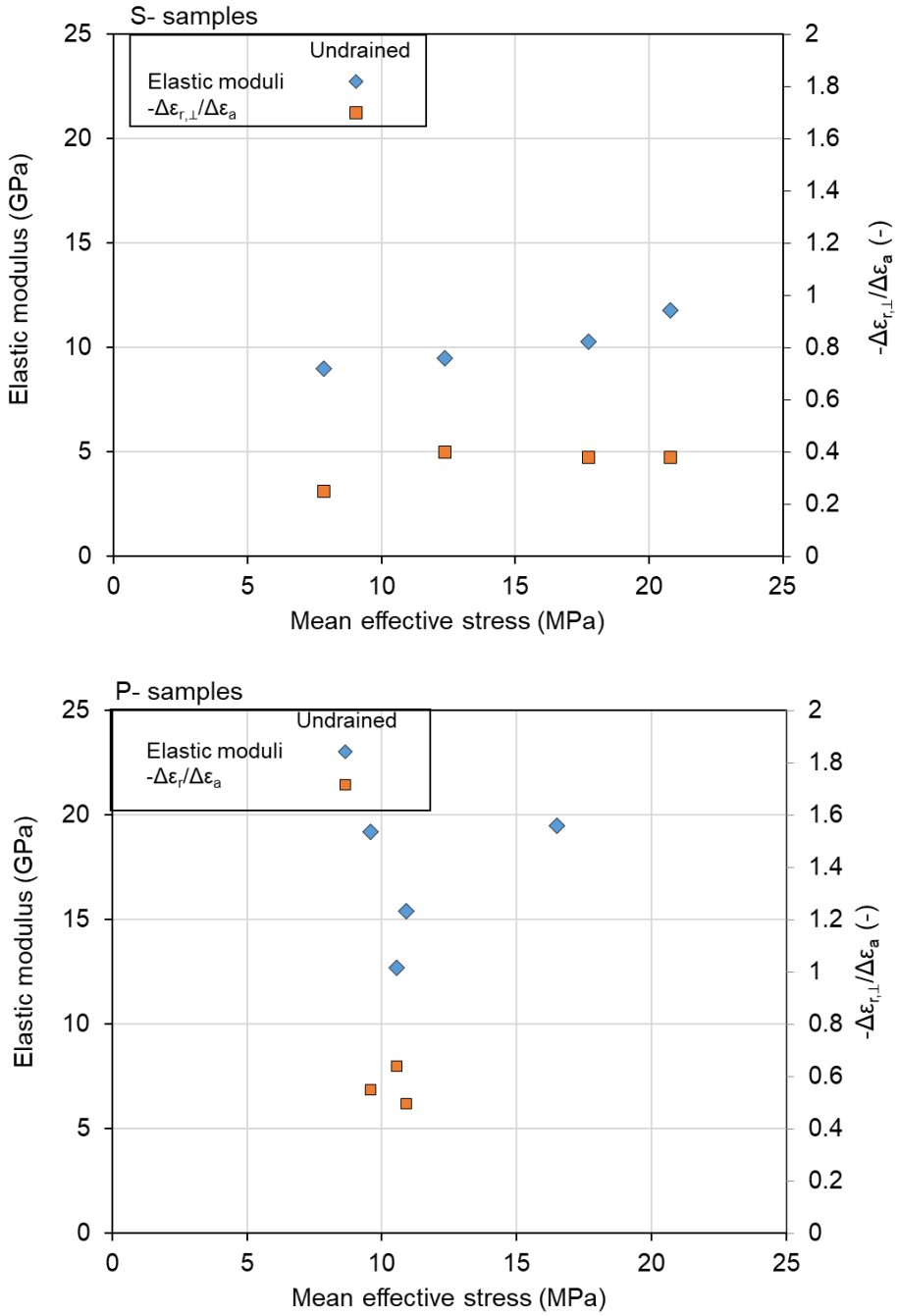

Fig. 6-10: Elastic undrained properties

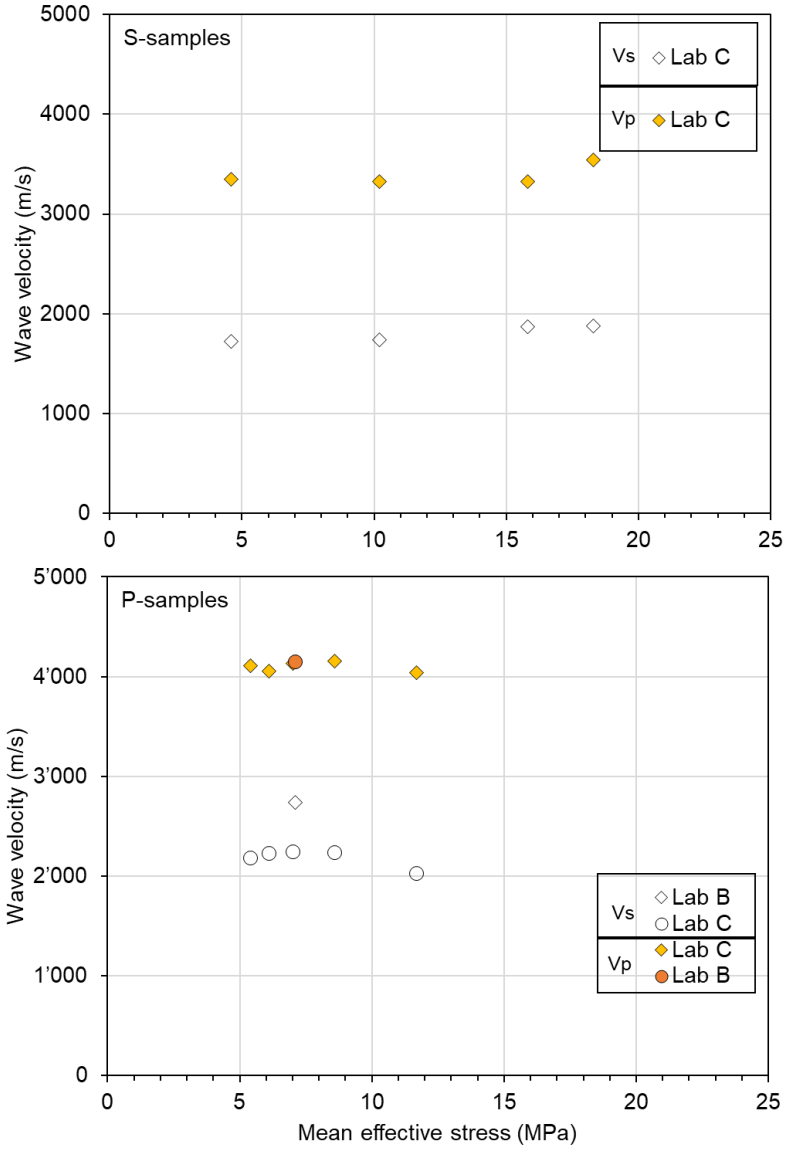

Fig. 6-11: Wave velocities at the beginning of the shearing phase

Results are divided by specimen geometry (data in Appendix E).

6.2.2.3 Pore pressure evolution

In Fig. 6-12, the stress levels ($p' - q$), at which the maximum value of the *AB* parameter and the maximum pore pressure u_w are reached, are plotted along with the peak shear strength for all test results (data in Appendix B). q is the deviatoric stress, p' is the mean effective stress, Δu_w is the variation of pore fluid pressure from the beginning of the shearing, *AB* is the ratio between Δu_w and q. The results are divided by specimen geometry. In test C4, an usual pore pressure response was observed, since maximum u_w and maximum *AB* values were achieved after peak shear strength. These two points are highlighted with a dotted marker line in Fig. 6-12.

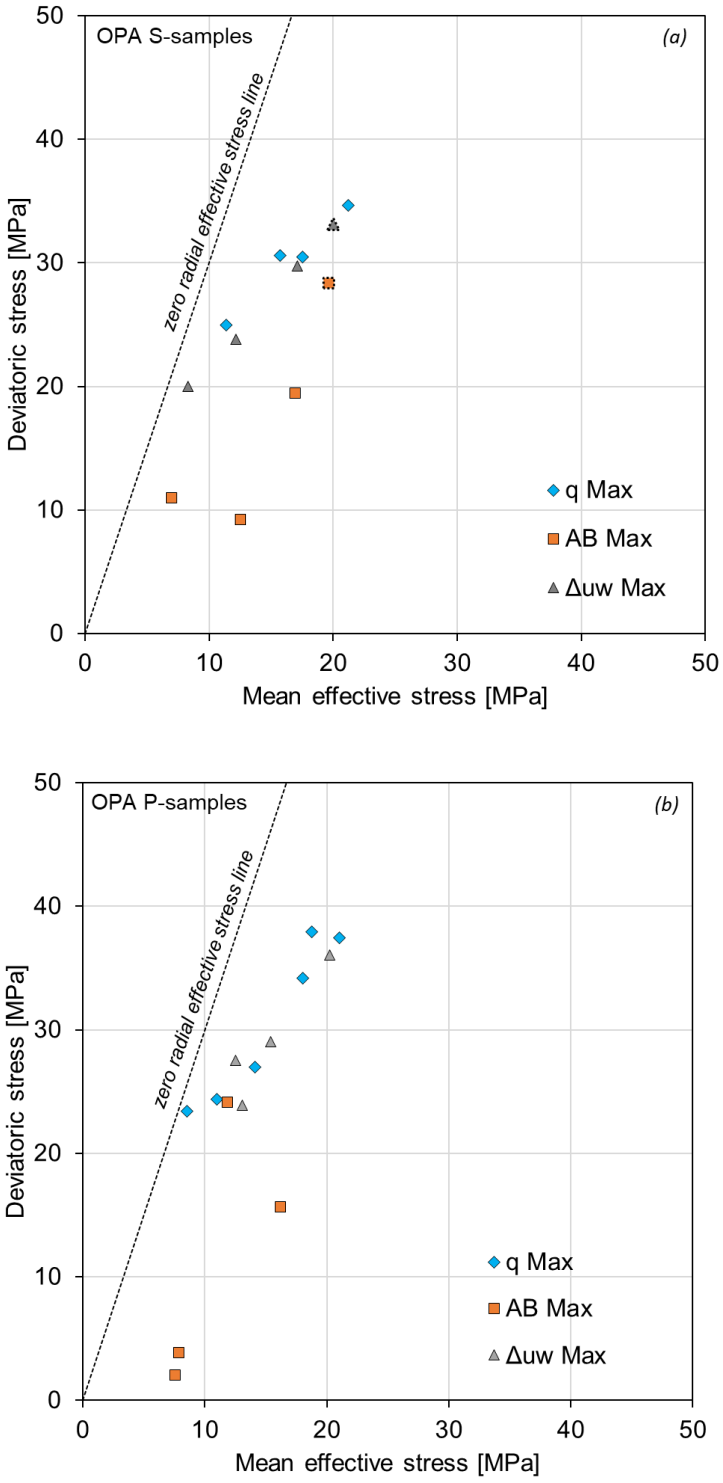

Fig. 6-12: Stress level at which the maximum deviatoric stress, the maximum value of pore pressure and the maximum value of the *AB* parameter are achieved

Opalinus Clay results, all geometries (a) S-samples, (b) P-samples.

6.2.2.4 Shear strength

For all tested specimens, during shearing, a peak in deviatoric stress was achieved, before softening occurred, followed by near-constant deviatoric stress. The peak value is reported below, as the *peak shear strength*, while the constant deviatoric stress achieved during continuing shearing (axial strain up to 1.5 – 3%) is hereafter referred to as *post-peak shear strength*.

In Fig. 6-13, peak (a) and post-peak shear strength (b) are reported in the $p' - q$ plane. The dotted lines highlight the pair of $p' - q$ values, at which radial effective stress equals zero. This line would correspond to the same boundary conditions as a UCS test if pore fluid pressure was zero. The stress states on the left side of this line cannot be achieved (negative radial effective stress) in a triaxial apparatus.

In Fig. 6-14 the peak shear strength results are analysed, sorted by the water content (Fig. 6-14a) of the specimens (obtained at the end of the test) and by the clay mineral content (Fig. 6-14b), where available. The plot includes the results of S-samples of Opalinus Clay. The results are reported also in Fig. 6-15 in terms of radial versus axial effective stress.

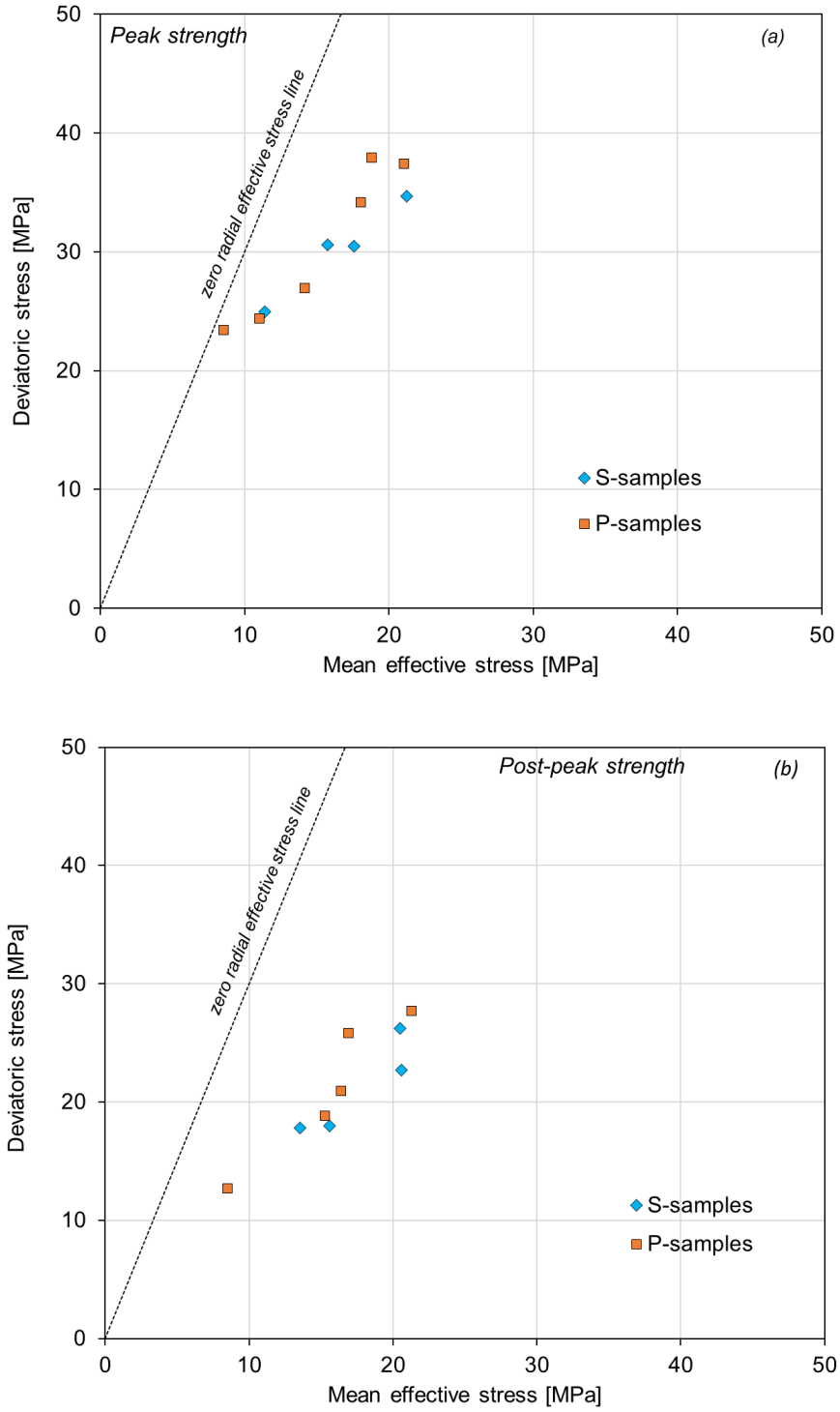

Fig. 6-13: Peak (a) and post-peak (b) shear strength of Opalinus Clay STA2-1 specimens
Results divided by geometry.

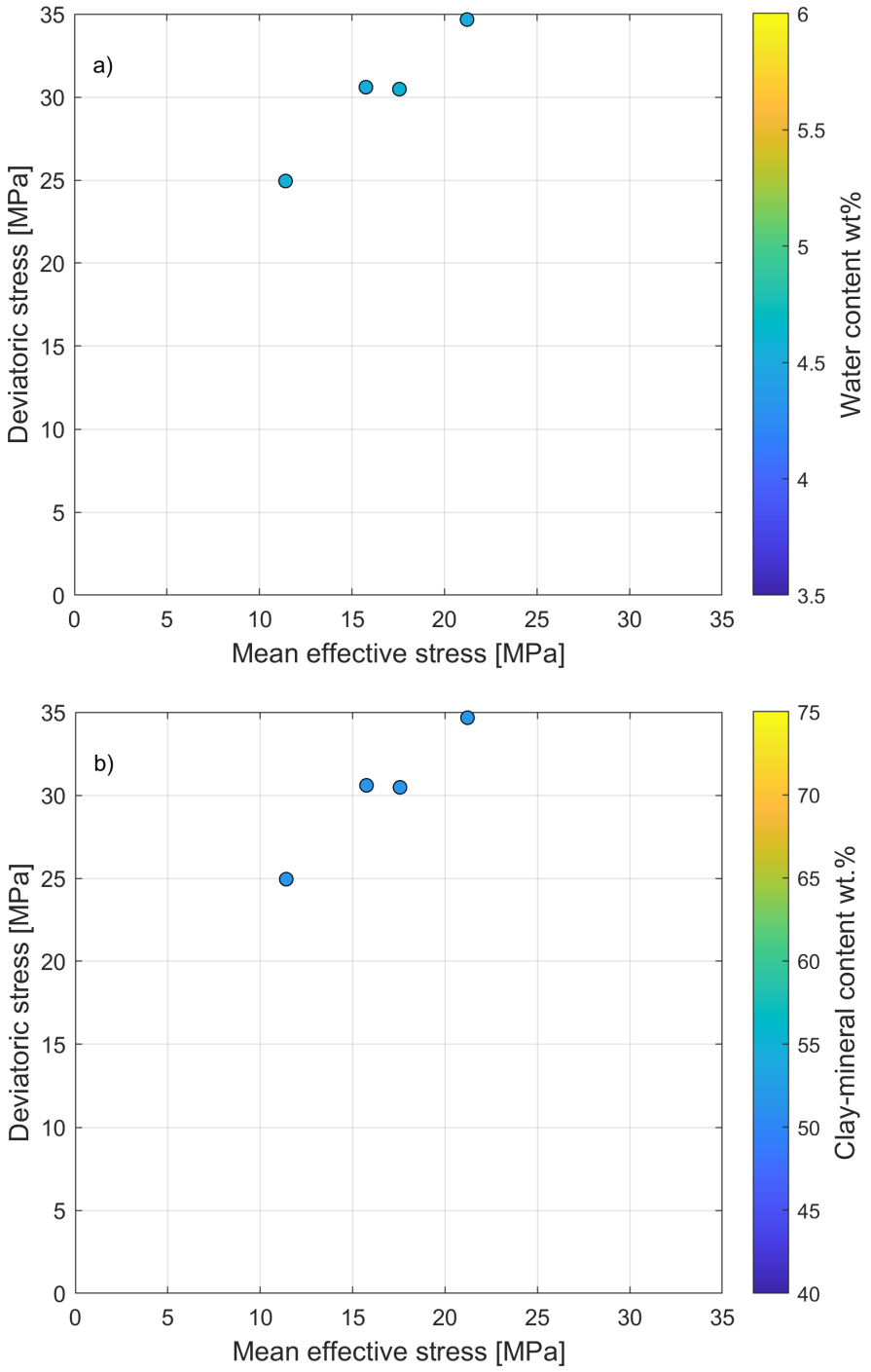

Fig. 6-14: Peak shear strength of Opalinus Clay specimens

Results in mean effective versus deviatoric stress, sorted by (a) water content and (b) clay mineral content, when available. Only S-samples are reported.

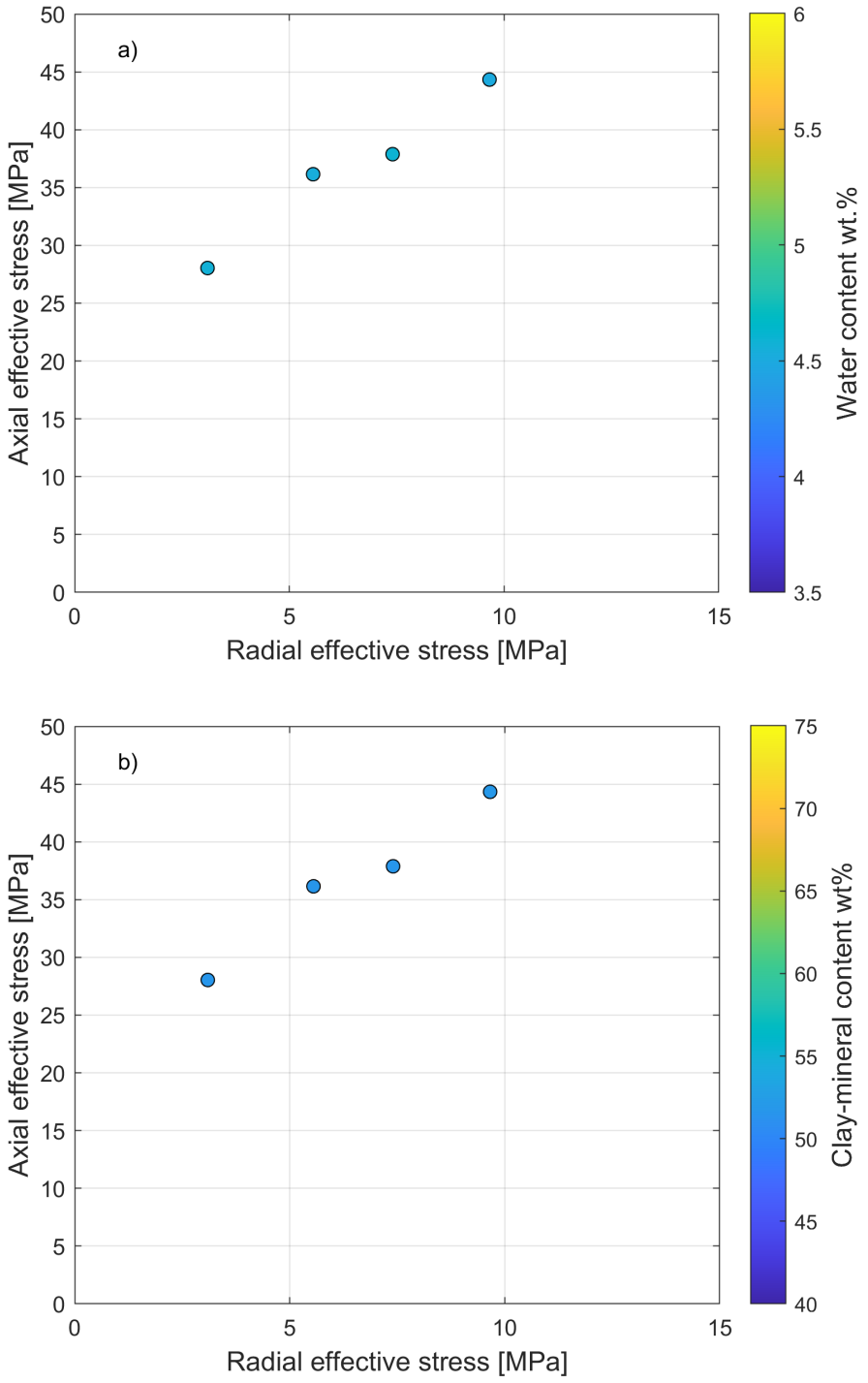

Fig. 6-15: Peak shear strength of Opalinus Clay specimens

Results in radial versus axial effective stress, sorted by (a) water content and (b) clay mineral content, when available. Only S-samples are reported.

6.2.2.5 Analysis of the anomalous results

The two conducted TC tests (C8_STA2_1_842_63P11TC and C9_STA2_1_842_63P8TC) showed fluctuations in axial stress during shearing, due to a problem with the load cell. Test C8 was further interrupted as soon as the deviatoric stress reached potential peak, as the sample breakage broke the membrane around the sample. The results of both tests are reported in the current Dossier with reference to the best estimate of the peak deviatoric stress. A detailed analysis was conducted and allowed to bound the uncertainty in the peak shear strength. For tests C8 the uncertainty is the best estimate (q_{Max} = 24.4 MPa) +1.3 and -2.0 MPa. For test C9 the uncertainty on the best estimate (q_{Max} =2 3.4 MPa) is of +2.0 and -2.5 MPa. The uncertainty on the mean effective stress at peak is limited to few tenth of MPa.

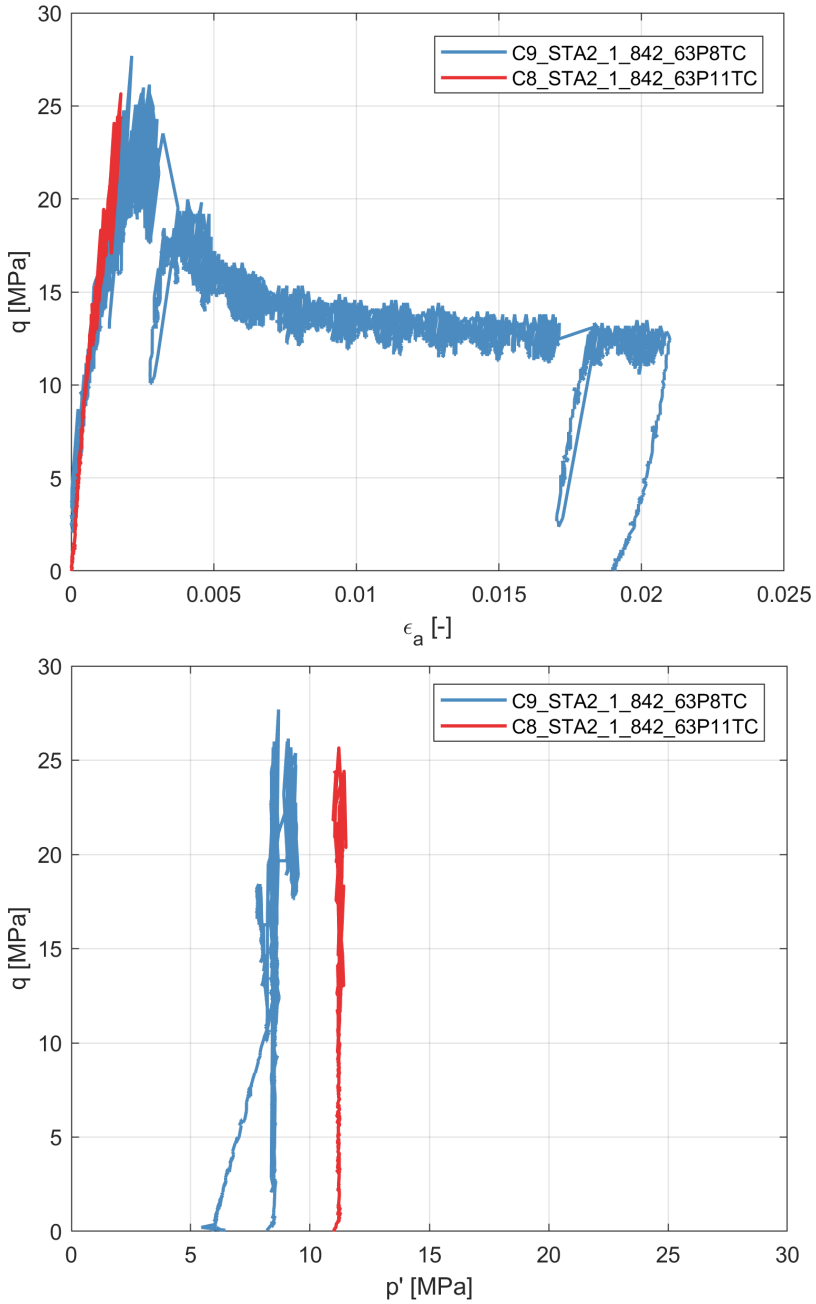

Fig. 6-16: Results from the TC drained tests

Axial strain (top) and mean effective stress (bottom) versus deviatoric stress.

Test C4_STA2_1_842_63S20CTCU showed an anomalous pore pressure response, where pore pressure kept increasing after peak strength is reached. Also the *AB* value kept increasing after peak, where it reached a maximum and then dropped. The diagnostic plots, with the evolution of all the quantities are reported in Appendix C.

6.3 Lateral strain prevented tests in triaxial conditions (K0)

This section includes the results of the triaxial test results in zero lateral strain conditions (K0). Results of test B2_STA2_1_845_33S_K0 are depicted in Figs. 6-17 and 6-18 as an example, in terms of: Fig. 6-17(a) mean effective stress versus volumetric strain, Fig. 6-17(b) axial versus radial effective stress and, Fig. 6-18, the evolution of the ratio of the radial to axial effective stresses (K0) with the applied axial effective stress upon loads and unloads.

The remaining test results are reported in Appendix E.

In Tab. 6-2, a summary of the performed tests is provided, together with the K0 value obtained for the vertical effective stress close to the in situ values. Where multiple loads and unloads were available, the reported K0 was obtained as the average ± the error, and the amount of available points is reported in parenthesis (from 1 to 4).

As expected, in all the test results the ratio of radial to axial effective stress in zero-radial-strain conditions (K0) was found to vary with the applied stress. For Opalinus Clay samples, ratios were fairly constant from the initial towards higher stress levels, but increased upon unloading. This is in agreement with the literature relating K0 to the overconsolidation ratio (OCR) (e.g Schmidt 1966, Alpan 1967).

Tab. 6-2: K0 test results

* Vertical effective stress is calculated as the overburden stress minus the pore pressure assumed hydrostatic. ** Range of obtained values, number of measurements for the considered vertical effective stress is reported in parenthesis.

ID	**Depth** [m]	**Laboratory**	**Specimen geometry**	**Formation**	**Estimated vertical effective stress *** [Mpa]	**K0 **** [-]
A1_STA2_1_626_58S_K0	626.58	A	S	Villigen	9	0.19 ± 0.01 (2)
A2_STA2_1_795_93S_K0	795.93	A	S	«Muchisonae-Oolith»	11	0.49 ± 0.09 (4)
B3_STA2_1_814_60S_K0	814.60	B	S	Opalinus Clay	11	0.52 ± 0.10 (3)
B2_STA2_1_845_33S_K0	845.33	B	S	Opalinus Clay	12	0.57 (1)

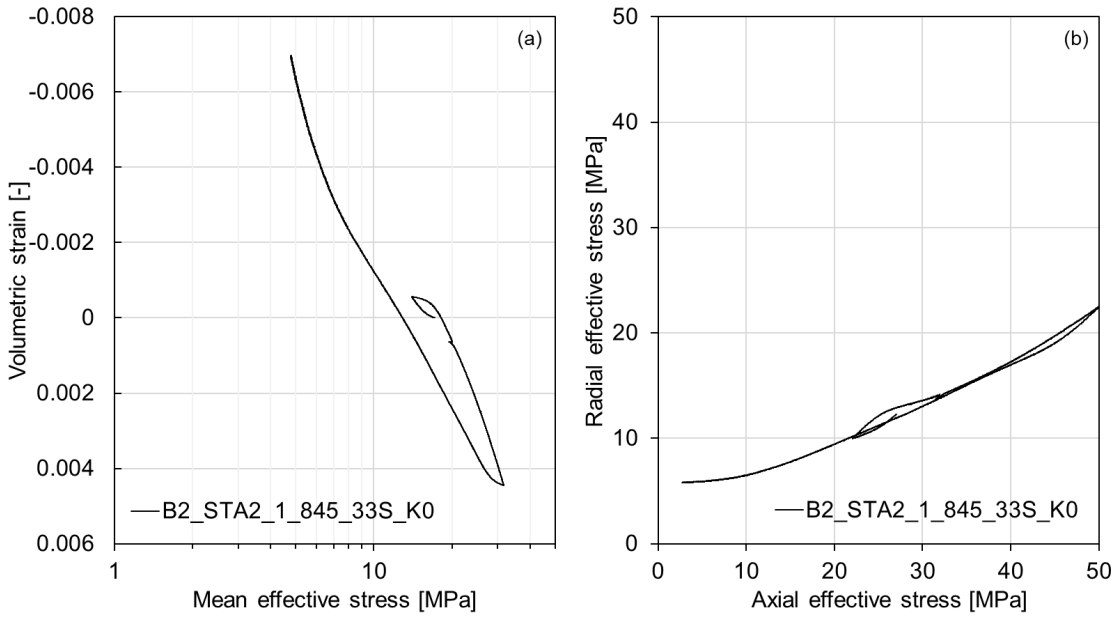

Fig. 6-17: Results of a lateral strain prevented test in triaxial conditions (K0)

(a) Mean effective stress versus volumetric strain and (b) axial versus radial effective stress.

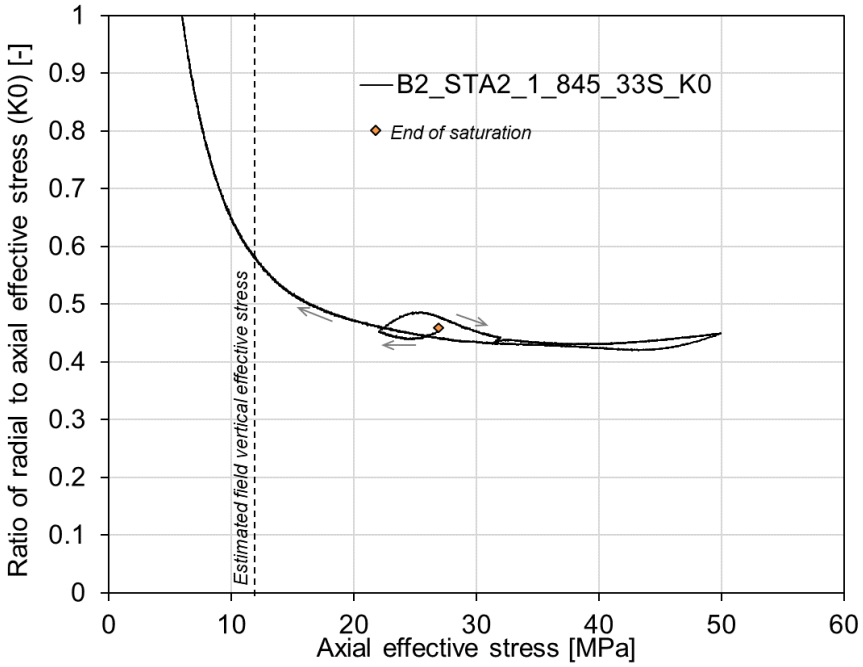

Fig. 6-18: Results of a lateral strain prevented test in triaxial conditions (K0)

Evolution of the ratio of radial to axial effective stress (K0) with the axial effective stress.

6.4 Constant-head permeability tests

This section includes the results obtained on:

- Constant-head permeability tests (PERM) obtained in oedometric conditions
- Constant-head permeability tests during K0 triaxial test (lateral strain prevented)

6.4.1 Overview of the performed tests and initial specimen conditions

An overview of the performed tests is provided in Tab. 6-3.

Tab. 6-3: Permeability tests performed in oedometric or triaxial conditions

For specimen geometry see Fig. 4-1.

ID	OED	K0	Depth [m]	Laboratory	Specimen geometry	Formation
A1_STA2_1_626_58S_K0		×	626.58	A	S	Villigen
A2_STA2_1_795_93S_K0		×	795.93	A	S	«Muchisonae-Oolith»
D1_STA2_1_PERM	×		965.58	D	P	Klettgau
D2_STA2_1_PERM	×		965.35	D	P	Klettgau
D3_STA2_1_PERM	×		965.35	D	P	Klettgau
D4_STA2_1_PERM	×		965.35	D	P	Klettgau
D5_STA2_1_PERM	×		965.29	D	P	Klettgau

The tests in oedometric conditions were labeled by indicating the letter of the laboratory that performed the test (e.g. Lab A), a sequential number (1) and the type of test (PERM = constant-head permeability).

6.4.2 Hydraulic conductivity: direct measurements

In Fig. 6-19, the hydraulic conductivity of P- and S-samples obtained from constant-head permeability measurements are reported and labelled with the values of vertical effective stress at which the test was performed. Data of hydraulic conductivity are reported in Tab. 6-4.

Tests in the Klettgau Formation were conducted to assess the variability in the hydraulic conducitivity in this section, which present lithological heterogeneity (see corresponding core picture in Appendix B).

Three tests (D2 to D4) were conducted on a same sample, in oedometric conditions from Lab D. For this sample, the gap between the ring and the sample was filled with a thin layer of bentonite. The sample was unmounted, and the bentonite checked and restored after each test. It is noted, that a high k-value was obtained in the first test, but the following two tests (done at lower pore pressure) showed consistent results. Hence, the elevated pore pressure may have eroded and affected the bentonite seal, and thereby leading to an elevated k-value.

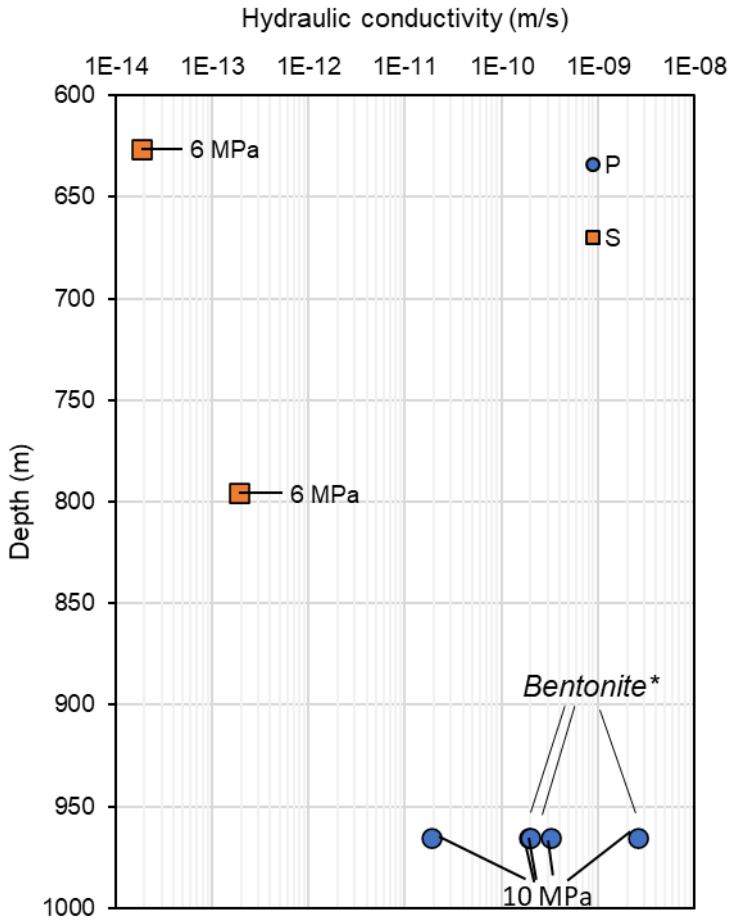

Fig. 6-19: Hydraulic conductivity versus depth

Results obtained from the analysis consolidation test, for the range of effective vertical stress 5 – 20 MPa, and constant-head tests in oedometric conditions. * A layer of bentonite was placed between the sample and oedometric ring to seal the contact.

Tab. 6-4: Hydraulic conductivity test results: from consolidation and constant-head tests

Specimen ID	**Specimen geometry**	**Depth**	**Constant-head tests**			
			σ_v	u_{bottom}	Δu	k
		[m]	[MPa]	[MPa]	[MPa]	[m/s]
A1_STA2_1_K0	S	626.58	8	3.0	1.9	1.86E-14
A2_STA2_1_K0	S	795.93	8	2.5	1.0	1.88E-13
D1_STA2_1_PERM	P	965.58	15	5.05	0.05	1.86E-11
D2_STA2_1_PERM	P	965.35	15	5.01	0.009	2.62E-09
D3_STA2_1_PERM	P	965.35	10	0.055	0.005	3.23E-10
D4_STA2_1_PERM	P	965.35	10	0.056	0.006	1.94E-10
D5_STA2_1_PERM	P	965.29	10	0.055	0.005	1.99E-10

7 Representativeness of test results

A critical question revolving around any rock-mechanical or geomechanical laboratory programme is how representative the chosen specimens are for a given formation. This depends on several factors, notably material heterogeneity.

One possible way to address this is to compare wave velocities derived from the sonic scanner in situ (Fig. 7-1, blue line) and ultrasonic velocities constrained in triaxial tests on cores in the laboratory (*cf.* Tabs. 5-3 and E-1, orange squares in Fig. 7-1). Such correlations can be used for both i) checking the plausibility of test results and ii) estimating the variability of material properties in (sub-)formations. Therefore, the tests conducted in the rock-mechanical testing programme with formations other than Opalinus Clay (and confining units) are used as guidance to estimate rock-mechanical formation properties.

In contrast, the ambition of the geomechanical testing programme (of Opalinus Clay in particular) is to cover the relevant spectrum of material properties by actual laboratory testing. Whether this was achieved is primarily assessed by comparing the basic properties and mineralogy of tested specimens with the larger database (*cf.* Dossier VIII). In this larger database, water content and mineralogy were constrained every 2 to 3 m along the 107 m thick interval of Opalinus Clay, and each measurement reflects a mean value over a 25 cm core interval.

The water content of geomechanically tested specimens was measured on trimming material from the specimen preparation and on the specimens themselves (before and after testing). For a same specimen, these values were averaged, and the error bars constructed to include the variability in the measurements. Those results are reported versus the specimens sourcing depth in Fig. 7-2. Based on the water content, the comparison with the larger database reveals that the spectrum of water contents is covered by the geomechanical tests.

The bulk mineralogy was also assessed for the tested specimens. However, it is noted that for a given depth interval, multiple «twin specimens» were sourced to constrain stress-dependent properties of the same material. As the material's variability in the horizontal direction in the Opalinus Clay is generally considered very small compared to the variability in the vertical direction, only one specimen was generally used for a given depth interval as a reference mineralogy for other specimens. This assumption was verified with repeated analyses of two plugs from an identical depth interval. Therefore, the bulk mineralogy obtained on one specimen was attributed to the other specimens from the same vertical interval of the core. The clay-mineral content (wt.-%) is reported in Fig. 7-3 against depth, together with the large database obtained from University of Bern (*cf.* Dossier VIII).

The comparisons of Figs. 7-2 and 7-3 demonstrate that tested specimens in the geomechanical testing programme capture the material variability and can thus be considered representative of the entire formation.

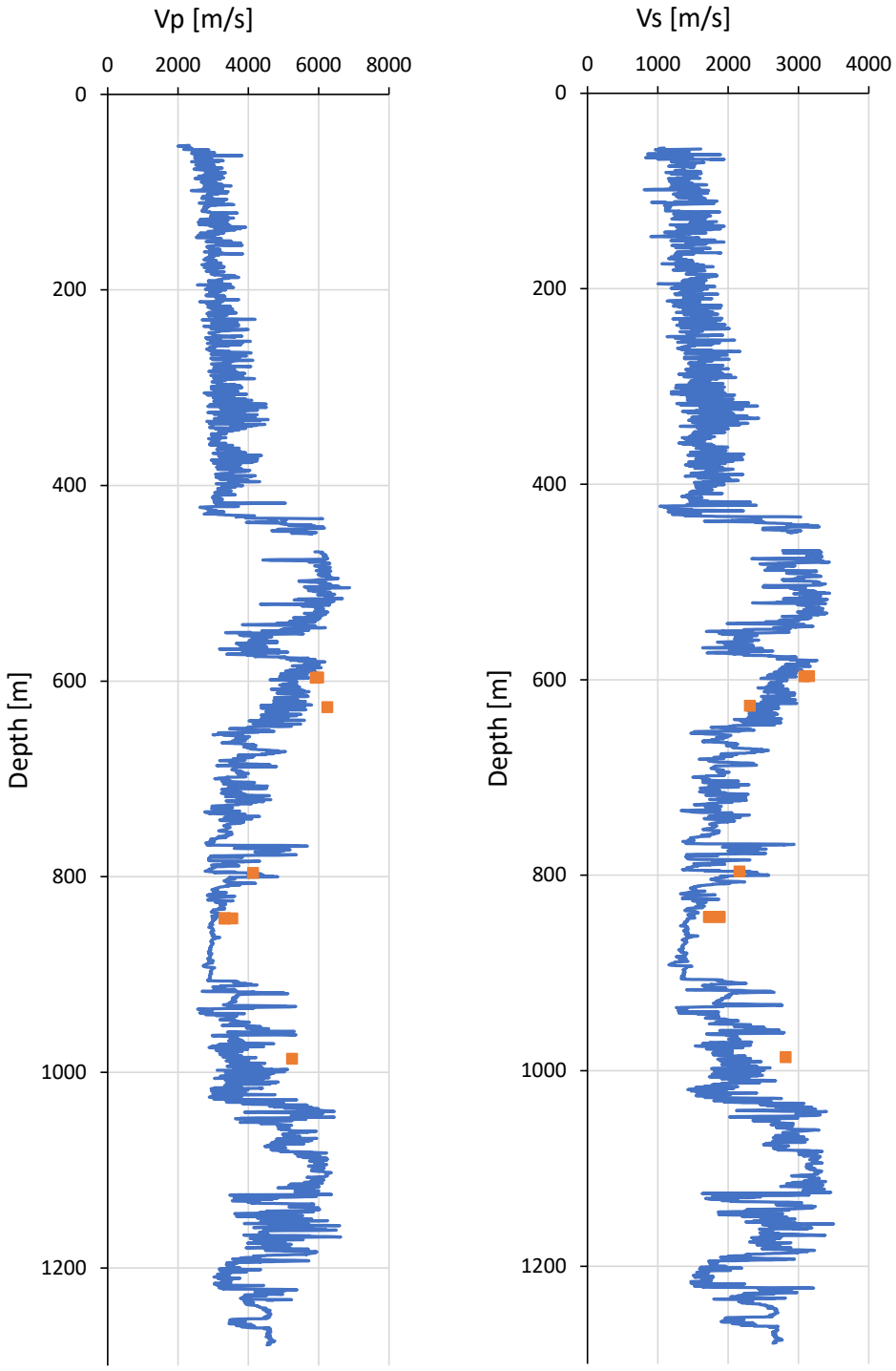

Fig. 7-1: Compressional (left) and shear-wave velocities (right) from borehole and lab testing

Blue line: continuous measurements from borehole sonic scanner (kHz frequency). Orange squares: lab measurements (MHz frequency).

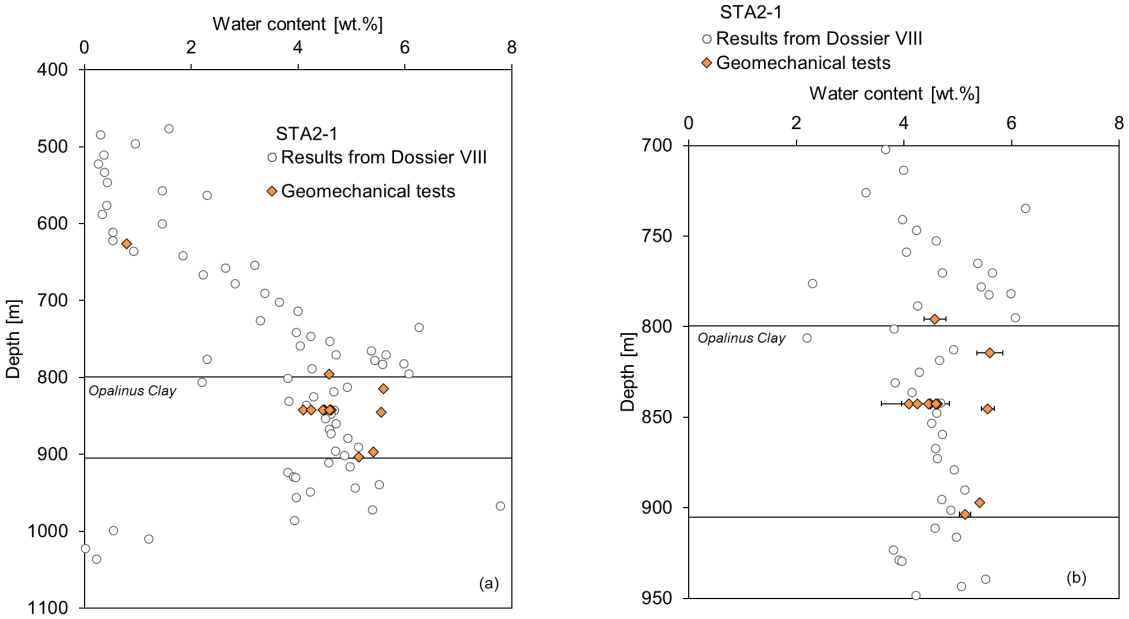

Fig. 7-2: Water content vs. depth from the large database and from tested specimens

Results include those from Dossier VIII for the STA2-1 borehole (a) and zoom into the Opalinus Clay and confining units' section (b).

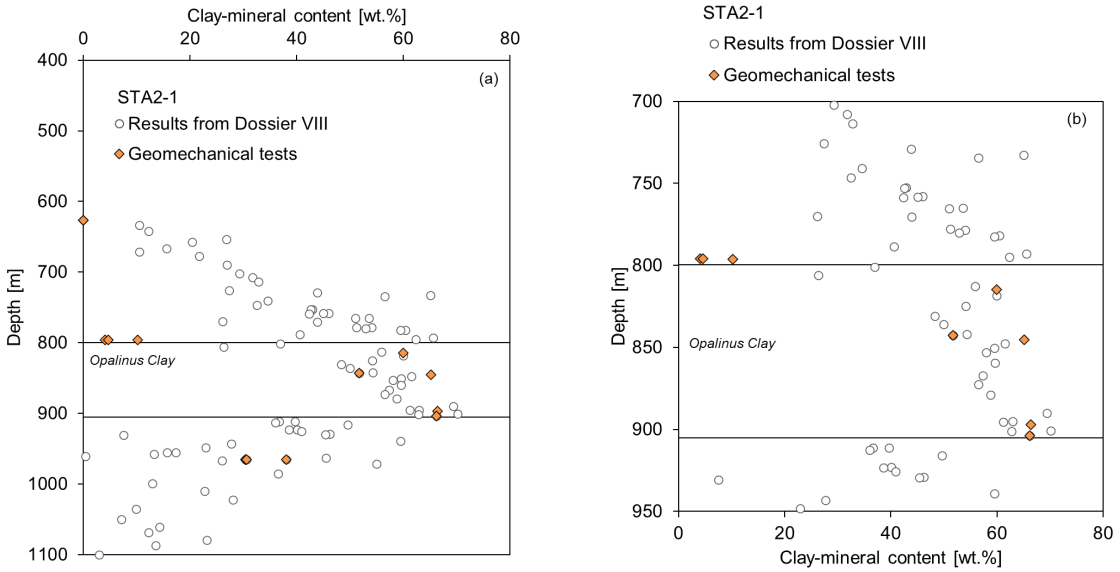

Fig. 7-3: Clay-mineral content vs. depth from the large database and from tested specimens

Results include those from Dossier VIII for the STA2-1 borehole (a) and zoom into the Opalinus Clay and confining units' section (b).

8 References

Alpan, I. (1967): The empirical evaluation of the coefficient K0 and K0R. Soils and Foundations 7, 31-40. https://doi.org/10.3208/sandf1960.7.31.

ASTM (2014): D7012-14e1: Standard test method for compressive strength and elastic moduli of intact rock core specimens under varying states of stress and temperatures. ASTM International, West Conshohocken, PA.

ASTM (2016): D3967-16: Standard test method for splitting tensile strength of intact rock core specimens. ASTM International, West Conshohocken, PA.

ASTM (2017a): D4318-17e1: Standard test methods for liquid limit, plastic limit, and plasticity index of soils. ASTM International, West Conshohocken, PA.

ASTM (2017b): D6913/D6913M-17: Standard test methods for particle-size distribution (gradation) of soils using sieve analysis. ASTM International, West Conshohocken, PA.

ASTM (2017c): D7928-17: Standard test method for particle-size distribution (gradation) of fine-grained soils using the sedimentation (hydrometer) analysis. ASTM International, West Conshohocken, PA.

ASTM (2019): D4543-19: Preparing rock core as cylindrical specimens and verifying conformance to dimensional and shape tolerances. ASTM International, West Conshohocken, PA.

Aydin, A. (2014): Upgraded ISRM suggested method for determining sound velocity by Ultrasonic Pulse Transmission Technique. Rock Mechanics and Rock Engingeering 47, 255-259.

Biot, M.A. (1941): General theory of three-dimensional consolidation. Journal of Applied Physics 12/2, 155-164.

Crisci, E., Ferrari, A., Giger, S.B. & Laloui, L. (2019): Hydro-mechanical behaviour of shallow Opalinus Clay shale. Eng. Geol. 251, 214-227. https://doi.org/10.1016/j.enggeo.2019.01.016.

Crisci, E., Laloui, L. & Giger, S. (2021a): TBO Bülach-1-1: Data Report. Dossier IX: Rock-mechanical and Geomechanical Laboratory Testing. Nagra Arbeitsbericht NAB 20-08.

Crisci, E., Laloui, L. & Giger, S. (2021b): TBO Trüllikon-1-1: Data Report. Dossier IX: Rock-mechanical and Geomechanical Laboratory Testing. Nagra Arbeitsbericht NAB 20-09.

Ewy, R.T. (2014): Shale swelling/shrinkage and water content change due to imposed suction and due to direct brine contact. Acta Geotech. 9, 869-886. https://doi.org/10.1007/s11440-013-0297-5.

Ewy, R.T. (2015): Shale/claystone response to air and liquid exposure, and implications for handling, sampling and testing. International Journal of Rock Mechanics and Mining Sciences 80, 388-401. https://doi.org/10.1016/j.ijrmms.2015.10.009.

Favero, V. (2017): Multiphysical behaviour of shales from Northern Switzerland. https://doi.org/10.5075/epfl-thesis-7539, urn:nbn:ch:bel-epfl-thesis7539-7.

Favero, V., Ferrari, A. & Laloui, L. (2018): Anisotropic behaviour of Opalinus Clay through consolidated and drained triaxial testing in saturated conditions. Rock Mechanics and Rock Engineering 51, 1305-1319.

Ferrari, A., Favero, V. & Laloui, L. (2016): One-dimensional compression and consolidation of shales. Int. J. Rock Mech. Min. Sci. 88, 286-300. https://doi.org/10.1016/j.ijrmms.2016.07.030.

Fischer, M.P., Elsworth, D., Alley, R.B., and Engelder, T. (1996): Finite element analysis of the modified ring test for determining mode I fracture toughness, Int. J. Rock. Mech. and Min. Sci. 33, 1-15.

Ghabezloo, S. & Sulem, J. (2010): Effect of the volume of the drainage system on the measurement of undrained thermo-poro-elastic parameters. International Journal of Rock Mechanics and Mining Sciences 47, 60-68. https://doi.org/10.1016/j.ijrmms.2009.03.001.

Giger, S.B., Ewy, R.T., Favero, V., Stankovic, R. & Keller, L.M. (2018): Consolidated-undrained triaxial testing of Opalinus Clay: Results and method validation. Geomechanics for Energy and the Environment 14, 16-28.

Head, K.H. (1998): Manual of soil laboratory testing. Volume 3: Effective stress tests. Second Edition John Wiley and Sons.

Isler, A., Pasquier, F. & Huber, M. (1984): Geologische Karte der zentralen Nordschweiz 1:100'000. Herausgegeben von der Nagra und der Schweiz. Geol. Komm.

Keller, L.M. & Giger, S.B. (2019): Petrophysical properties of Opalinus Clay drill cores determined from Med-XCT images. Geotech. Geol. Eng. 37/4, 3507-3522. https://doi.org/10.1007/s10706-019-00815-2.

Kuruppu, M.D., Obara, Y., Ayatollahi, M.R., Chong, K.P. & Funatsu, T. (2014): ISRM-suggested method for determining the mode I static fracture toughness using semi-circular bend specimen. Rock Mechanics and Rock Engineering 47/1, 267-274.

Minardi, A., Ferrari, A. & Laloui, L. (2019): Benchmark study on triaxial testing of Opalinus Clay: Analysis and comparative evaluation of tests results. Nagra Arbeitsbericht NAB 19-18.

Minardi, A., Giger, S.B., Ewy, R.T., Stankovic, R., Stenebråten, J., Soldal, M., Rosone, M., Ferrari, A. & Laloui, L. (2020): Benchmark study of undrained triaxial testing of Opalinus Clay shale: Results and implications for robust testing. Geomechanics for Energy and the Environment 25, 100210.

Nagra (2014): SGT Etappe 2: Vorschlag weiter zu untersuchender geologischer Standortgebiete mit zugehörigen Standortarealen für die Oberflächenanlage. Geologische Grundlagen. Dossier II: Sedimentologische und tektonische Verhältnisse. Nagra Technischer Bericht NTB 14-02.

Pietsch, J. & Jordan, P. (2014): Digitales Höhenmodell Basis Quartär der Nordschweiz – Version 2013 (SGT E2) und ausgewählte Auswertungen. Nagra Arbeitsbericht NAB 14-02.

Rufer, D. (2019): Field manual: Drill core sampling for analytical purposes. Nagra Arbeitsbericht NAB 19-13.

Saxena, A. & Hudak, S.J. (1978): Review and extension of compliance information for common crack growth specimens. Int. J. Fract. 14, 453-468. https://doi.org/10.1007/BF01390468.

Schmidt, B. (1966): Earth ressures at rest related to stress history. Can. Geotech. J. 3, 239-242. https://doi.org/10.1139/t66-028.

Thiercelin, M. & Roegiers, J.-C. (1988): Fracture toughness determination with the modified ring test. *In:* Chengxiang, L. & Ling, Y. (eds.): Proceedings of the International Symposium on Engineering in Complex Rock Formations, Pergamon, 284-290, ISBN 9780080358949, https://doi.org/10.1016/B978-0-08-035894-9.50041-X.

Tuttolomondo, A. (2021): Effective stress for unsaturated active clays and in-situ effective stress estimation methodology. EPFL PhD Thesis n° 8291.

Wissa, A.E.Z. (1969): Pore pressure measurement in saturated stiff soils. Journal of the Soil Mechanics and Foundations Division 95, 1063-1074.

Wersin, P., Mazurek, M., Waber, H.N., Mäder, U.K., Gimmi, T., Rufer, D. & de Haller, A. (2013): Rock and porewater characterisation on drillcores from the Schlattingen borehole. Nagra Arbeitsbericht NAB 12-54.

Witteveen, P., Ferrari, A. & Laloui, L. (2013): An experimental and constitutive investigation on the chemo-mechanical behaviour of a clay. Geotechnique 63/3, 244-255.

Appendix A: Photo documentation of the rock mechanical testing programme

UCS (average sample depth) **STA2-1**

before testing **after testing**

484.21 m

484.34 m

484.52 m

before testing **after testing**

561.32 m

561.55 m

596.18 m

596.58 m

before testing **after testing**

701.22 m

701.56 m

961.04 m

961.25 m

before testing **after testing**

986.07 m

986.33 m

1073.73 m

1074.03 m

before testing **after testing**

1108.75 m

1109.06 m

1220.18 m

1220.45 m

before testing **after testing**

1273.24 m

1273.60 m

TRX (average depth)

before testing

561.32 m

STA2-1

after testing

596.18 m

596.58 m

before testing **after testing**

626.56 m

TRX8_626_56

701.22 m

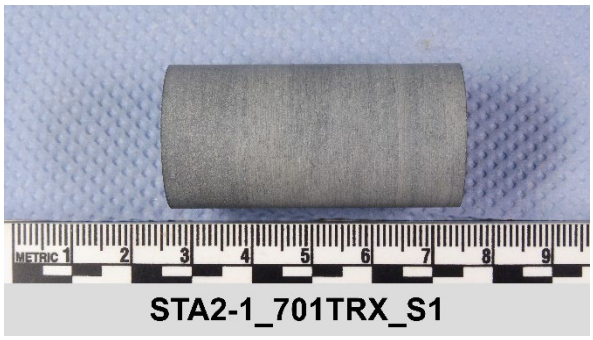

before testing **after testing**

796.13 m

TRX9_796_13

796.13 m

TRX10_796_13

before testing **after testing**

796.13 m

TRX11_796_13

986.07 m

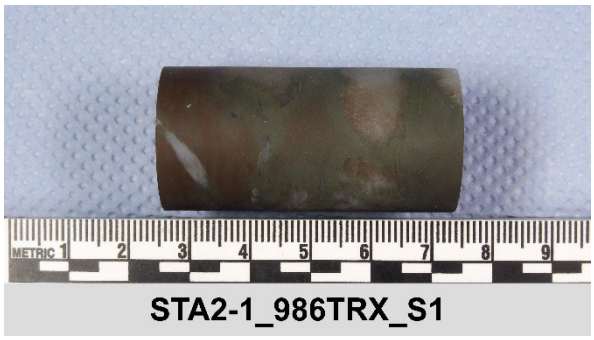

986.34 m

before testing **after testing**

1008.75 m

Appendix B: XCT cross-sections with selection of test specimens

The computed tomography scans of the tested cores are here reported, and the sections used in the testing programme are indicated.

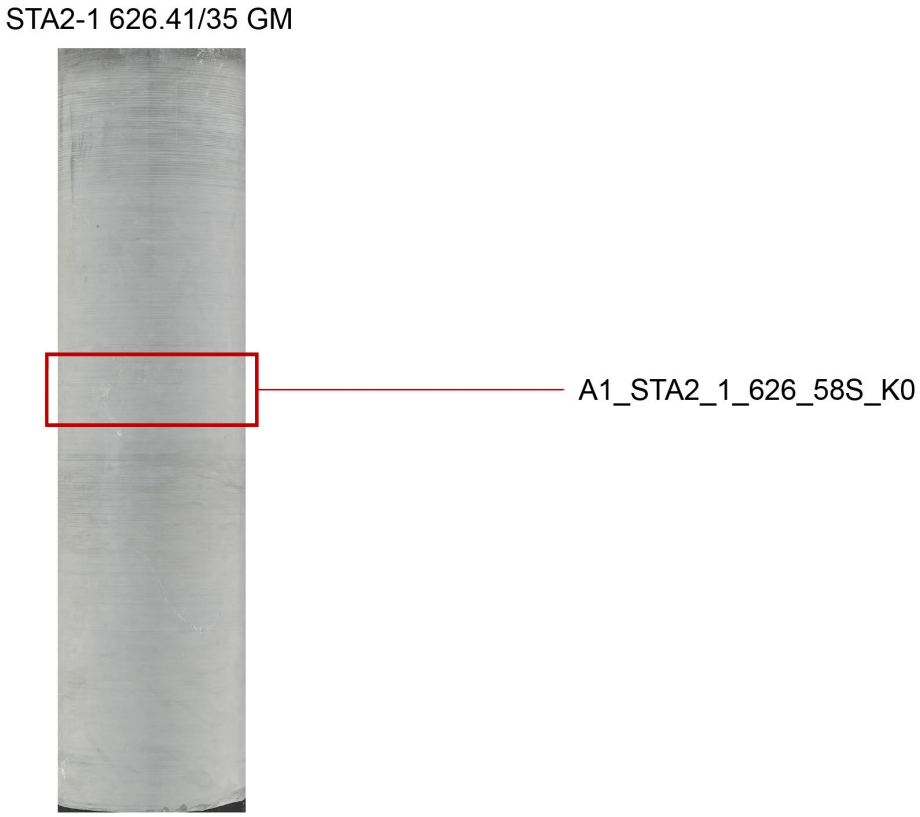

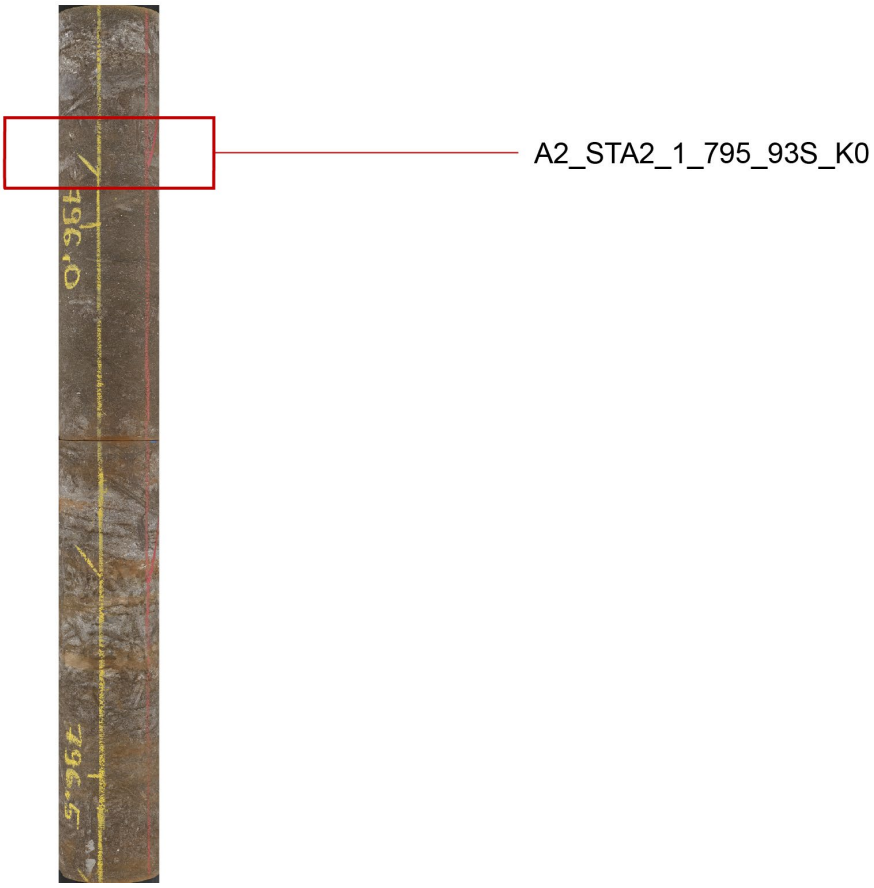
A2_STA2_1_795_93S_K0
795,0
795,5

STA2-1 814.52/40 GM

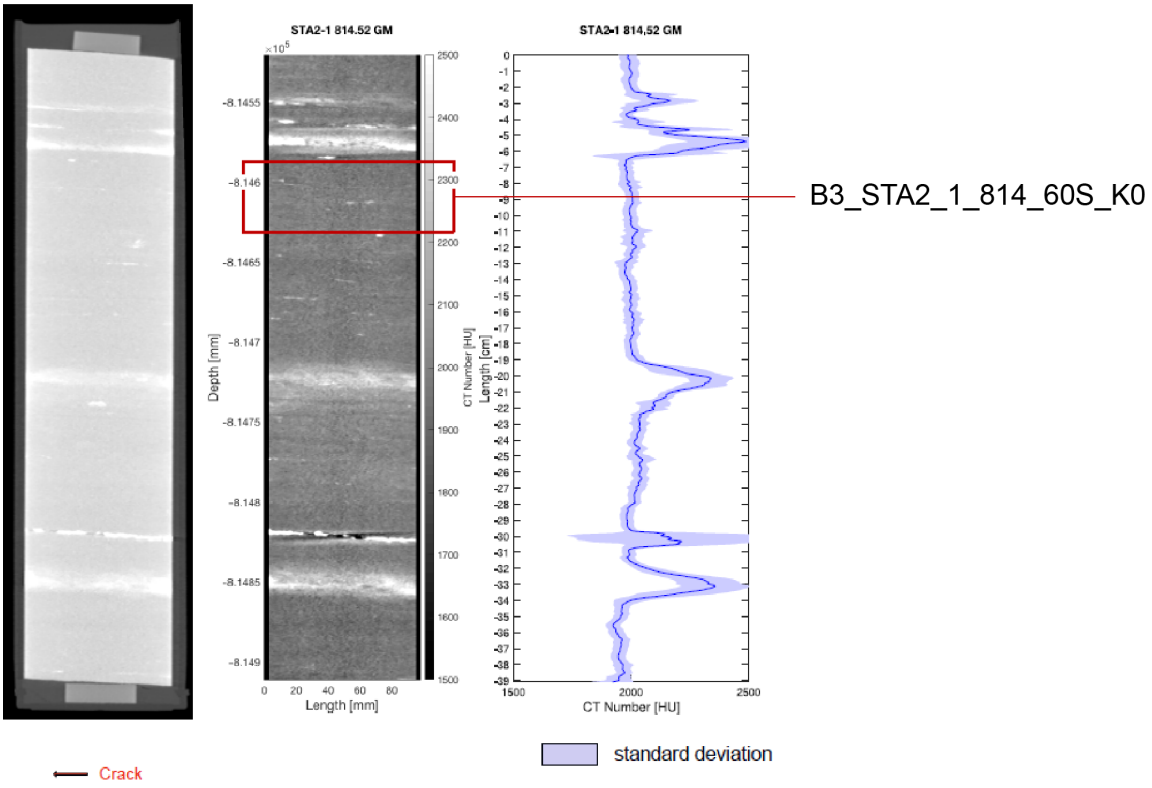

STA2-1 842.52/40 GM

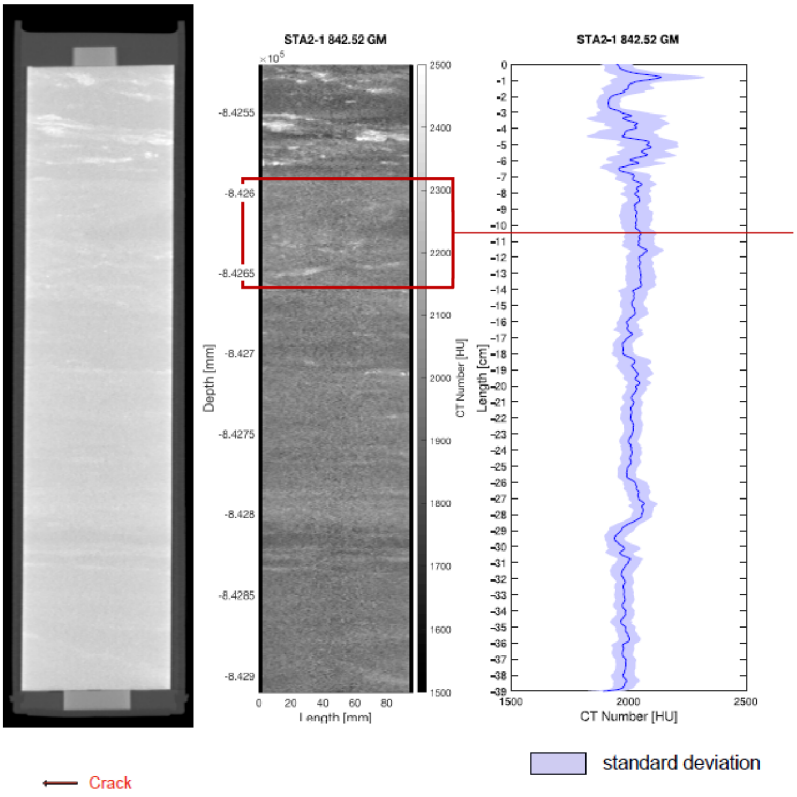

C6_STA2_1_842_62P13CTCU
C7_STA2_1_842_62P8CTCU
C8_STA2_1_842_63P11TC
C9_STA2_1_842_63P8TC
C2_STA2_1_842_63S7CTCU
C3_STA2_1_842_62S13CTCU
C4_STA2_1_842_63S20CTCU
C5_STA2_1_842_63S18CTCU

STA2-1 845.28/45 GM

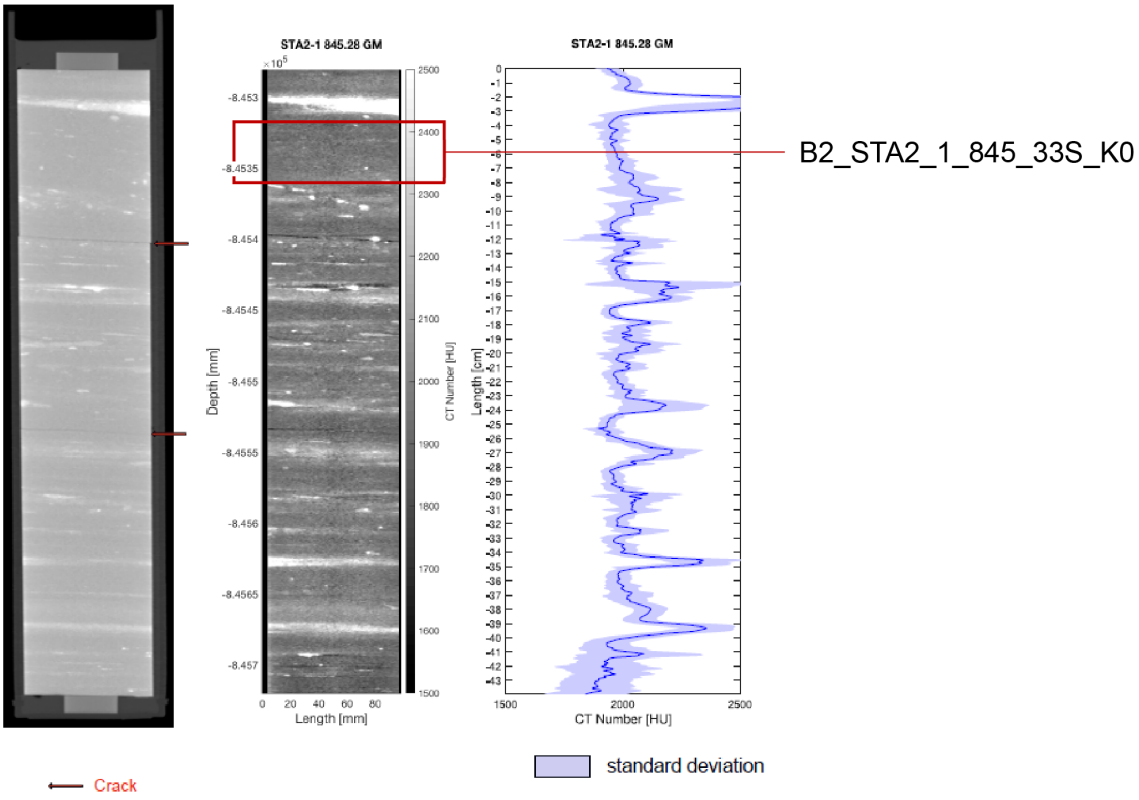

STA2-1 896.99/50 GM

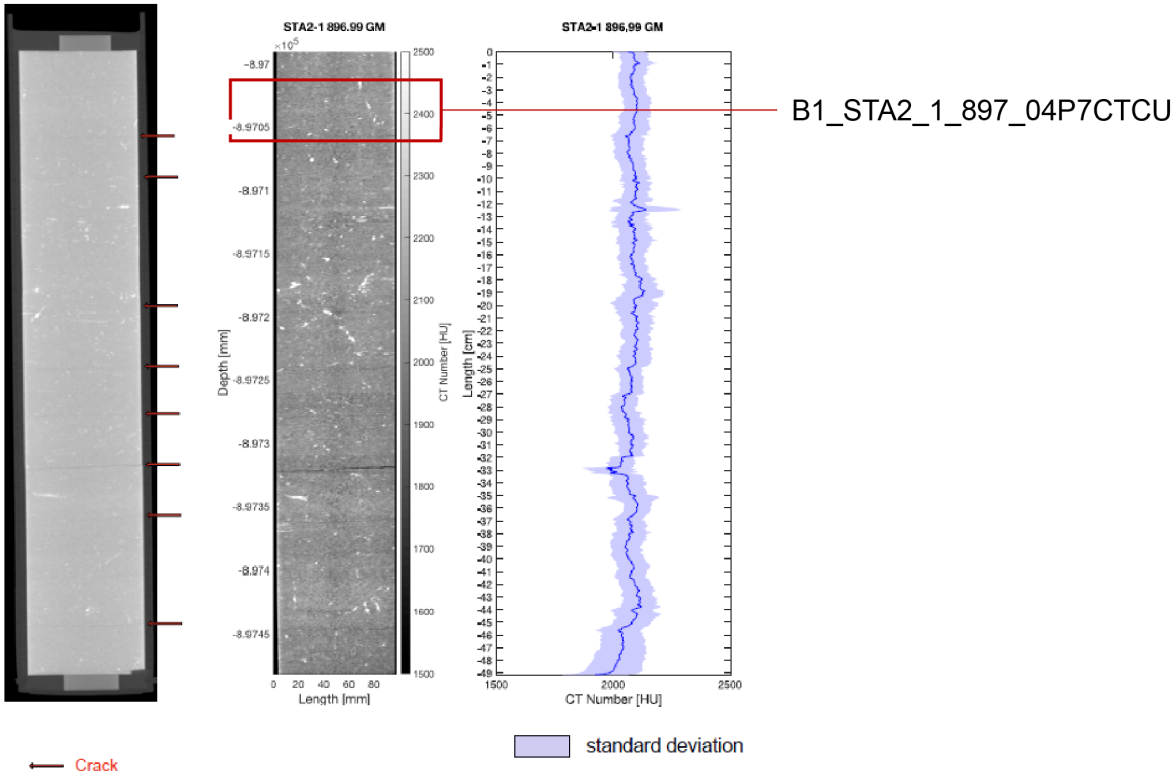

STA2-1 903.62/49 GM

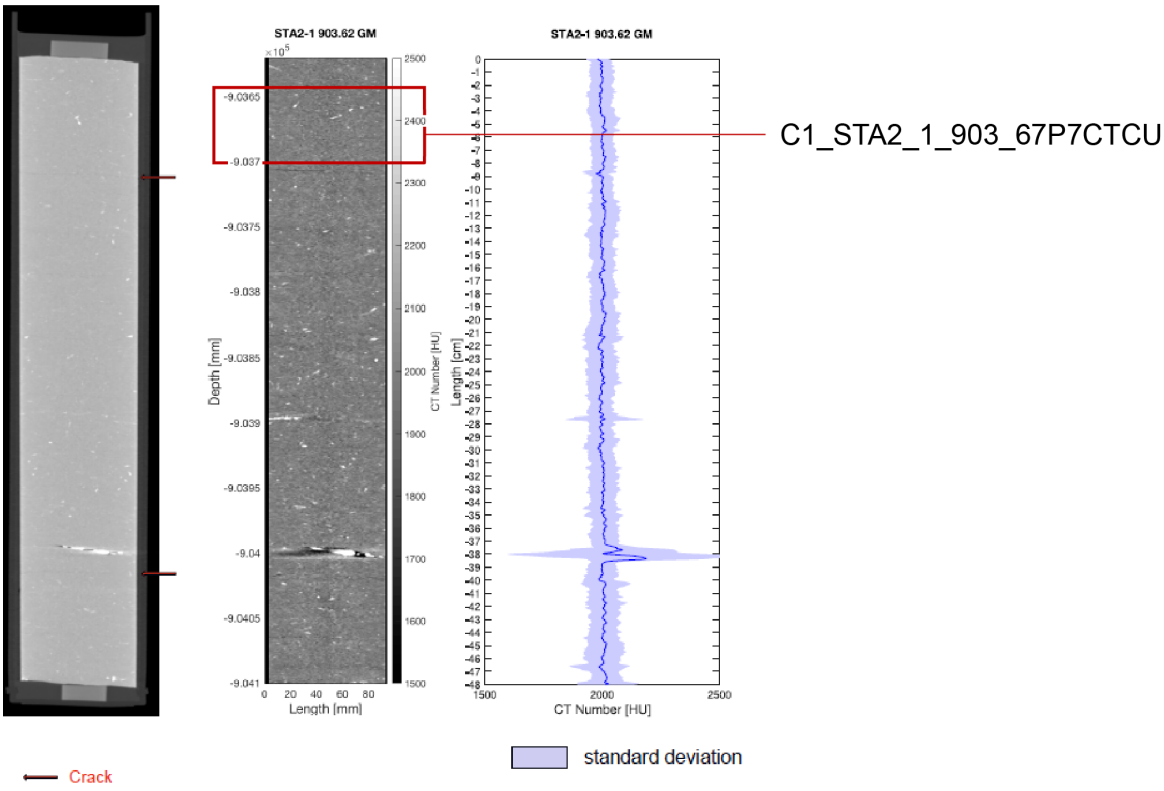

STA2-1 065.15/50 GM

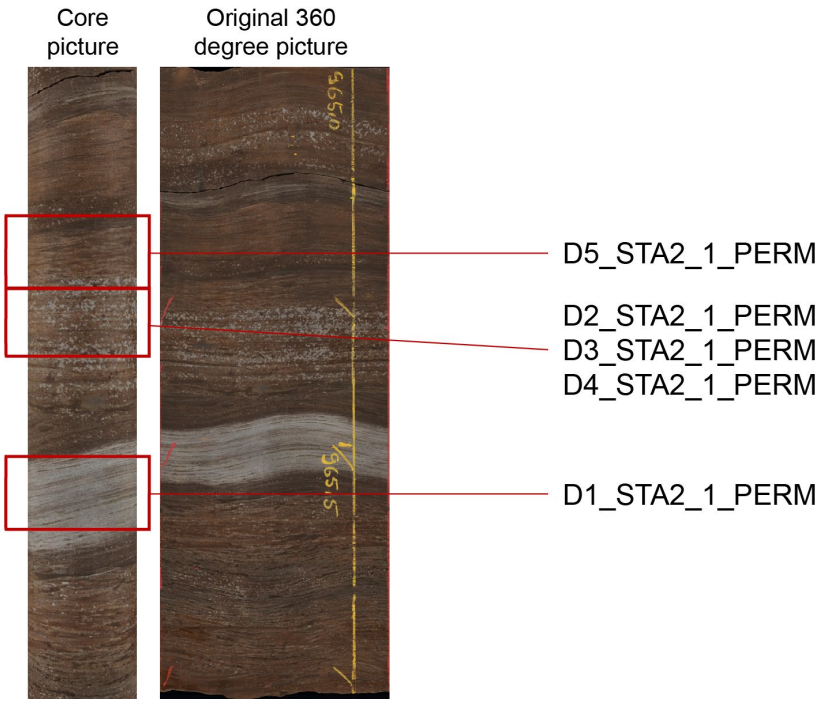

Appendix C Diagnostic plots of triaxial tests (geomechanical testing programme)

For each triaxial test, the diagnostic plots are here reported (order of tests according to Tab. E-2). The plots include: the evolution of axial and radial strains with deviatoric stress q, the pore pressure change Δu_w during shearing versus the axial strain ε_a, the stress path in the p'-q plane, the pore pressure variation Δu_w and the AB parameter evolution with q. In all the plots, the conditions at which the maximum deviatoric stress (Max q), the maximum pore pressure change (Max Δu_w) and the maximum AB (Max AB) (excluding evolution during unload/reload loops) are marked, as mentioned in Section 6.2.2.4. Testing conditions are reported in Tab. 6-2.

C6_STA2_1_842_62P13CTCU

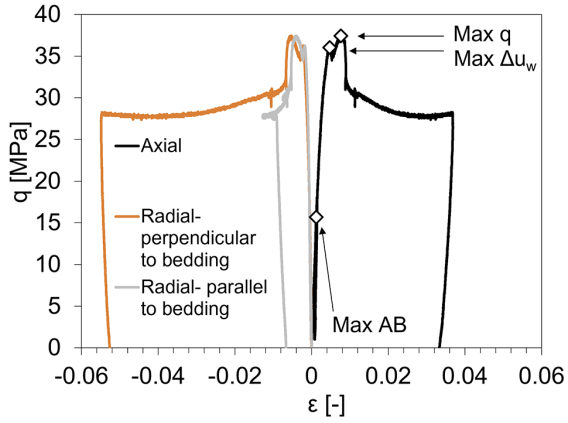

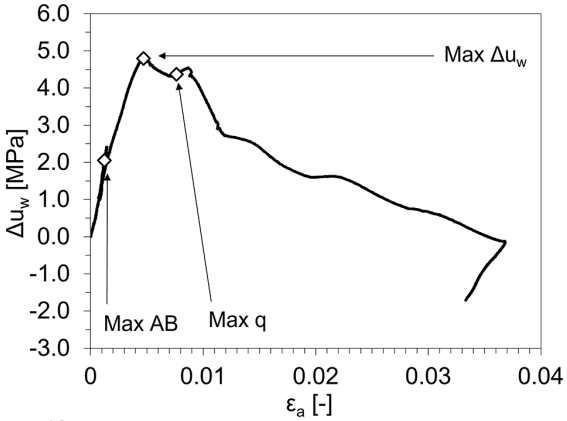

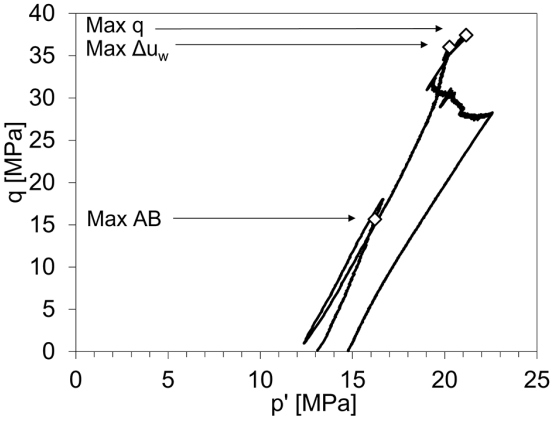

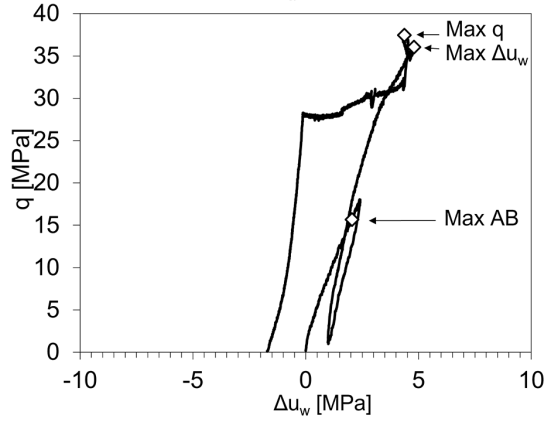

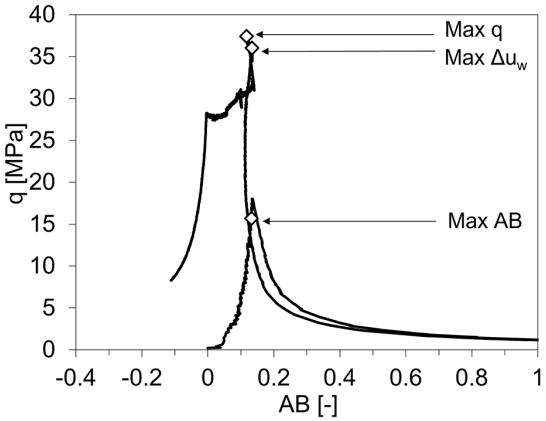

C7_STA2_1_842_62P8CTCU

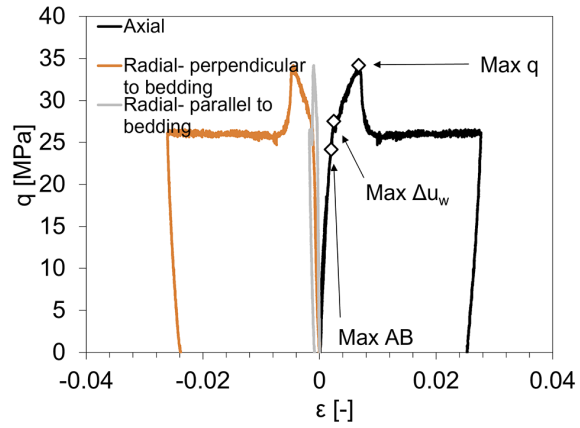

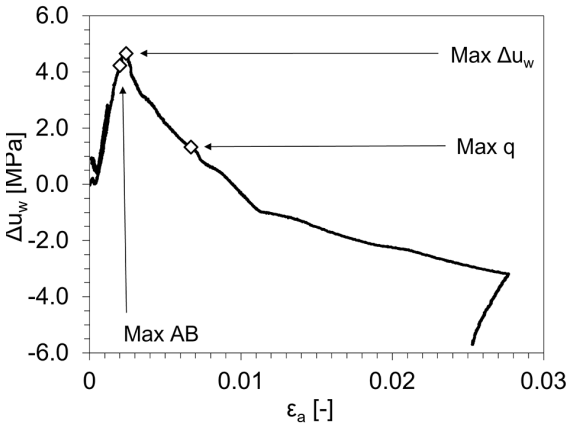

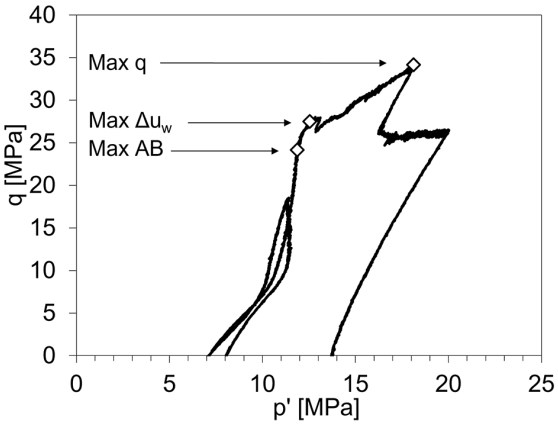

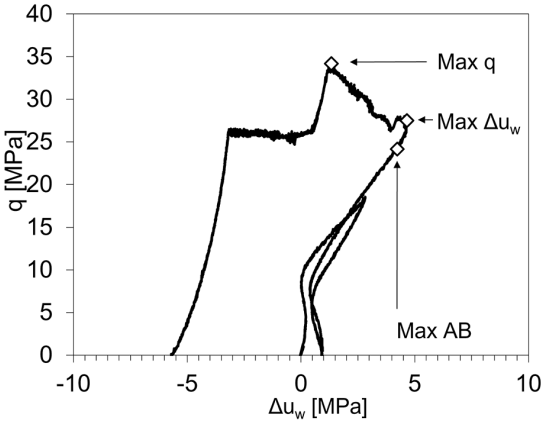

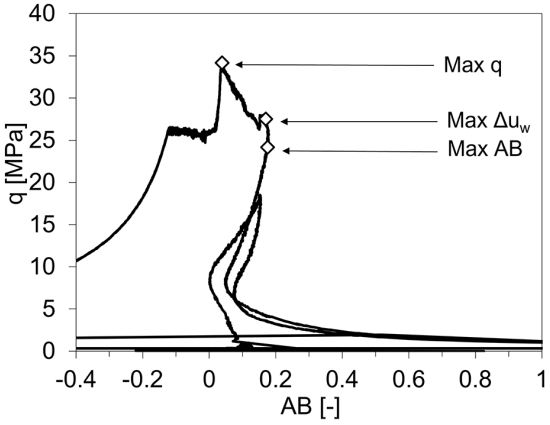

C8_STA2_1_842_63P11TC

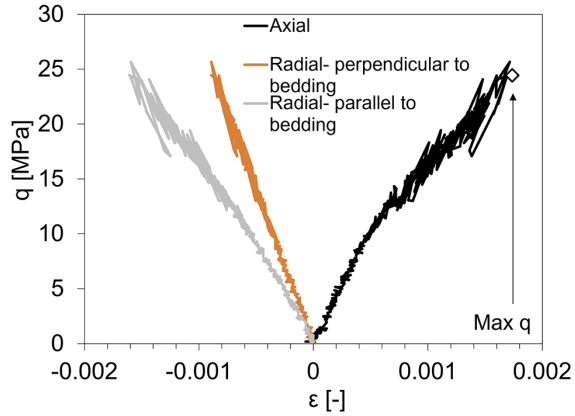

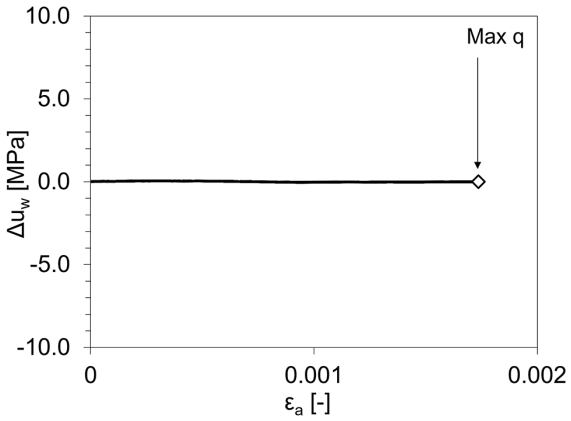

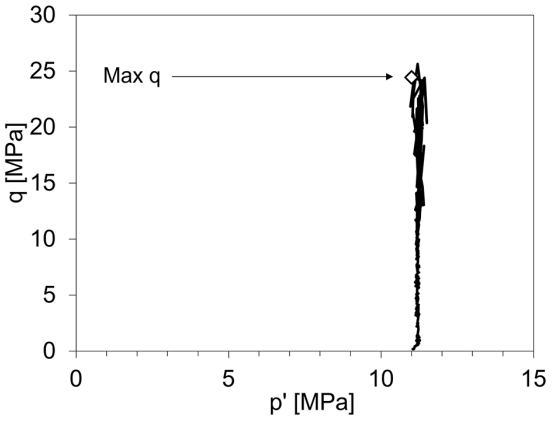

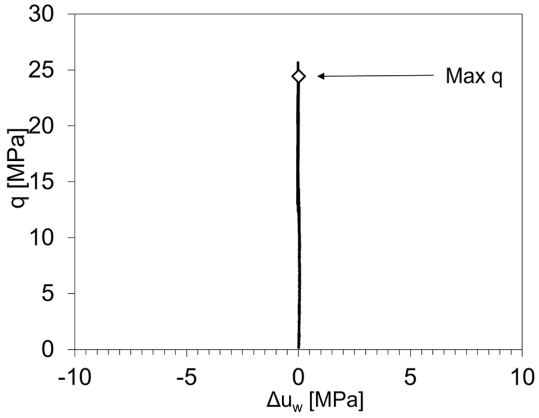

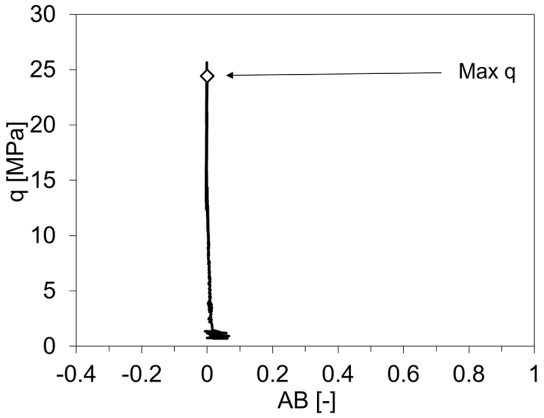

C9_STA2_1_842_63P8TC

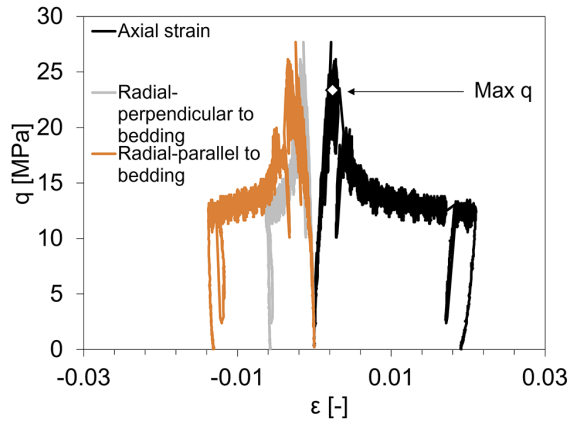

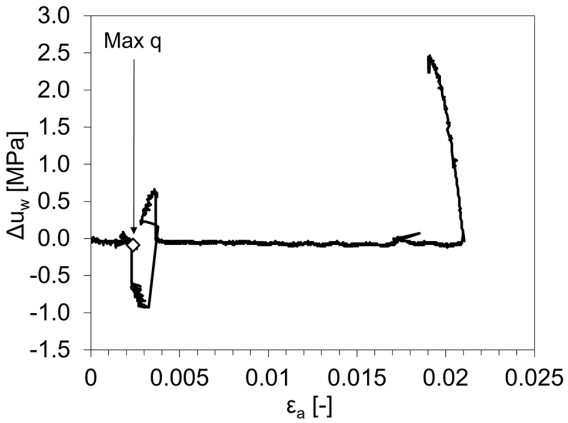

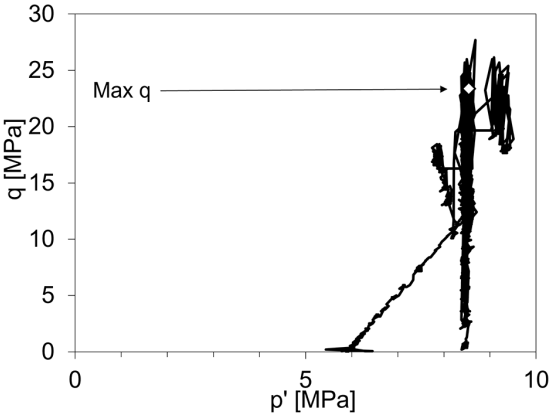

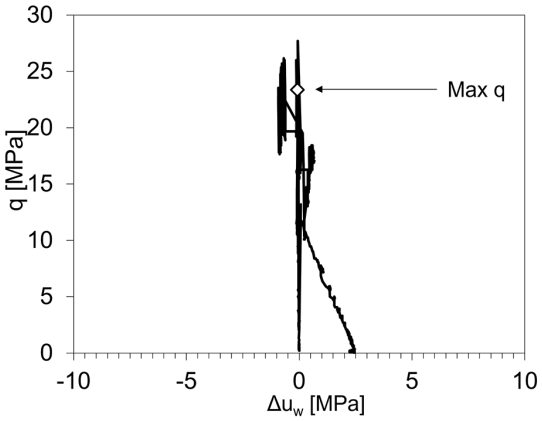

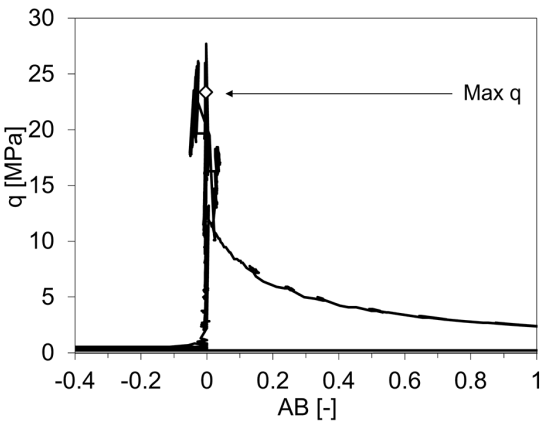

C2_STA2_1_842_63S7CTCU

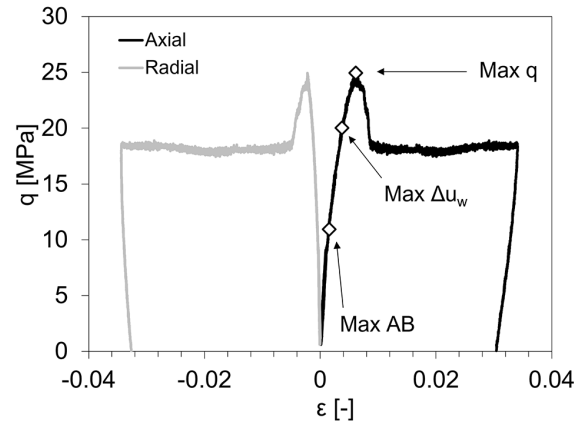

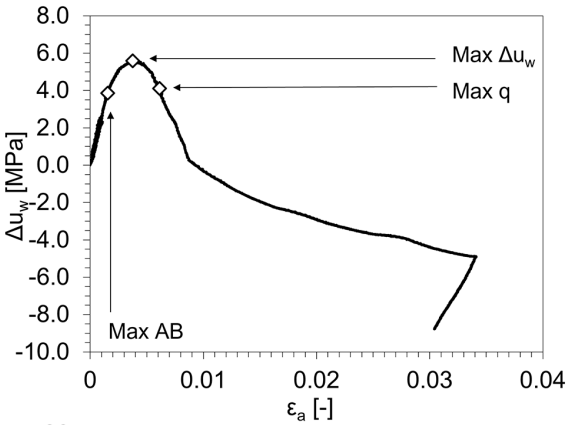

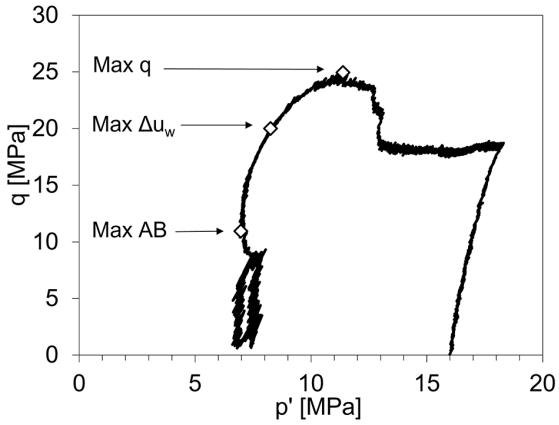

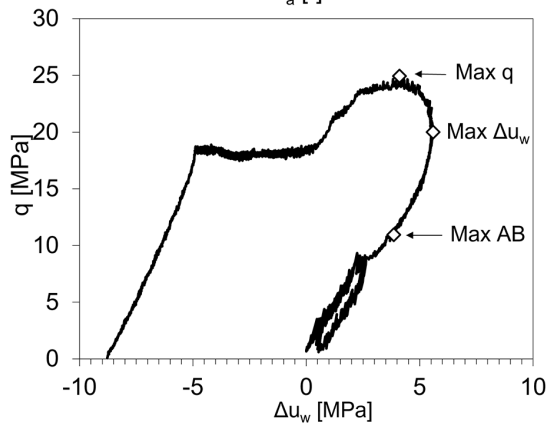

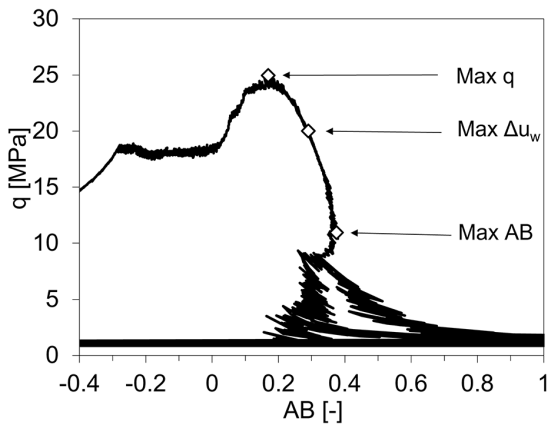

C3_STA2_1_842_62S13CTCU

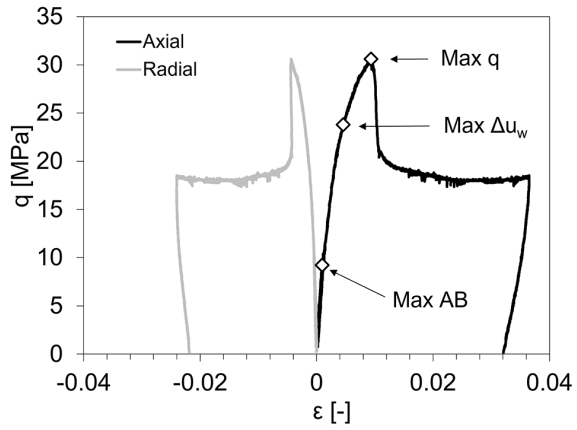

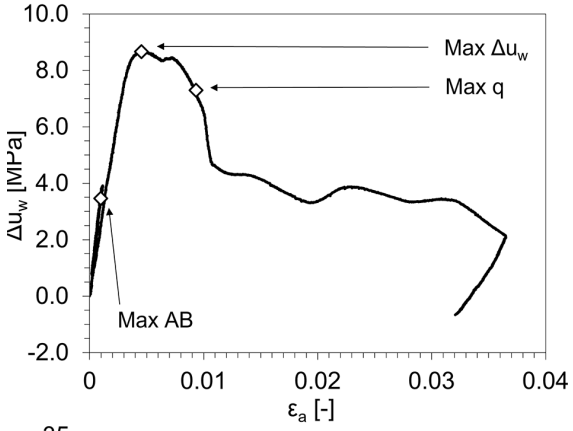

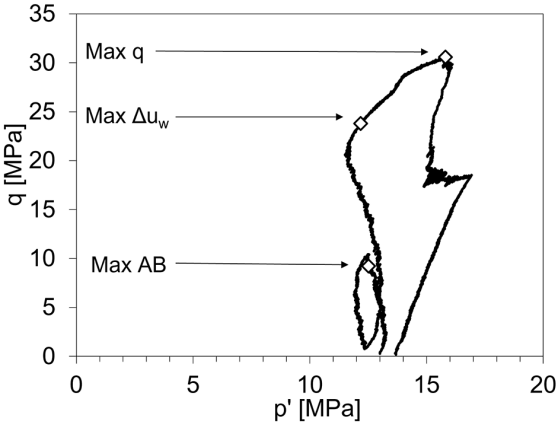

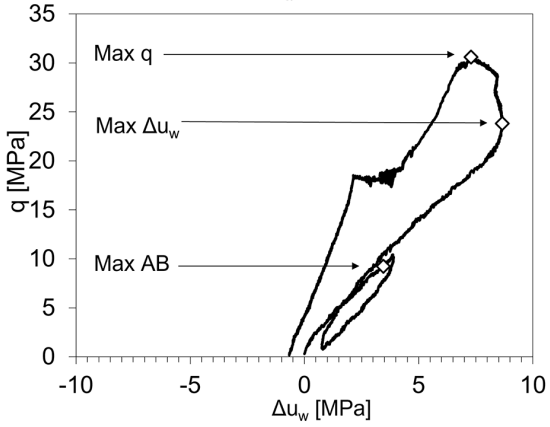

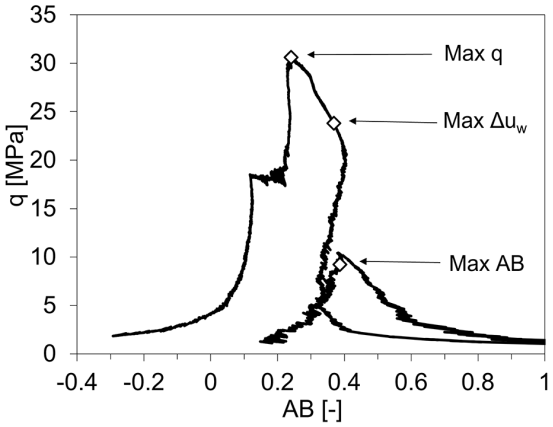

C4_STA2_1_842_63S20CTCU

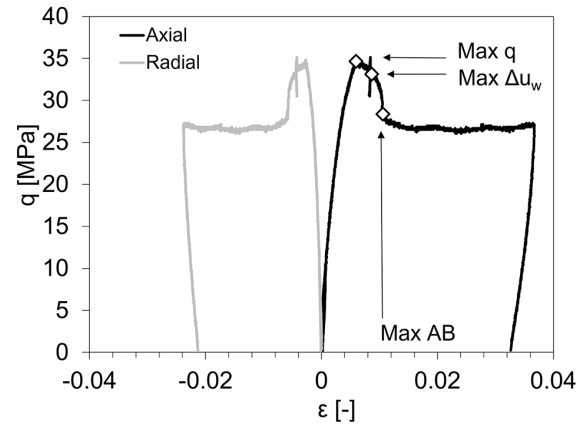

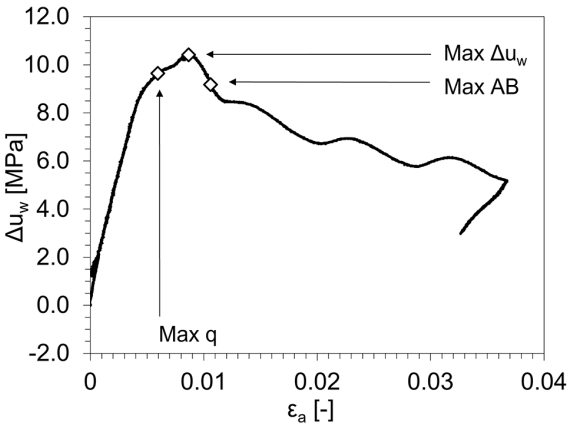

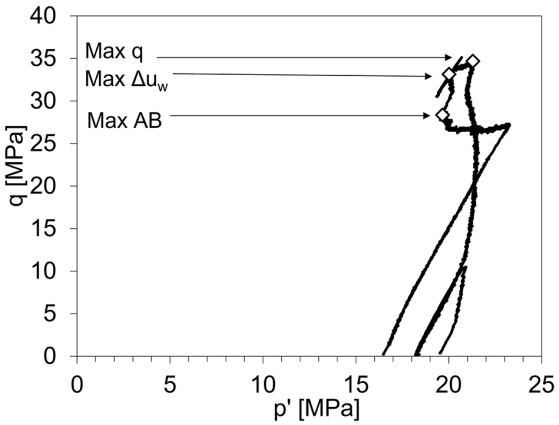

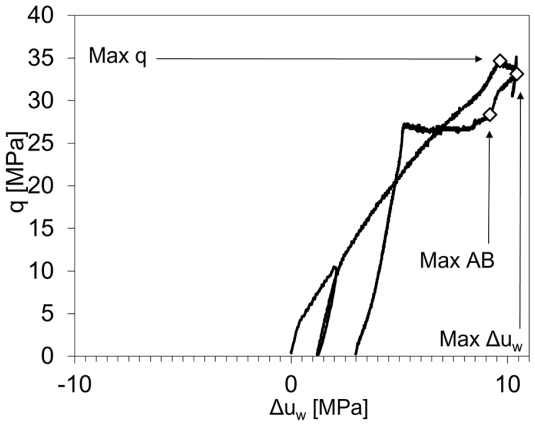

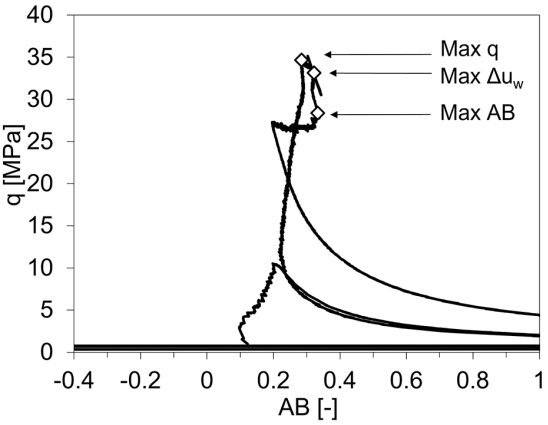

C5_STA2_1_842_63S18CTCU

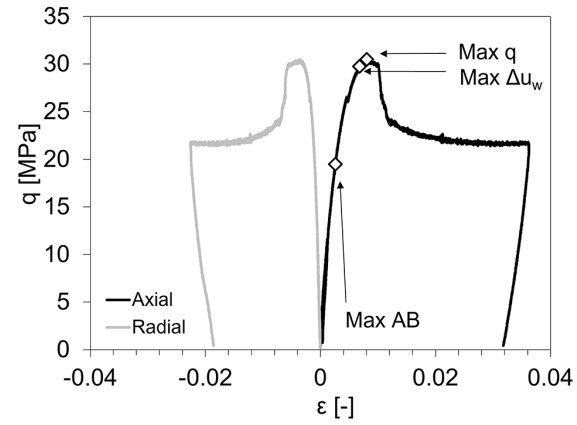

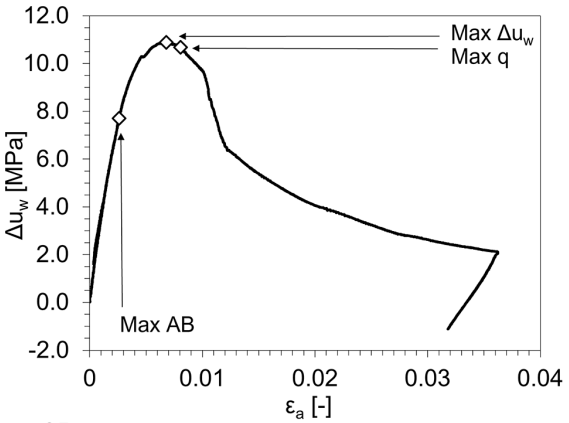

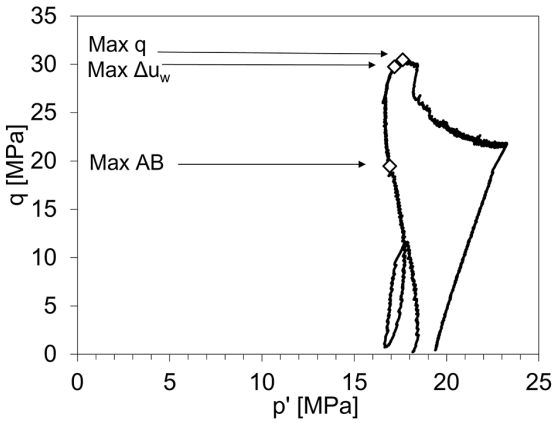

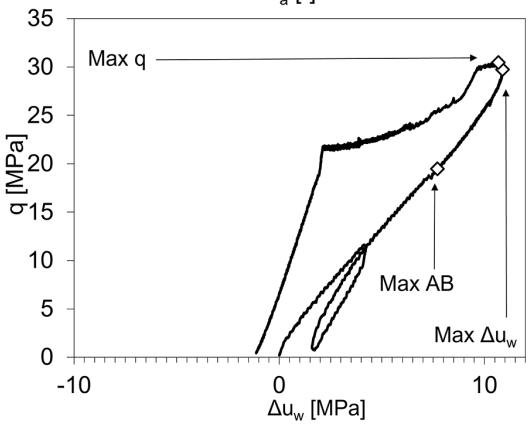

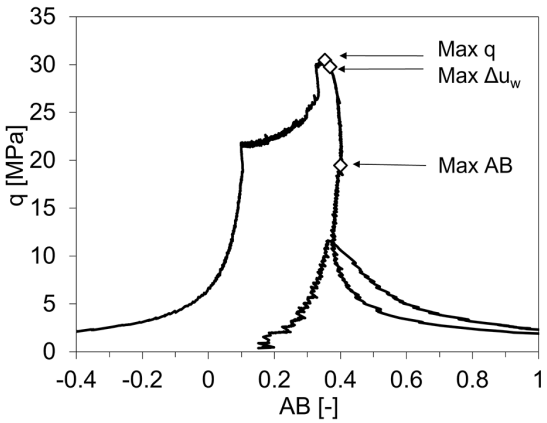

B1_STA2_1_897_04P7CTCU

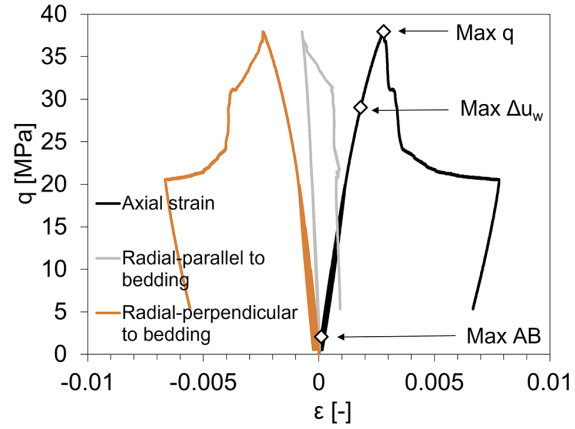

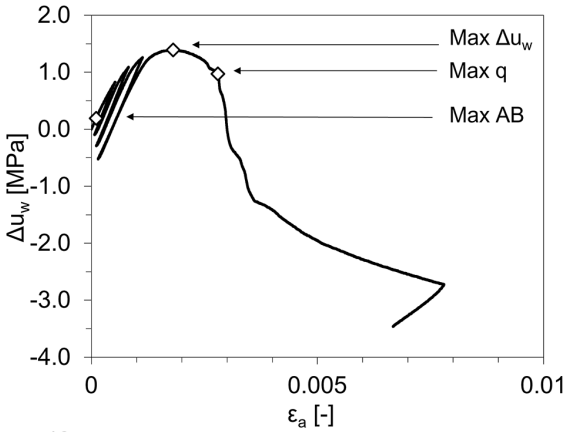

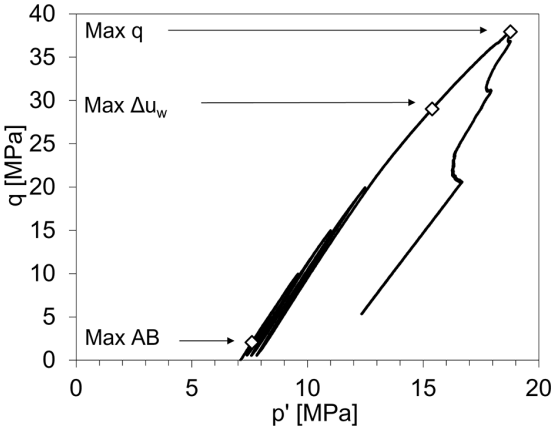

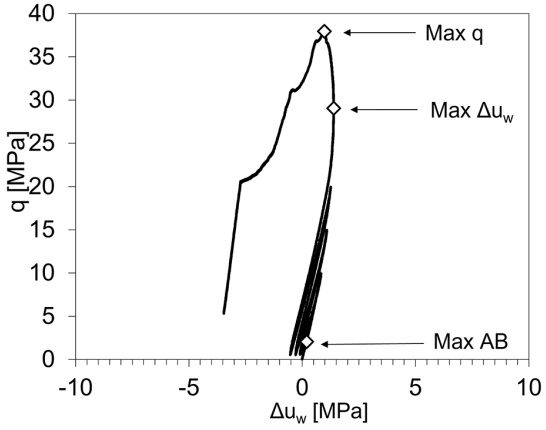

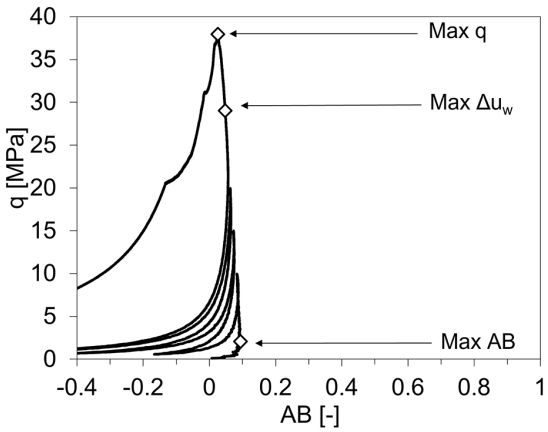

C1_STA2_1_903_67P7CTCU

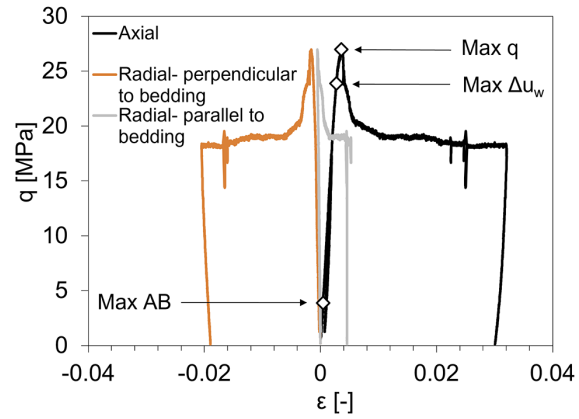

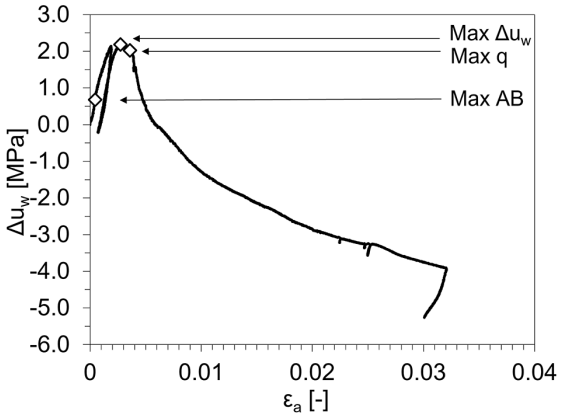

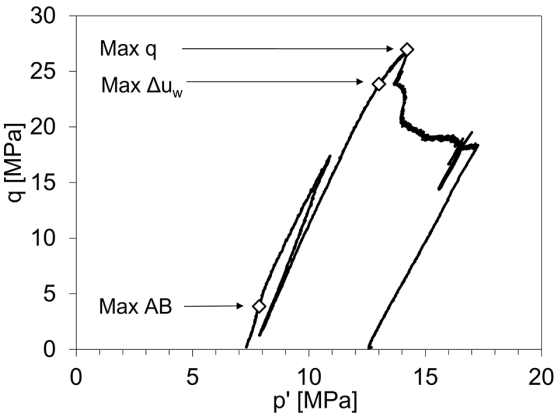

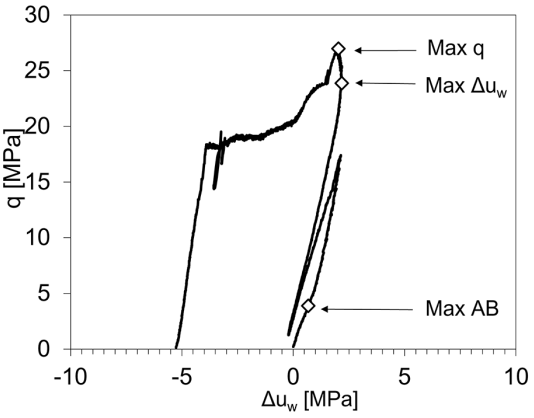

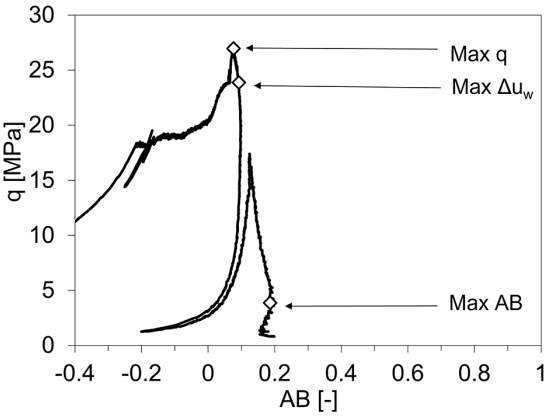

Appendix D Mineralogical analysis of the tested samples

Mineralogical analysis and grain density performed by the University of Bern on a series of specimens. Mineralogical analyses were performed on specimens that were not used in the mechanical programme, or negatives and chuncks from the specimen preparation. The ID of one of the specimens sourced from the same depth is reported. [a] Organic carbon content value altered by sample oil-contamination.

Specimen ID from same depth	**Depth** [m]	**S** [wt.-%]	**C(inorg)** [wt.-%]	**C(org)** [wt.-%]	**Quartz** [wt.-%]	**K-feldspar** [wt.-%]	**Plagioclase** [wt.-%]	**Calcite** [wt.-%]	**Dolomite/Ankerite [wt.-%]**	**Siderite** [wt.-%]	**Pyrite** [wt.-%]	**Clay minerals** [wt.-%]	**Grain density** [g/cm^3]	**Grain density STDEV** [10^{-4}/cm^3]
STA2-1_TRX8_626_56	626.56	< 0.1	12.0	0.2	1			98	1		< 0.2	0	2.717	8
A1_STA2_1_626_58S_K0	626.59	0.14	12.0	0.3	2			97	1		0.3	0	2.713	4
A2_STA2_1_795_93S_K0	795.92	< 0.1	7.5	0.3	5		3	51	9	3	< 0.2	4	2.973	10
Additional measurement	795.94	< 0.1	6.9	0.7	6		3	45	10	2	< 0.2	5	2.946	5
STA2-1_TRX9_796_13	796.13	< 0.1	5.5	0.3	8		4	37	8		< 0.2	10	3.041	8
B3_STA2_1_814_60S_K0	814.61	0.3	1.5	1.4[a]	23	1	1	12			0.6	60	2.669	9
C2_STA2_1_842_63S7CTCU	842.63	0.04	2.27	1.3	24	2	1	12		8	0.1	52	2.696	5
B2_STA2_1_845_33S_K0	845.35	0.2	0.9	1.1 [a]	22	2	2	6	1	1	0.4	65	2.675	9
B1_STA2_1_897_04P7CTCU	897.04	0.6	1.6	1.2 [a]	15	1	2	11	1	2	1.1	66	2.692	10
C1_STA2_1_903_67P7CTCU	903.67	0.5	1.3	1.1	17	2	2	11			0.9	66	2.690	7
D5_STA2_1_PERM	965.27	1.0	0.1	0.1	43	9	10					30	2.687	8
D2_STA2_1_PERM	965.34	1.8	< 0.1	0.1	42	8	10					31	2.707	4
D1_STA2_1_PERM	965.55	0.6	< 0.1	< 0.1	38	8	11					38	2.683	7

Appendix E Triaxial test results

Tab. E-1: Wave velocities recorded at the beginning of the shearing phase

Specimen ID, specimen geometry, mean effective and deviatoric stress (if applicable) at which the measurements were performed, P and S waves in the cylinder axis direction (*Vp*, *Vs*). For specimen geometry see Fig. 4-1.

Specimen ID	**Specimen geometry**	*p'* [MPa]	*q* [MPa]	*Vp* [m/s]	*Vs* [m/s]
C6_STA2_1_842_62P13CTCU	P	15	11	4'039	2'024
C7_STA2_1_842_62P8CTCU	P	11	11	4'131	2'244
C8_STA2_1_842_63P11TC	P	11	8	4'155	2'235
C9_STA2_1_842_63P8TC	P	8	9	4'106	2'180
C2_STA2_1_842_63S7CTCU	S	7	9	3'349	1'725
C3_STA2_1_842_62S13CTCU	S	13	8	3'327	1'734
C4_STA2_1_842_63S20CTCU	S	21	7	3'542	1'880
C5_STA2_1_842_63S18CTCU	S	18	7	3'322	1'873
B1_STA2_1_897_04P7CTCU	P	7		4'148	2'736
C1_STA2_1_903_67P7CTCU	P	9	8	4'052	2'229

Specimen ID and corresponding initial characteristics are reported in Tab. 6-2, along with the results from the triaxial tests from the pre-shearing phases. Tab. E-2 includes:

- Specimen ID
- Core depth
- Formation
- Specimen geometry
- Bulk modulus ρ_{bulk} [g/cm^3]
- Initial void ratio, computed using a reference solid density of 2.70 g/cm^3
- Initial and final water content
- Measured values of the Skempton's B check, without correction (average B value over multiple determinations and corresponding mean effective stress)
- Swelling pressure obtained at the end of the saturation (radial and axial)
- Consolidation coefficient, obtained during the consolidation phase, and corresponding mean effective stress

Tab. E-2: Triaxial test results (part 1)

For specimen geometry see Fig. 4-1.

Specimen ID	**Specimen geometry**	ρ_{bulk}	e_0	**Water content**		**B check**		**Swelling pressure**		**Consolidation phase**		**Strain rate**	**Stress path**
				Initial	Final	p'	B	Axial	Radial	p'	c_v	$\dot{\varepsilon}$	
		[g/cm³]	[-]	[%]	[%]	[MPa]	[-]	[MPa]	[MPa]	[MPa]	[mm²/s]	[s⁻¹]	
C6_STA2_1_842_62P13CTCU	P	2.521	0.121	4.71	4.48	9	0.81					5E-08	CTCU
C7_STA2_1_842_62P8CTCU	P	2.538	0.112	4.54	4.44							5E-08	CTCU
C8_STA2_1_842_63P11TC	P	2.522	0.120	4.60	3.58							2E-08	TC
C9_STA2_1_842_63P8TC	P	2.532	0.111	4.13	4.85	17	0.72			8	1.9E-04	2E-08	TC
C2_STA2_1_842_63S7CTCU	S	2.521	0.120	4.57	4.68	20	0.71					5E-08	CTCU
C3_STA2_1_842_62S13CTCU	S	2.504	0.127	4.53	3.96							5E-08	CTCU
C4_STA2_1_842_63S20CTCU	S	2.518	0.121	4.50	4.42							5E-08	CTCU
C5_STA2_1_842_63S18CTCU	S	2.521	0.120	4.59	4.60	4	0.75					5E-08	CTCU
B1_STA2_1_897_04P7CTCU	P	2.541	0.119	5.36	5.45	29	0.80	28.7	28.7	7	6.1E-04	7E-08	CTCU
C1_STA2_1_903_67P7CTCU	P	2.495	0.137	5.03	5.24	10	0.81					5E-08	CTCU

Tab. E-3 presents the results from the shearing phases, including:

- Undrained elastic properties: Elastic modulus [GPa], Small Strain elastic modulus [GPa], Ratio of radial to axial strain [-], Ratio of radial (parallel to bedding) to axial strain [-] (only for P-samples), Mean effective stress at which the elastic properties were computed [MPa]
- Peak strength: Mean effective stress and deviatoric stress at peak
- Maximum *AB* value: Mean effective stress and deviatoric stress at the maximum *AB* value
- Maximum pore pressure: Mean effective stress and deviatoric stress attained at the maximum pore pressure
- Post peak strength: Mean effective stress and deviatoric stress

Tab. E-3: Triaxial test results (part 2)

* Best estimates of the peak shear strength. See Section 6.2.2.5.

** Maximum pore water pressure and maximum AB value were achieved after the peak shear strength. See Section 6.2.2.5 and diagnostic plots in Appendix C.

Specimen ID	**Undrained elastic properties**					**Peak strength** [MPa]		**Max. *AB* value** [MPa]		**Max. pore pressure** [MPa]		**Post peak strength** [MPa]		**Post peak elastic properties**	
	p' [MPa]	**Elastic modulus** [GPa]	**Small Strain modulus** [GPa]	**Ratio radial (perpendicular to bedding) to axial strain** [-]	**Ratio radial** (parallel to bedding) **to axial strain** [-]	q [MPa]	p' [MPa]	q [MPa]	p' [MPa]	q [MPa]	p' [(MPa]	q [MPa]	p' [MPa]	p' [MPa]	E [GPa]
C6_STA2_1_842_62P13CTCU	16.5	19.5	28.4			37.4	21.0	15.7	16.2	36.0	20.2	27.7	21.3	22.3	10.9
C7_STA2_1_842_62P8CTCU	10.6	12.7	14.8	0.64	0.26	34.2	18.0	24.2	11.9	27.5	12.5	25.8	16.9	19.9	13.7
C8_STA2_1_842_63P11TC						24.4 *	11.0								
C9_STA2_1_842_63P8TC						23.4 **	8.5								
C2_STA2_1_842_63S7CTCU	7.9	9	13.5	0.25		24.9	11.4	11.0	7.0	20.0	8.3	17.8	13.56	21.1	6.3
C3_STA2_1_842_62S13CTCU	12.4	9.5	11.5	0.40		30.6	15.8	9.2	12.5	23.8	12.2	18.0	15.6	16.8	5.4
C4_STA2_1_842_63S20CTCU **	20.8	11.8		0.38		34.7	21.2	28.4	20.0	33.1	20.0	26.2	20.5	23.1	8.3
C5_STA2_1_842_63S18CTCU	17.7	10.3	11.62	0.38		30.5	17.6	19.5	16.9	29.8	17.1	22.71	20.6	23.1	5.8
B1_STA2_1_897_04P7CTCU	9.6	19.2	24.8	0.55	0.28	37.9	18.8	2.1	7.6	29.0	15.4	21.0	16.4	16.7	14.1
C1_STA2_1_903_67P7CTCU	10.9	15.4	21.8	0.50	0.34	27.0	14.1	3.9	7.9	23.9	13.1	18.83	15.3	17.2	12.7

Appendix F Test results in radial strain prevented conditions

Tab. F-1 includes:

- Specimen ID
- Specimen geometry
- Bulk modulus ρ_{bulk} [g/cm^3]
- Solid density ρ_s [g/cm^3], (i) measured or (ii) assumed
- Initial void ratio
- Initial and final water content
- Swelling pressure obtained at the end of the saturation (radial and axial)
- Strain rate
- Stress path

Tab. F-1: K0 test results

Specimen ID	**Specimen geometry**	ρ_{bulk}	ρ_s	e_0	**Water content**		**Swelling pressure**		**Strain rate**	**Stress path**
		[g/cm^3]	[g/cm^3]	[-]	Initial [%]	Final [%]	Axial [MPa]	Radial [MPa]	$\dot{\varepsilon}$ [s^{-1}]	
A2_STA2_1_795_93S_K0	S	2.707	3.0	0.172	4.37	4.78	2.8	1.2	7E-08	K0
A1_STA2_1_626_58S_K0	S	2.662	2.7	0.021	0.71	0.87	4.5	1.6	7E-09	K0
B2_STA2_1_845_33S_K0	S	2.503	2.7	0.138	5.44	5.68	27.0	12.3	2E-08	K0
B3_STA2_1_814_60S_K0	S	2.492	2.7	0.141	5.36	5.84	25.6	8.5	2E-08	K0

B3_STA2_1_814_60S_K0

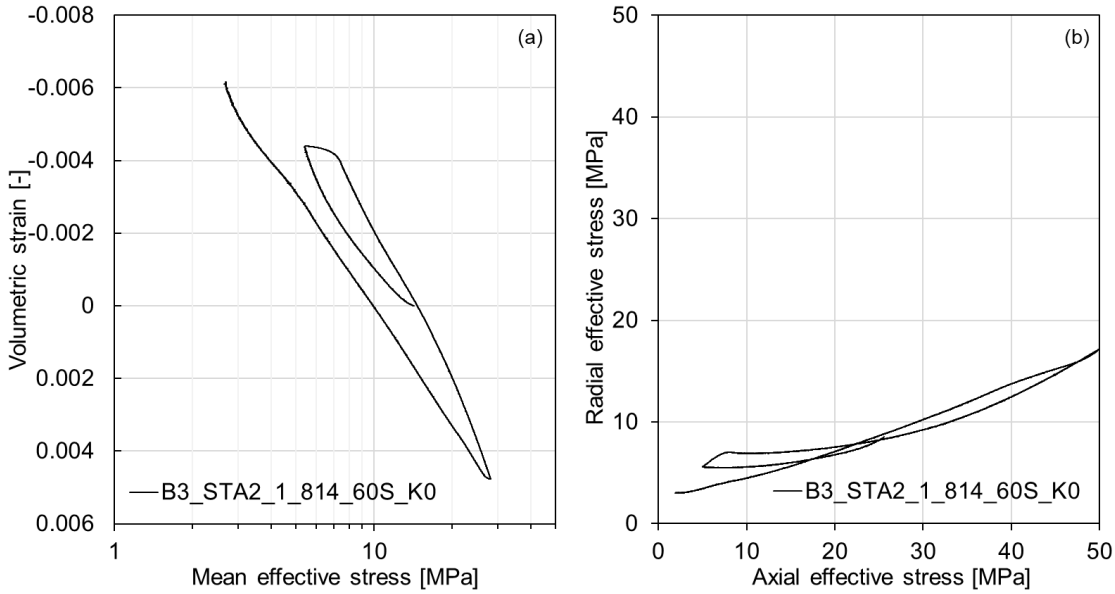

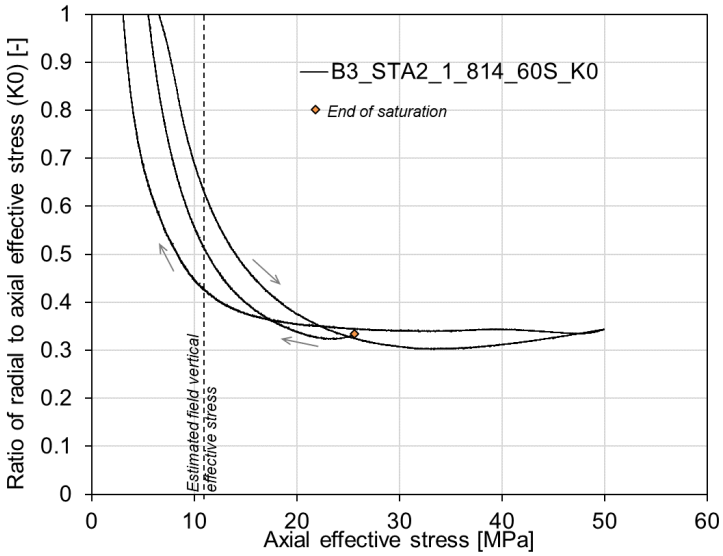

A1_STA2_1_626_58S_K0

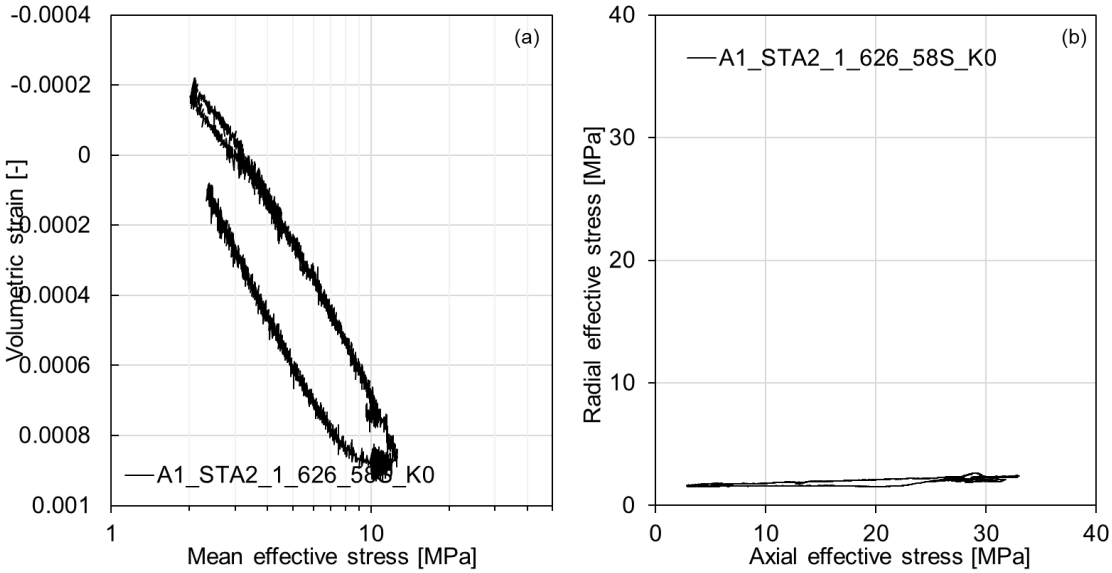

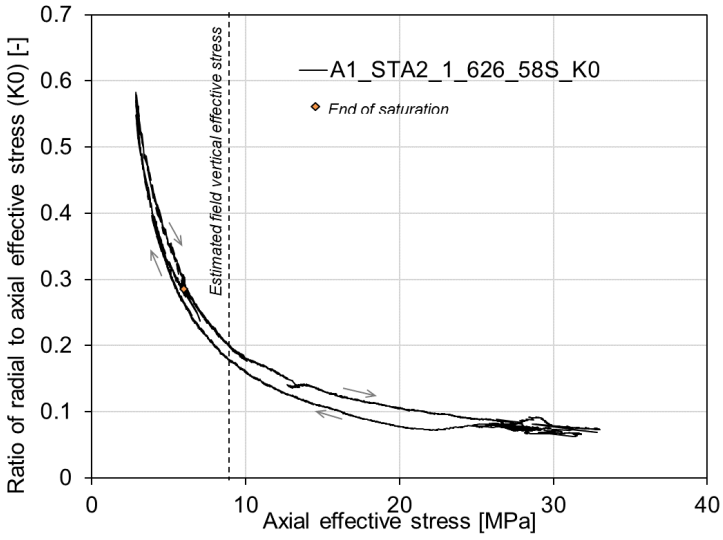

A2_STA2_1_795_93S_K0